Quantum Reflection at Strong Magnetic Fields

seit 1558

Masterarbeit zur Erlangung des akademischen Grades
Master of Science (M.Sc.)

eingereicht von Nico Seegert
geboren am 23.06.1986 in Berlin
Matrikelnummer: 98387

Contents

Introduction

The advent of quantum mechanics in the 1920s marked an important step in the development of modern physics. In 1928, P.A.M. Dirac published his relativistic theory of the electron [1] and offered an interpretation of the occurring negative energy states of the particles. In his "hole theory", he identified the vacuum as an infinite sea of occupied negative energy states, which is stable due to the Pauli exclusion principle. Electrons which are removed from this sea by means of a sufficient energy transfer leave behind "holes", which he associated with positively charged electrons, i.e. positrons, for the first time at the Solvay conference in 1933 [2]. Owing to the uncertainty principle of quantum mechanics, energy fluctuations are always present and therefore the vacuum constantly produces (virtual) electron-positron pairs which have the ability to modify the propagation of (real) light fields through vacuum. In 1936, W. Heisenberg and his PhD student H. Euler published a generalization of the Maxwell Lagrangian which is now known as the Heisenberg-Euler Lagrangian [3]. It describes the nonlinear dynamics of slowly varying electromagnetic fields at one loop order, taking into account couplings to all orders. The resulting equations of motion for the photon fields are similar to those known from nonlinear optics and thus, one can adopt the viewpoint that the vaccuum exhibits medium-like properties. Dirac's theory was eventually developed further and culminated in the formulation of quantum electrodynamics (QED), which constitutes the basic theory for the fundamental interaction of light and matter. In the context of QED, J. Schwinger rederived the results of Euler and Heisenberg, employing proper-time methods and effective action approaches, and hence put the results on firmer theoretical grounds [4].

The signatures of the quantum vacuum nonlinearity, as described by the Heisenberg-Euler Lagrangian, are manifold (for a recent overview see for example [5]). One of the earliest discussed effects on the vacuum is the acquisition of a dielectric constant differing from unity. Hence, real probe photons subject to a strong magnetic background field will experience vacuum magnetic birefringence [6, 7] as well as vacuum dichroism [8]. Other effects resulting from the self-interactions of electromagnetic fields by means of induced electron-positron pairs are, for example, light-by-light scattering [9] and photon splitting [10]. Conceptionally, all of these signatures differ in the order to which the microscopic photon field $f^{\mu\nu}$ couples to the virtual electron-positron pair, whose dynamics itself are modified by the coupling to the macroscopic background field $F^{\mu\nu}$ (to all orders). Photon splitting as a higher order process has already been observed experimentally [11], albeit by employing atomic fields as background fields and only for hard photons, i.e. with frequency $\omega \gg m$, where m denotes the electron mass. In contrast, light-by-light scattering and magnetic birefringence still await their experimental verification. To this end, several experiments such as PVLAS [12] and BMV [13] are currently underway and results should be expected in the upcoming years. Further consequences of the structure of the QED vacuum are the well studied and established Casimir effect [14] as well as the Schwinger effect, describing electron-positron pair production in strong electric fields E. The Schwinger effect is a representative of a process which cannot be treated perturbatively since the pair production rate for weak fields is suppressed exponentially in the parameter E_{cr}/E, where $E_{\mathrm{cr}} = e/m^2$ denotes the Schwinger limit of the electric field strength.

The present work aims at introducing and investigating the effect of quantum reflection as a new means of probing the quantum vacuum nonlinearity. The term quantum reflection is commonly employed to describe the reflection of atoms, quantum mechanically regarded as matter waves, from attractive potentials [15]. This effect can be used to investigate the surface of condensed matter by shining probe particles onto it at grazing incident angles. The reflected particles are then a superposition of both atoms reflected classically at the repulsive surface of the condensed matter as well as atoms subjected to quantum reflection due to the attractive long range potential.

This work now suggests to carry over this mechanism to the purely optical case by employing a highly sensitive "pump-probe" setup. A strong magnetic background field, created by a pump laser, modifies the QED vacuum to act as an effective potential for traversing probe photons. Since the magnetic field exhibits a spatial (as well as temporal) inhomogeneity, we expect the incoming probe photons to be partially reflected from the region of the inhomogeneity. In our analogy the probe photons play the role of the atoms, while the magnetized quantum vacuum plays the role of the attractive potential created by the condensed matter surface. However, probe photons unaffected by the vacuum fluctuations simply pass the entire region of inhomogeneity. This is in contrast to quantum reflection in the atomic case, where the repulsive potential of the condensed matter gives rise to a large background. We therefore end up with a highly sensitive setup possessing an inherent signal-background separation, which should prove to be an important advantage compared to other experiments aiming to probe fluctuation-induced nonlinearities of the quantum vacuum. Owing to the smallness of the nonlinear effects, one of the biggest challenges for such standard experiments is usually given by the separation of photons carrying the optical signatures from such photons which were unaffected by the fluctuations.

The first chapter of this work is devoted to outline the quantum electrodynamical foundations. We derive an equation of motion ("Quantum Maxwell equation") to one loop order for photons traveling through a slowly varying magnetic background field. The central quantity of interest is the photon polarization tensor, whose derivation is outlined very briefly and which is expanded in terms of the field strength ratio eB/m^2. The second chapter then treats the specific phenomenon of optical quantum reflection in the limit of small background field strengths. We show two different ways to derive a closed-form formula for the reflection coefficient for the case of time independent magnetic fields. By employing this formula, the reflection for various field profiles is investigated and numerical values based on the soon-to-be available laser facilities POLARIS and JETI200 in Jena are calculated. The goal is to maximize the effect by suitably shaping the background laser profile to yield a measurable rate of reflection. The third chapter then gives a first overview and introduction to space as well as time dependent magnetic background fields. The formulae complicate noticeably, and final results for the reflection have not yet been obtained. The last chapter concludes with a summary and prospects for further investigations.

1. Quantum electrodynamical fundamentals

The first chapter intends to give a brief overview of the quantum electrodynamical fundamentals. In the first section we use the effective action approach to derive the equation of motion, which describes the propagation of photons in an electromagnetic background field. The central quantity of interest is the photon polarization tensor in a constant magnetic background field, whose derivation we outline very briefly and which is evaluated perturbatively for magnetic fields which are small compared to a critical magnetic field strength $B_{\mathrm{cr}} = m^2/e$.

1.1. Effective action and equation of motion

Our goal is to derive the equation of motion ("Quantum Maxwell equation") of the photons from an effective action, which includes the full information about the propagation in an external magnetic background field at one-loop accuracy. The derivation closely follows [16]. The starting point is the usual "bare" QED action

$$S[\psi, \bar{\psi}, \mathcal{A}] = \int d^4x \, \mathcal{L}_{\mathrm{QED}} = \int d^4x \left(i\bar{\psi}\slashed{D}\psi - m\bar{\psi}\psi - \frac{1}{4}F_{\mu\nu}F^{\mu\nu} \right), \tag{1.1}$$

where $\slashed{D} = \gamma_\mu D^\mu = \gamma_\mu(\partial^\mu - ie\mathcal{A}^\mu)$ denotes the contracted gauge covariant derivative and $F_{\mu\nu} = ie\,[D_\mu, D_\nu]$ the field strength tensor. The 4-component Dirac spinors ψ and $\bar{\psi} = \psi^+\gamma^0$ represent fermionic particles and anti-particles respectively. Switching to the Euclidean formulation of QFT, connected correlation functions, or n-point functions $\langle \chi(x_1)\dots\chi(x_n)\rangle$, can be obtained from the generating functional

$$Z[J] = e^{W[J]} = \int_\Lambda \mathscr{D}\chi \, e^{-S[\chi]+\int J\chi} = \langle 0|0\rangle_J \tag{1.2}$$

via the relation

$$\langle \chi(x_1)\cdots\chi(x_n)\rangle = \frac{\int_\Lambda \mathscr{D}\chi \, \chi(x_1)\dots\chi(x_n)e^{-S[\chi]}}{\int_\Lambda \mathscr{D}\Phi \, e^{-S[\chi]}} = \frac{\delta}{\delta J(x_1)} \cdots \frac{\delta}{\delta J(x_n)} W[J]\bigg|_{J=0}. \tag{1.3}$$

As a shorthand notation, the so-called "super-vector" $\chi = (\psi, \bar{\psi}, \mathcal{A})$ has been introduced and the product χJ is understood to be over all possible field components. $Z[J]$ is the vaccuum-vacuum transition amplitude in the presence of an external source field J, $W[J]$ is called "Schwinger functional" and presents a more effective way of storing the relevant information by generating the connected n-point functions. A lower integration bound Λ (UV cut-off) has been introduced, since the occurring integrals formally diverge and have to be properly renormalized. We can now introduce the effective action $\Gamma[\phi]$ by means of a Legendre transformation

$$\Gamma[\phi] := \sup_J \left(-W[J] + \int J\phi \right), \tag{1.4}$$

where the classical field $\phi(x)$ is defined by

$$\phi(x) = \frac{\delta W}{\delta J(x)} = \langle \chi(x) \rangle_J. \tag{1.5}$$

and represents the vacuum expectation value of the quantum field χ in the presence of a source term J. $\Gamma[\phi]$ is the generating functional of the 1PI-irreducible correlation functions and governs the dynamics of the "classical fields" by means of the "quantum equation of motion"

$$\frac{\delta \Gamma[\phi]}{\delta \phi(x)} = J(x), \tag{1.6}$$

much in the same way in which real classical fields are governed by the classical action S. Employing a coordinate shift $\chi \to \chi + \phi$, we can derive from Eq. (1.2) a relation to determine Γ, i.e.,

$$e^{-\Gamma[\phi]} = \int_\lambda \mathscr{D}\chi \; e^{-S[\phi+\chi]+\int \frac{\delta\Gamma[\phi]}{\delta\phi}\chi}. \tag{1.7}$$

Since Eq. (1.7) is rather hard to solve for any interacting theory, we perform an expansion of the right-hand-side exponent

$$-S[\phi] - \int \left(\frac{\delta S[\phi]}{\delta \phi} - \frac{\delta \Gamma[\phi]}{\delta \phi} \right) \chi - \frac{1}{2} \int \int \chi \frac{\delta^2 S[\phi]}{\delta \phi^2} \chi + O\left(\chi^3\right). \tag{1.8}$$

We note that in a perturbative expansion in the parameter $\hbar$, the order of $\hbar$ counts the numbers of loops of a graph [17]. The explanation can be given as follows: Reinstating $\hbar$ for the time being, it only enters as a factor $1/\hbar$ in front of the action S and Γ in Eq. (1.7). Since the propagator corresponding to a line in a graph is given by the inverse of the differential operator in the interaction-free Lagrangian, each internal line I has a factor of $\hbar$. Furthermore, each vertex V introduces a factor of $1/\hbar$, so that the power of $\hbar$ is given by

$$P = I - V \tag{1.9}$$

and with the known relation $L = I - V + 1$, where L denotes the number of loops, we get

$$P = L - 1. \tag{1.10}$$

Note, that $L - 1$ includes the overall factor of $1/\hbar$ and therefore $\hbar$ on the right-hand-side indeed counts the number of loops. With a substitution $\chi' = \sqrt{\hbar}\chi$ and realizing that the term in brackets in Eq. (1.8) must be at least of the order $\hbar$, we obtain to the lowest order the general equation for the one-loop effective action

$$\Gamma[\phi] = S[\phi] + \Gamma^{(1)}[\phi] = S[\phi] + \frac{1}{2}\mathrm{Tr}\ln\left(\frac{\delta^2 S[\phi]}{\delta \phi^2}\right). \tag{1.11}$$

The trace "Tr" denotes integration in momentum or position space as well as summation over Dirac-indices. Using the QED-Lagrangian (1.1) and setting $\psi, \bar{\psi} = 0$ after the differentiation (we are only interested in light propagation in a fermionic vacuum), we obtain

$$\Gamma[\mathcal{A}] = S[\mathcal{A}] - i\mathrm{Tr}\ln(-i\slashed{D} + m). \tag{1.12}$$

Here, we have switched back to the usual Minkowski space (hence the factor of i) and the "$-$" is due to the Grassmann integration when evaluating the Gaussian integral. Note, that Γ is

equivalent to an action where the fermionic contributions have been integrated out [18]. Equation (1.12) is the starting point to obtain the famous Euler-Heisenberg action, which for the first time allowed the investigation of quantum vacuum effects like birefringence, light-by-light scattering and electron-positron pair production in strong electric fields. In light of the physical situation under consideration, we now split the vector potential $\mathcal{A}^\mu(x) = A^\mu(x) + a^\mu(x)$ into the vector potential of the background field A^μ and the potential of the probe photon field a^μ. We then perform an expansion in the number of photon fields a^μ which couple to the loop, while at the same time retain the coupling of the background field A^μ to all orders. The intention of this splitting is to later regard the background field as constant or at most "slowly" varying. To this end, we make use of the free additive constant to rewrite $\Gamma^{(1)}$, i.e.,

$$\Gamma^{(1)}[a, A] = -i\operatorname{Tr}\ln\left[1 + (\not{p} - e\not{A} + m)^{-1}(-e\not{a})\right] \tag{1.13}$$

and use the expansion of the logarithm $\ln(1 + x) = x - (1/2)x^2 + \mathcal{O}(x^3)$ to obtain

$$\Gamma^{(1)}[a, A] = -i\operatorname{Tr}\left[\frac{1}{\not{p} - e\not{A} + m}(-e\not{a})\right] + \frac{i}{2}\operatorname{Tr}\left[\frac{1}{\not{p} - e\not{A} + m}(-e\not{a})\frac{1}{\not{p} - e\not{A} + m}(-e\not{a})\right]$$

$$+ \mathcal{O}\left(\left[\frac{1}{\not{p} - e\not{A} + m}(-e\not{a})\right]^3\right) \tag{1.14}$$

$$= \quad\bigcirc\!\!\!\!\bigcirc\!\!\!\!\sim \quad + \quad \sim\!\!\!\!\bigcirc\!\!\!\!\bigcirc\!\!\!\!\sim \quad + \mathcal{O}\left(\left[\frac{1}{\not{p} - e\not{A} + m}(-e\not{a})\right]^3\right).$$

The doubled fermion lines in the Feynman diagrams represent the coupling of the fermions to the external field to all orders.

The individual terms occurring in Eq. (1.14) can be directly interpreted. The first sum term, which is of first order in $\not{a}$, corresponds to a tadpole-like diagram: The incoming probe photon field is absorbed by the magnetic background field. For constant background fields, this process can be neglected due to the requirement of energy and momentum conservation at the single vertex. This still holds true for background fields varying slowly in time and space, if only lower order couplings to the external field are considered. However, an infinite number of couplings should result in a non-perturbative effect of photon absorption even for slowly varying fields.

We can identify the second order term with photon propagation in a magnetic background field. The imaginary part of this diagram corresponds to mode specific photon losses by virtue of electron-positron pair creation. Higher order terms correspond to photon splitting and light-by-light scattering. Note that terms involving an odd number of a^μ and A^μ vanish identically, which is known as Furry's theorem: Only an even number of fields can couple to a closed fermion loop. This is a direct consequence of the charge conjugation symmetry of QED.

Here, we are solely interested in effects related to photon propagation in at most slowly varying magnetic background fields and furthermore, we will only consider lowest order couplings. This allows us to only keep the second order term and discard the rest. The second term can be evaluated explicitly to yield

$$i\frac{e^2}{2}\int d^4x\, d^4y\, a^\mu(x)\operatorname{tr}_\gamma\left[\gamma_\mu\langle x|\frac{1}{\not{p} - e\not{A} + m}|y\rangle\gamma_\nu\langle y|\frac{1}{\not{p} - e\not{A} + m}|x\rangle\right]a^\nu(y)$$

$$= i\frac{e^2}{2}\int d^4x\, d^4y\, a^\mu(x)\operatorname{tr}_\gamma\left[\gamma_\mu\frac{1}{i}G_+(x, y|A)\gamma_\nu\frac{1}{i}G_+(y, x|A)\right]a^\nu(y), \tag{1.15}$$

where

$$G_+(x,y|A) = \langle x| \frac{i}{\not{p} - e\not{A} + m} |y\rangle = \quad x \overline{\quad\quad\quad\quad} y \tag{1.16}$$

denotes the dressed electron-propagator in position space, which describes electron propagation in a background field involving couplings to all orders. We now define the photon polarization tensor $\Pi_{\mu\nu}^{(2)}(x,y|A)$ in an electromagnetic background field at one loop order by

$$\Pi_{\mu\nu}^{(2)}(x,y|A) = -ie^2 \mathrm{tr}_\gamma \left[\gamma_\mu G_+(x,y|A) \gamma_\nu G_+(y,x|A) \right] \tag{1.17}$$

and hence we arrive at the effective action

$$\Gamma[a,A] = -\frac{1}{4} \int d^4x F_{\mu\nu}F^{\mu\nu} \Big|_{a+A} - \frac{1}{2} \int d^4x \, d^4y \, a^\mu(x) \Pi_{\mu\nu}^{(2)}(x,y|A) a^\nu(y). \tag{1.18}$$

We now obtain the equations of motion for the probe field a^μ from Equation (1.18). The field strength tensor $F_{\mu\nu}|_A$ is considered constant and we can therefore neglect the contribution of A^μ in the first integral of (1.18) in the following calculation. Switching to momentum space by means of the Fourier transformations (A.11) and evaluation of the emerging delta-functions leads to

$$\Gamma[a] = \int \frac{d^4q}{(2\pi)^4} \int \frac{d^4p}{(2\pi)^4} \left[-\frac{1}{2}\delta(p+q) \left(a_\nu(q)a^\nu(p)p^2 - p_\nu p^\mu a_\mu(q)a^\nu(p) \right) \right.$$
$$\left. -\frac{1}{2} a_\mu(q)\Pi^{\mu\nu}(-q,-p|A)a_\nu(p) \right]. \tag{1.19}$$

The corresponding Lagrange equations can be obtained from the variational principle

$$\frac{\delta \Gamma[a]}{\delta a_\alpha(k)} = 0 \tag{1.20}$$

and are given by

$$k^2 a^\alpha(-k) - k_\nu k^\alpha a^\nu(-k) = -\frac{1}{2} \int \frac{d^4p}{(2\pi)^4} \left[\Pi^{\alpha\nu}(-k,-p|A)a_\nu(p) + \Pi^{\mu\alpha}(-p,-k|A)a_\mu(p) \right]. \tag{1.21}$$

The polarization tensor is symmetric in the indices, and hence we arrive at the equations of motion

$$(k^2 g^{\mu\nu} - k^\mu k^\nu)a_\nu(k) = -\int \frac{d^4k'}{(2\pi)^4} \tilde{\Pi}^{\mu\nu}(k,-k'|A)a_\nu(k'). \tag{1.22}$$

Here, the symmetrized polarization tensor $\tilde{\Pi}^{\mu\nu}(k,k'|A) = \frac{1}{2}\left[\Pi^{\mu\nu}(k,k'|A) + \Pi^{\mu\nu}(k',k|A)\right]$, which generally mediates between two distinct momenta k and $-k'$, has been introduced. For the case of a constant background field, momentum conservation dictates the polarization tensor to be of the form

$$\Pi^{\mu\nu}(k,k'|A) = 2\pi\delta(k+k')\Pi^{\mu\nu}(k|A), \tag{1.23}$$

and the equations of motion simplify to

$$\left[k^2 g^{\mu\nu} - k^\mu k^\nu + \Pi^{\mu\nu}(k|A) \right] a_\nu(k) = 0. \tag{1.24}$$

In our case, however, Eq. (1.22) serves as the starting point for the calculation of the reflected field. As a simplification, we neglect the effect, which the induced field $a_{\mathrm{ind}}(k)$ will have on its

own further propagation and on the magnetic field. Therefore, we regard the right-hand side of Eq. (1.22) as a current $j(k)$, which is solely generated by the incoming beam $a_{\text{in}}(k')$, i.e.

$$j^\mu(k) = \int \frac{d^4k'}{(2\pi)^4} \tilde{\Pi}^{\mu\nu}(k, -k'|A)(a_{\text{in}})_\nu(k').\tag{1.25}$$

This current in turn is being interpreted as the source for the induced photon beam, and the equations of motion take on the form

$$(k^2 g^{\mu\nu} - k^\mu k^\nu)(a_{\text{ind}})_\nu(k) = -j^\mu(k).\tag{1.26}$$

Eq. (1.26) is a tensor equation of rather complicated structure, since the interaction with electromagnetic fields generally mixes different polarization modes of the photon field. Later on we will see, how this equation can be cast into a simpler one with trivial tensor structure for certain polarization modes.

1.2. The photon polarization tensor in a constant magnetic field

This section is devoted to giving an overview of the vacuum photon polarization tensor $\Pi^{\mu\nu}$. This quantity, also known as the "photon self energy", describes the modified propagation of photons in vacuum due to QED effects and plays a similar role for the photon as does the "mass operator" Σ for the electron. At the lowest loop order, the photon propagation is modified by the creation and subsequent annihilation of virtual electron-positron pairs, which now induce non-linear interactions between electromagnetic fields. Hence, the superposition principle of classical electromagnetism is no longer valid and effects, which should not exist classically, are predicted by QED. The vacuum therefore possesses the ability to modify photon propagation through external electromagnetic fields and acquire medium-like properties.

To elucidate the concept of the polarization tensor, we first consider photon propagation in a vacuum without external fields. The vacuum photon polarization tensor $\Pi^{\mu\nu}(k)$ is defined as the sum of all one-particle irreducible diagrams (1PI) without external legs, which contribute to the full photon propagator $G_A^{\mu\nu}(k)$, i.e.

$$\tag{1.27}$$

The direction of the momentum is omitted for the sake of clarity. The full photon propagator is given by the geometric series

$$\tag{1.28}$$

$$= D^{\mu\nu} + D_\kappa^\mu i\Pi^{\kappa\lambda} D_\lambda^\nu + D_\kappa^\mu i\Pi^{\kappa\lambda} D_{\lambda\delta} \Pi^{\delta\beta} D_\beta^\nu + \dots$$

where

$$D^{\mu\nu}(k) = \frac{i}{k^2}\left(\delta^{\mu\nu} + (\alpha - 1)\frac{k^\mu k^\nu}{k^2}\right)\tag{1.29}$$

denotes the photon propagator for the non-interacting theory for various Lorenz gauges ($\alpha \to 0$: Landau-gauge, $\alpha \to 1$: Feynman-gauge). The "Ward identity" now implies that the polarization tensor possesses no longitudinal components, i.e.

$$\Pi^{\mu\nu}(k) = (k^2 g^{\mu\nu} - k^\mu k^\nu)\Pi(k), \tag{1.30}$$

with a scalar function $\Pi(k)$. The polarization tensor can be calculated explicitly to one loop order, see for instance [18]. The calculation becomes more involved, if we consider photon propagation in an constant, external electromagnetic field. An explicit derivation is given in [19] for the case of a constant magnetic field, which shall be very briefly outlined here.

As a first step, the electron propagator G_+ in a constant, external magnetic field **B**, satisfying

$$\left[\gamma^\mu \left(\frac{1}{i}\partial'_\mu - e\,A_\mu(x')\right) + m\right] G_+(x', x'', A) = \delta(x' - x''), \tag{1.31}$$

has to be calculated. To simplify the computation, the magnetic field is chosen to point in the z-direction and equation (1.31) is solved employing the Schwinger-Fock gauge $A'^\mu(x') = -1/2\, F^{\mu\nu}(x' - x'')_\nu$. At the end, we multiply the "holonomy factor"

$$\Phi(x', x'', A) := \exp\left[ie \int_{x''}^{x'} dx_\mu \left\{A^\mu(x) - A'^\mu(x')\right\}\right] \tag{1.32}$$

to "transport" the gauge back from A' to any arbitrary gauge A. Furthermore, the magnetic field sets an external reference direction and Lorentz vectors as well as tensors can be decomposed in directions parallel and perpendicular to the magnetic field $\mathbf{B} = B\mathbf{e}_z$, i.e.

$$a_\parallel := (a^0, 0, 0, a^3), \quad a_\perp := (0, a^1, a^2, 0) \quad \text{and} \quad (ab)_\parallel := -a^0 b^0 + a^3 b^3, \quad (ab)_\perp := a^1 b^1 + a^2 b^2 \tag{1.33}$$

as well as

$$g_\parallel = \begin{pmatrix} -1 & 0 & 0 & 0 \\ 0 & 0 & 0 & 0 \\ 0 & 0 & 0 & 0 \\ 0 & 0 & 0 & 1 \end{pmatrix} \quad \text{and} \quad g_\perp = \begin{pmatrix} 0 & 0 & 0 & 0 \\ 0 & 1 & 0 & 0 \\ 0 & 0 & 1 & 0 \\ 0 & 0 & 0 & 0 \end{pmatrix}. \tag{1.34}$$

The result for the electron propagator $g(k)$ in momentum space, defined by

$$G_+(x', x'', A) = \Phi(x', x'', A) \int \frac{d^4k}{(2\pi)^4} e^{ik(x'-x'')} g(k), \tag{1.35}$$

reads

$$g(k) = i \int_0^\infty ds\, \exp\left\{-is\left[m^2 - ie + k_\parallel^2 + \frac{\tan z}{z}k_\perp^2\right]\right\} \cdot \frac{e^{i\sigma^{12}z}}{\cos z}\left(m - (\gamma k)_\parallel - \frac{e^{-i\sigma^{12}z}}{\cos z}(\gamma k)_\perp\right), \tag{1.36}$$

where $z := eBs$.

Employing the usual Feynman rules, the polarization tensor in an external magnetic field to the lowest order is given by

$$\Pi_{\mu\nu}^{(2)}(k|\mathbf{B}) = -ie^2 \text{tr}_\gamma \int \frac{d^4p}{(2\pi)^4} \gamma_\mu g(p)\gamma_\nu g(p-k) \quad + \quad \text{c.t.} \tag{1.37}$$

and corresponds to the Feynman graph
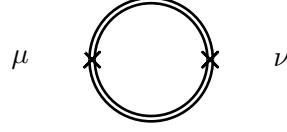
$$\mu \qquad \qquad \nu \qquad \qquad . \qquad (1.38)$$

The coupling of the electron-positron pair to the external magnetic field to all orders is accounted for by means of the dressed electron propagator $g(p)$. The additional contact terms (c.t.) renormalize the expression and can be chosen in such a way that the polarization tensor vanishes for the combined limit of vanishing momentum k and magnetic field B, i.e. $\Pi^{(2)}_{\mu\nu}(k \to 0, B \to 0) = 0$. Such a choice relates the QED coupling α to the cross section of Thomson scattering. The γ traces and the momentum integration can be evaluated explicitly and the polarization tensor be expressed in terms of a double parameter integral. The end result reads (omitting the label (2) from here on)

$$\Pi^{\mu\nu}(k|\mathbf{B}) = P_0^{\mu\nu}\Pi_0(k|\mathbf{B}) + P_\parallel^{\mu\nu}\Pi_\parallel(k|\mathbf{B}) + P_\perp^{\mu\nu}\Pi_\perp(k|\mathbf{B}) \qquad (1.39)$$

with

$$\begin{Bmatrix} \Pi_0 \\ \Pi_\parallel \\ \Pi_\perp \end{Bmatrix} = \frac{\alpha}{2\pi} \int_0^\infty \frac{ds}{s} \int_{-1}^1 \frac{d\nu}{2} \left(e^{-is\tilde{\phi}_0} \begin{Bmatrix} k^2 N_0 \\ N_0 k_\perp^2 + N_1 k_\parallel^2 \\ N_2 k_\perp^2 + N_0 k_\parallel^2 \end{Bmatrix} - e^{-im^2 s} k^2 (1 - \nu^2) \right), \qquad (1.40)$$

where

$$
\begin{aligned}
N_0 &= \cos\nu z - \nu \sin\nu z \cot z, \\
N_1 &= (1 - \nu^2)\cos z, \\
N_2 &= 2\frac{\cos\nu z - \cos z}{\sin^2 z} \qquad \text{and} \\
\tilde{\phi}_0 &= m^2 + \frac{1 - \nu^2}{4}k_\parallel^2 + \frac{1}{2}\frac{\cos\nu z - \cos z}{z \sin z}k_\perp^2.
\end{aligned} \qquad (1.41)
$$

The contour of the s integration is implicitly understood to lie slightly below the real positive s-axis, i.e. $m^2 \to m^2 - i\epsilon$. Furthermore, we introduced the projectors

$$P_\parallel^{\mu\nu}(k) = g_\parallel^{\mu\nu} - \frac{k_\parallel^\mu k_\parallel^\nu}{k_\parallel^2}, \quad P_\perp^{\mu\nu}(k) = g_\perp^{\mu\nu} - \frac{k_\perp^\mu k_\perp^\nu}{k_\perp^2} \quad \text{and} \quad P_0^{\mu\nu}(k) = g^{\mu\nu} - \frac{k^\mu k^\nu}{k^2} - P_\parallel^{\mu\nu}(k) - P_\perp^{\mu\nu}(k),$$

$$(1.42)$$

which span the transverse subspace, i.e. the subspace defined by the projector

$$P_T(k) = g^{\mu\nu} - \frac{k^\mu k^\nu}{k^2}. \qquad (1.43)$$

They fulfill the usual projector identities ($p \in \{\parallel, \perp, 0, k\}$)

$$
\begin{aligned}
(P_p)^{\mu\nu}(P_p)^\rho_\nu &= (P_p)^{\mu\rho}, \\
(P_p)^{\mu\nu}(P_{p'})^\rho_\nu &= 0 \qquad \text{for } p \neq p', \\
g^{\mu\nu} &= P_\parallel^{\mu\nu} + P_\perp^{\mu\nu} + P_0^{\mu\nu} + P_k^{\mu\nu},
\end{aligned} \qquad (1.44)
$$

where the remaining projector $P_k^{\mu\nu} = k^\mu k^\nu / k^2$ spans the longitudinal eigenspace. The result Eq. (1.39) still fulfills the Ward identity, which requires $k_\mu \Pi^{\mu\nu}(k) = 0$. For the case of $\mathbf{e}_B \nparallel \mathbf{k}$ and the

magnetic field pointing into the z-direction, explicit representations of the first two projectors defined by (1.42) are given by

$$P_\parallel^{\mu\nu} = \frac{1}{k_\parallel^2} \begin{pmatrix} -k_z^2 & 0 & 0 & -\omega k_z \\ 0 & 0 & 0 & 0 \\ 0 & 0 & 0 & 0 \\ -\omega k_z & 0 & 0 & -\omega^2 \end{pmatrix}, \qquad P_\perp^{\mu\nu} = \frac{1}{k_\perp^2} \begin{pmatrix} 0 & 0 & 0 & 0 \\ 0 & k_y^2 & -k_x k_y & 0 \\ 0 & -k_x k_y & k_x^2 & 0 \\ 0 & 0 & 0 & 0 \end{pmatrix}. \qquad (1.45)$$

In the presence of an external magnetic field, there hence exist three independent photon propagation modes onto which the quantities (1.42) project. For $\mathbf{k} \nparallel \mathbf{B}$, $P_\parallel$ and $P_\perp$ refer to photon polarization modes parallel and perpendicular to the plane spanned by $\mathbf{k}$ and $\mathbf{B}$. These modes can be continuously related to the corresponding ones in the limit of a vanishing external field. In the case of $\mathbf{k} \parallel \mathbf{B}$, only one externally set direction is left. Now the projectors P_0 and $P_\perp$ correspond to the two photon modes in the limit of a vanishing magnetic field (see [20]).

For the sake of completeness, let us give the result for a vanishing magnetic field. In the limit $B \to 0$, the quantities $N_i \to (1 - \nu^2)$ as well as $\tilde{\phi}_0 \to m^2 + (1 - \nu^2)/4 \; k^2$ simplify and the polarization tensor can be written as

$$\Pi_{\mu\nu}(k|\mathbf{B} = 0) = (g_{\mu\nu}k^2 - k_\mu k_\nu)\frac{\alpha}{2\pi}\int_0^\infty \frac{ds}{s}\int_{-1}^1 \frac{d\nu}{2}(1 - \nu^2)e^{-im^2 s}\left[e^{-is\frac{1-\nu^2}{4}k^2} - 1\right]. \qquad (1.46)$$

This result naturally complies with Eq. (1.30).

A derivation of the photon polarization tensor to the lowest order for the case of arbitrary constant magnetic and electric fields was first obtained in 1971 [21]. A nice presentation of the derivation can be found in [22]. There, use has been made of the fact that an explicit representation of the polarization tensor was obtained in [23] for the case of parallel magnetic and electric fields. Employing the knowledge, that the final Lorentz and gauge invariant solution for an arbitrary field configuration may only depend on Lorentz and gauge invariants, which are made up of the basic building blocks $F^{\mu\nu}$, $^\star F^{\mu\nu}$ and k^μ, a one-to-one correspondence between those invariants and the dynamical variables E, B, $k_\perp^2$ and $k_\parallel^2$ of the special polarization tensor can be established. Furthermore, the tensor structure can as well be related unambiguously to the appropriate one in a general, arbitrary Lorentz frame. The obtained general result then reduces to Eq. (1.39) in the case of vanishing electric fields.

Another convenient representation of the projectors $P_\parallel$ and $P_\perp$ is given by

$$P_\parallel^{\mu\nu} = \frac{v_\parallel^\mu v_\parallel^\nu}{v_\parallel^2} \qquad \text{and} \qquad P_\perp^{\mu\nu} = \frac{v_\perp^\mu v_\perp^\nu}{v_\perp^2}, \qquad (1.47)$$

where

$$v_\parallel^\mu = |\mathbf{k}|\,[\mathbf{e}_k \cdot \mathbf{e}_B, \bar{v}\,\mathbf{e_B}] \qquad \text{and} \qquad v_\perp^\mu = |\mathbf{k}|\,[0\,, \mathbf{e}_k \times \mathbf{e}_B]\,, \qquad (1.48)$$

and the phase velocity is defined by $\bar{v} = \omega/|\mathbf{k}|$. The equivalence with (1.45) can be quickly verified.

Perturbative treatment: The weak field limit

In this section, we give expressions for a Taylor expansion of the photon polarization tensor in terms of $eB/m^2 = B/B_{\mathrm{cr}}$. For any present and near future laser facility, attainable magnetic fields strengths are well below the critical field strength B_{cr}, as will be discussed in more detail

later. Hence, to simplify the computation and obtain analytical insights into the processes related to quantum reflection, an inspection of only the lowest orders seems justified. This expansion corresponds to neglecting higher order couplings of the external magnetic field to the virtual electron-position pairs. Hence, the polarization tensor can be written as

$$
\begin{aligned}
\Pi^{\mu\nu}(k|\mathbf{B}) &= \sum_{n=0}^{\infty} \Pi^{\mu\nu}_{(2n)}(k)\,(eB)^{2n} \\
&= \Pi^{\mu\nu}_{(0)}(k) + \Pi^{\mu\nu}_{(2)}(k)\,(eB)^2 + \mathcal{O}\left[(eB)^4\right],
\end{aligned}
\tag{1.49}
$$

which, as a consequence of Furry's theorem, is in even powers of eB only. The calculation of the expansion coefficients is straightforward and shall not be demonstrated here. The $(n=0)$ - coefficient is already given by Eq. (1.46). The s integration can be performed using proper-time integration techniques, keeping in mind the actual contour of integration ($m^2 \to m^2 - i\epsilon$). The result in its most compact form reads

$$
\Pi_{p,(0)}(k) = \left(k^2\right)^2 \frac{\alpha}{4\pi} \int_0^1 d\nu \left(\frac{\nu^2}{3} - 1\right) \frac{\nu^2}{\phi_0},
\tag{1.50}
$$

with

$$
\phi_0 = m^2 - i\epsilon + \frac{1-\nu^2}{4}\,k^2.
\tag{1.51}
$$

The label p shall henceforth refer to the three different polarization modes $p = 0, \|, \perp$. The second order can be calculated analogously and is given by (see also [24])

$$
\Pi_{p,(2)}(k) = -\frac{\alpha}{12\pi} \int_0^1 d\nu \frac{(1-\nu^2)^2}{\phi_0^2} \left[\left\{\begin{matrix} -\frac{1}{2} \\ \frac{2}{1-\nu^2} \\ 1 \end{matrix}\right\} k_\|^2 + \left(\left\{\begin{matrix} 1 \\ 1 \\ \frac{5-\nu^2}{2(1-\nu^2)} \end{matrix}\right\} - \frac{k^2(1-\nu^2)}{4\phi_0}\right) k_\perp^2\right].
\tag{1.52}
$$

The polarization tensor in this form will constitute the basis of our further studies. It is important to note, that each coefficient still contains the complete information about the entire momentum dependence. This fact is of great importance, since the upcoming considerations require a representation of the polarization tensor in position space by means of Fourier transformations in order to properly deal with the boundary conditions inherent to our problem. Concerning this aspect, the treatment shows some similarity with the theoretical treatment of axion-like-particle searches, where the proper inclusion of boundary conditions requires Fourier transformations to position space as well [25]. On the contrary, many signatures of the quantum electrodynamical nonlinearity of the vacuum can properly be dealt with theoretically by means of "on the light-cone dynamics", i.e. by treating the problem exclusively in momentum space and imposing the vacuum light-cone condition $k^2 = 0$. The most prominent example is the calculation of the vacuum refractive indices in the presence of strong electromagnetic fields, which leads to the effect of vacuum birefringence (see also [26]).

2. Reflection at static magnetic fields

Having derived an expression for the photon polarization tensor in a constant magnetic field, this chapter now deals with the specific phenomenon of quantum reflection. Since reflection manifestly requires the inhomogeneity of the background potential, we have to alter the expression for the photon polarization tensor to include position dependent magnetic fields. We will neglect a possible time dependency of the magnetic field to gain some first insights into the structure of the equations and magnitude of the effects. The subsequent chapter will extend the treatment to time dependent magnetic field backgrounds.

In the first section, we specify the setup and derive an expression for the reflection coefficient R. The second section shows an alternative derivation similar to ordinary, one dimensional quantum mechanics. In the third section, we investigate some specific beam profiles and compute numerical values of R in order to get a notion of the magnitude of the effect.

2.1. The derivation of the reflection coefficient

The effect of quantum reflection describes the reflection of atoms off an attractive potential, which is a direct consequence of the quantum mechanical nature of particles. Atoms must be regarded as matter waves and therefore exhibit wave-like behavior. Partial reflection of light waves at both positive and negative refractive index steps are well known phenomena, which from a quantum mechanical viewpoint must also arise for matter waves. A massive particle with the energy E_{kin}, traveling in a potential $V(\mathrm{x})$ with maximum V_{max}, will therefore experience scattering even if $E_{\mathrm{kin}} > V_{\mathrm{max}}$. Such "above-the-barrier" scattering depends on the spatial variation of the potential. Particles with $E_{\mathrm{kin}} < V_{\mathrm{max}}$ on the other hand will experience reflection at the potential barrier in both the classical and quantum mechanical theory, although the latter allows for classically forbidden processes like "tunneling", depending on the specific shape of the potential. Quantum reflection is currently put to use to very accurately measure the surface properties of condensed-matter specimens, since reflection is very sensitive to the spatial profile of the potential generated by the surface atoms. To this end, polarizable probe atoms hit the surface at a grazing angle of incidence and are reflected both "classically" by the repulsive potential of the surface as well as "quantum mechanically" by the attractive long range potential owing to the Casimir-Polder and Van der Waals force. The discrete surface potential usually produces diffuse reflection, while quantum reflection generates a specular reflection which can then be investigated accordingly [27]. Usually, the separation of these two signals of different origin may provide a big challenge depending upon the specific experiment.

Carrying over the scenario of quantum reflection to the purely optical case, we now aim to investigate how a strong, inhomogeneous magnetic background field, which acts as an effective potential for traversing probe photons, will alter the propagation of these probe photons. In analogy to the case of atomic quantum reflection, we expect a part of these probe photons to be reflected by the inhomogeneity and the rate of the reflection to depend on the spatial shape of background field. However, in contrast to the aforementioned surface experiments, there exists no optical analogon of a repulsive potential and therefore very little background noise can be
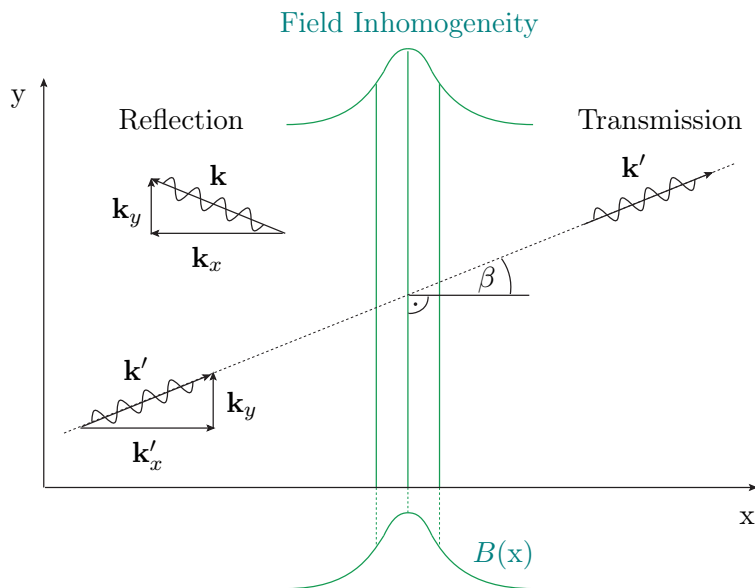
Figure 2.1.: A basic visualization of the effect of quantum reflection from [28]. Roman letters x and y denote the spatial components of the spatio-temporal four-vector x, see appendix A. The static, one dimensional field inhomogeneity of amplitude $B(x)$ is infinitely extended in the transversal directions, but falls off to zero asymptotically for large values of $|x|$. The probe photons with wave vector $\mathbf{k}'$ hit the inhomogeneity under an angle β, which denotes the direction of $\mathbf{k}'$ with respect to the x axis. The reflected photons with wave vector $\mathbf{k}$ are measured by a suitably placed detector spanning the y-z plane.

expected. This should allow for a clear signal-background separation and facilitate the use of very sensitive methods of measurement such as single photon detection techniques.

To investigate the phenomenon of quantum reflection, we consider the following setup (see Fig. 2.1, [28]): Let the spatial inhomogeneity of the magnetic field be centered around the origin x = 0 and directed along the x axis, while the field is homogeneous along the y and z direction. Furthermore, it is assumed that the magnetic field decreases rapidly enough along the x direction for $|x| \to \infty$. Here, Roman letters are used to denote spatial components of the spatio-temporal four-vector x, for more detail see the appendix A. The spatial extension of the inhomogeneous magnetic field is assumed to be of the order of width w. Additionally, the direction of the magnetic field $\mathbf{B} = B(x)\mathbf{e}_B$ is fixed and only its amplitude varies. Then, the magnetic field still defines a global reference direction, according to which the polarization tensor can be decomposed along the lines of the last chapter. Without loss of generality, the incident probe beam is considered to travel within the x-y-plane, having the momentum vector $\mathbf{k}' = k_x' \, \mathbf{e}_x + k_y'\mathbf{e}_y$. The direction of the probe beam is described by the incidence angle $\beta = \arctan(k_y'/k_x')$. The asymptotic decline of the magnetic field implies that the light-cone condition $k^2 = 0$ has to be fulfilled far from the origin.

To simplify Eq. (1.26), we can make use of the fact that the inhomogeneity only affects momentum components along its direction. Therefore, the y and z components of the momentum remain unaffected throughout the whole process, i.e. $k_y' = k_y$ and $k_z' = k_z$. The reflected beam then has the momentum vector $\mathbf{k} = k_x\mathbf{e}_x + k_y\mathbf{e}_y = k_x\mathbf{e}_x + k_y'\mathbf{e}_y$. These assumptions effectively reduce the problem under consideration to a one dimensional problem. If only special photon polarization modes are considered, we can furthermore rid ourselves of the rather complicated tensor structure of Eq. (1.26). These two situations can be identified as follows:

Parallel case: For the case of the direction of the magnetic field inhomogeneity $\mathbf{e}_x$ and the direction of the magnetic field $\mathbf{e}_B$ being orthogonal to each other, i.e. $\mathbf{e}_x \cdot \mathbf{e}_B = 0$, the $\parallel$-component of the photon momentum $k'_\parallel$ remains unaffected by the inhomogeneity. Thus, the projectors

$$P_\parallel^{\mu\nu}(k) = P_\parallel^{\mu\nu}(k') = P_\parallel^{\mu\nu}$$

are the same for k and k'. The same holds especially true for $\mathbf{k}'_\parallel = 0$, i.e. the direction of photon momentum and magnetic field are orthogonal to each other. In view of our two dimensional discussion, the only fixed direction of the magnetic field to fulfill this requirement for arbitrary angles β is given by $\mathbf{e}_B = \mathbf{e}_z$. Note that the energy-component of $k' = (\omega, \mathbf{k}')$ remains naturally unaffected for time-independent magnetic fields. This fact also implies $|\mathbf{k}'| = |\mathbf{k}|$ at asymptotically large distances from the inhomogeneity, since $k^2 = 0$ and no frequency conversion can take place.

Perpendicular case: For the case of the inhomogeneity and the perpendicular momentum component of the photon $k'_\perp$ being orthogonal to each other, i.e. $\mathbf{k}'_\perp \cdot \mathbf{e}_x = 0$, the $\perp$-component of the photon momentum is not affected by the inhomogeneity and analogously

$$P_\perp^{\mu\nu}(k) = P_\perp^{\mu\nu}(k') = P_\perp^{\mu\nu}$$

are the same for k and k'. A closer examination shows that only one direction $\mathbf{e}_B$ of the magnetic field fulfills the requirement for arbitrary angles of incidence β. Since $\mathbf{k}'_\perp = \mathbf{k}' - (\mathbf{k}' \cdot \mathbf{e}_B)\mathbf{e}_B$ and we demand $\mathbf{k}'_\perp \cdot \mathbf{e}_x = 0$, the following condition

$$\mathbf{k}' \cdot \mathbf{e}_x = (\mathbf{k}' \cdot \mathbf{e}_B)(\mathbf{e}_B \cdot \mathbf{e}_x) \tag{2.1}$$

has to hold. Employing the two dimensional treatment

$$\mathbf{k}' = k'_x \mathbf{e}_x + k'_y \mathbf{e}_y = |\mathbf{k}|(\cos\beta\, \mathbf{e}_x + \sin\beta\, \mathbf{e}_y)$$

as well as $\mathbf{B} = B_x \mathbf{e}_x + B_y \mathbf{e}_y + B_z \mathbf{e}_z$ leads us to the requirement of

$$\left(B_y^2 + B_z^2\right) = \tan\beta\, B_x B_y. \tag{2.2}$$

For a fixed direction of $\mathbf{B}$, Eq. (2.2) can only be satisfied for arbitrary angles $\beta < \pi/2$ if $B_y = B_z = 0$, i.e. the magnetic field points into the direction of the inhomogeneity. Other directions of $\mathbf{B}$ fulfill Eq. (2.2) only for certain specific angles β, as can be seen in Fig. 2.2.

The invariance of the projectors can now be used to simplify Eq. (1.26) by simply contracting it with either projector. The resulting scalar equation of motion for the induced photon beam $a_{\text{ind},p}(k)$ is given by (cf Eq. (1.39))

$$k^2 a_{\text{ind},p}(k) = -\int \frac{d^4 k'}{(2\pi)^4} \tilde{\Pi}_p(k, -k'|\mathbf{B}) a_{\text{in},p}(k'), \tag{2.3}$$

where the index $p = \parallel, \perp$ represents exactly those field configurations described in the parallel and perpendicular case respectively. The incoming photon beam $a_{\text{in},p}(k')$ can be chosen freely. Limiting ourselves to the two-dimensional case as described above, Eq. (2.3) reduces to

$$\left(k_x^2 - \tilde{\omega}^2\right) a_{\text{ind},p}(\omega, k_x, k_y) = -\int \frac{dk'_x}{2\pi} \tilde{\Pi}_p(k_x, -k'_x, k_y|\mathbf{B}) a_{\text{in},p}(\omega, k'_x, k_y), \tag{2.4}$$
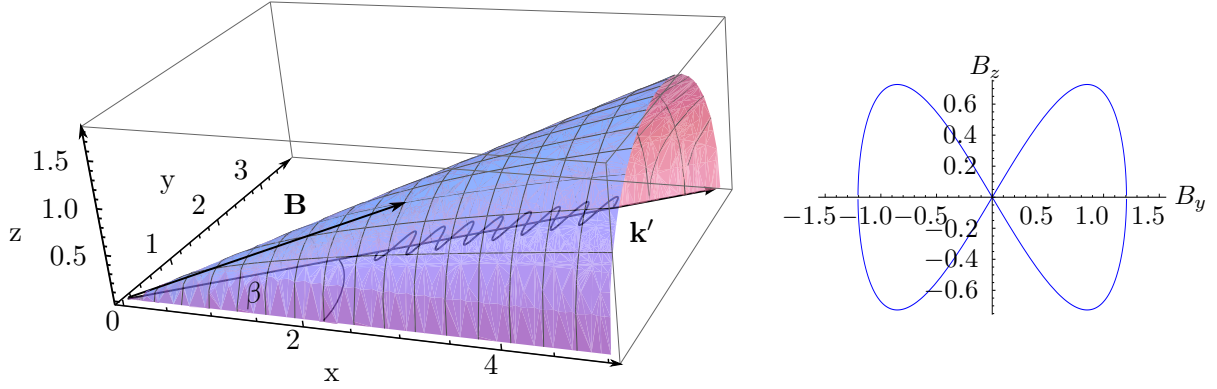
Figure 2.2.: The left figure shows a plot in arbitrary units of the possible values $B_x, B_y, B_z > 0$ of the magnetic field **B** for a given incident photon wave vector **k'** in the perpendicular case. The angle was chosen as $\beta = \pi/5$. The magnetic field has to satisfy Eq. (2.2), which defines an area of possible magnetic field directions. Note, however, that the absolute value of the magnetic field is not restricted. The figure on the right side shows a plot of all possible values of the magnetic field components B_y and B_z for a fixed value $B_x = 2$, again choosing $\beta = \pi/5$.

where the reduced frequency $\tilde{\omega}^2 = \omega^2 - k_y^2$ has been introduced. To increase the clarity of notation, references to the conserved quantities ω and k_y as well as the magnetic field **B** will be mostly omitted in the future. We can now solve the remaining equation with the help of the corresponding Green's function $G(x, x')$ for the equation

$$\left(-\partial_x^2 - \tilde{\omega}^2 - i\epsilon\right) G(x, x') = \delta(x - x'), \tag{2.5}$$

or in momentum space

$$\left(k_x^2 - \tilde{\omega}^2 - i\epsilon\right) G(k_x, k_x') = 2\pi\delta(k_x + k_x'). \tag{2.6}$$

Hence,

$$\begin{aligned}
G(x, x') &= \int \frac{dk_x}{2\pi} \int \frac{dk_x'}{2\pi} e^{ik_x x} \frac{2\pi\delta(k_x + k_x')}{(k_x - \tilde{\omega} - i\epsilon)(k_x + \tilde{\omega} + i\epsilon)} e^{ik_x' x'} \\
&= \int \frac{dk_x}{2\pi} \frac{e^{ik_x(x - x')}}{(k_x - \tilde{\omega} - i\epsilon)(k_x + \tilde{\omega} + i\epsilon)},
\end{aligned} \tag{2.7}$$

and the integral can be solved by closing the contour in the upper plane for $x - x' > 0$ and in the lower plane for $x - x' < 0$. Consequently,

$$G(x, x') = \frac{i}{2\tilde{\omega}} \begin{cases} e^{i\tilde{\omega}(x - x')} & \text{for} \quad x - x' > 0, \\ e^{-i\tilde{\omega}(x - x')} & \text{for} \quad x - x' < 0. \end{cases} \tag{2.8}$$

The solution of Eq. (2.4) in position space is given by

$$a_{\text{ind},p}(x) = -\int dx' \, G(x, x') \, j_p(x') = -\int dx' \int dx'' \, G(x, x') \, \tilde{\Pi}_p(x', x'') \, a_{\text{in},p}(x''), \tag{2.9}$$

where the symmetrized polarization tensor in position space,

$$\tilde{\Pi}_p(x, x') = \frac{1}{2} \left[\Pi_p(x, x') + \Pi_p(x', x) \right], \tag{2.10}$$

17

has been introduced. Since the background field is time independent, it is sufficient to deal exclusively with plane waves of fixed frequency ω and corresponding amplitude $A_{\text{in},p}$. We now restrict ourselves to incoming photons that are purely right-moving, i.e.

$$a_{\text{in},p}(\text{x}'') = A_{\text{in},p}(\tilde{\omega})e^{ik'_x \text{x}''} = A_{\text{in},p}(\tilde{\omega})e^{i\tilde{\omega}\text{x}''}, \tag{2.11}$$

where we have made use of the light-cone condition $k^2 = 0$, which has to hold far from the inhomogeneity. Furthermore, we assume the probe photons to be emitted from the source at large negative distances $-L$, where the magnetic field vanishes. As can be read off from the Green's function (2.8), the induced beam will consist of parts which are right-moving, i.e. transmitted, and left-moving, i.e. reflected. At asymptotic distances, these will be the parts proportional to $e^{i\tilde{\omega}\text{x}}$ and $e^{-i\tilde{\omega}\text{x}}$ respectively.

The reflected photons are assumed to be registered by a suitably placed detector spanning a part of the y-z plane, which is located at a large negative distance $\text{x}'' < -L$ from the inhomogeneity. With regard to an actual experimental realization we have to bear in mind that an actual detector must be of the same length scale as the inhomogeneity w. More precisely, for an incident beam with angle β, the detector size in the y direction must be of the order of $2w \tan \beta$. Here, the inherent signal-background separation of the setup becomes obvious and thus the particular suitability for experiments concerning QED effects, where only very small effects compared to the classical behavior are expected. The separation is maintained, if the incidence angle remains sufficiently small, i.e. $\beta \lesssim \pi/2$.

Implementing the above statements, the amplitude for the reflected photons is given by

$$\begin{aligned} a_{\text{ref},p}(\text{x} < -L) &= -\frac{i}{2\tilde{\omega}} \int_{-L}^{\infty} d\text{x}' \, j_p(\text{x}') e^{-i\tilde{\omega}(\text{x}-\text{x}')} \\ &= -\frac{i}{2\tilde{\omega}} \int_{-L}^{\infty} d\text{x}' \int_{-\infty}^{\infty} d\text{x}'' \, \tilde{\Pi}_p(\text{x}',\text{x}'') \, a_{\text{in},p}(\text{x}'') e^{-i\tilde{\omega}(\text{x}-\text{x}')}, \end{aligned} \tag{2.12}$$

where we have chosen the lower line of the Green's function (2.8). Specifying the incoming beam to (2.11), the solution can be written as

$$a_{\text{ref},p}(\text{x} < -L) = -\frac{i}{2\tilde{\omega}} A_{\text{in},p}(\tilde{\omega}) e^{-i\tilde{\omega}\text{x}} \int_{-L}^{\infty} d\text{x}' \int_{-\infty}^{\infty} d\text{x}'' e^{i\tilde{\omega}\text{x}'} \tilde{\Pi}_p(\text{x}',\text{x}'') e^{i\tilde{\omega}\text{x}''} =: A_{\text{ref},p}(\tilde{\omega};L) e^{-i\tilde{\omega}\text{x}}. \tag{2.13}$$

We define the reflection coefficient R in analogy to the static, quantum mechanical case as the squared ratio of the photon amplitudes of the reflected and incoming beam at asymptotic distances, i.e.

$$R_p = \lim_{L \to \infty} \left| \frac{A_{\text{ref},p}(\tilde{\omega};L)}{A_{\text{in},p}(\tilde{\omega})} \right|^2. \tag{2.14}$$

In our case, using the inverse Fourier transformation, we end up with the elegant and concise expression

$$R_p = \left| \frac{\tilde{\Pi}_p(-\tilde{\omega}, -\tilde{\omega})}{2\tilde{\omega}} \right|^2. \tag{2.15}$$

The label p should remind us of the fact that the reflection coefficient will in general differ for the different polarization modes and scenarios under consideration. Thus, the general formula for the reflection coefficient is given by the photon polarization tensor in momentum space evaluated on the light-cone, i.e. $k_x = -\tilde{\omega}$ and $k'_x = -\tilde{\omega}$ and thus accounting for the transferred momentum of $2\tilde{\omega}$ between reflected and incoming beam.

Transformation of the polarization tensor

The general strategy to include a one dimensional spatial dependence, which we choose w.l.o.g. to be along the x direction, into (1.49) is illustrated by the following scheme,

$$\tilde{\Pi}^{\mu\nu}(k_x')\,(2\pi)\,\delta(k_x + k_x') \xrightarrow{\text{F.T.}} \tilde{\Pi}^{\mu\nu}(\mathrm{x} - \mathrm{x}') \xrightarrow{B \to B(\mathrm{x})} \tilde{\Pi}^{\mu\nu}(\mathrm{x}, \mathrm{x}') \xrightarrow{\text{F.T.}^{-1}} \tilde{\Pi}^{\mu\nu}(k_x, k_x'). \quad (2.16)$$

The polarization tensor for constant magnetic fields is momentum conserving. After a first partial Fourier transformation (A.12) into position space it naturally depends only on the difference $\mathrm{x} - \mathrm{x}'$ due to the translational invariance of the considered problem. Now we substitute the constant magnetic field $\mathbf{B}$ by a spatially inhomogeneous field $\mathbf{B}(\mathrm{x})$ and therefore translational invariance is broken. Performing the inverse Fourier transformation, we end up with a polarization tensor of the kind required in (1.22), which mediates between two distinct momenta k_x and k_x'. The following argument motivates the simple substitution of $B \to B(\mathrm{x})$. First we note that in position space the polarization tensor probes distances of about the Compton wavelength $\lambda_c = 1/m$ of the virtual particles. In our context, $m \approx 511\,\mathrm{keV}$ corresponds to the electron mass and therefore $\lambda_c \approx 1.96 \cdot 10^{-6}\mathrm{eV}^{-1} \approx 3.9 \cdot 10^{-13}\mathrm{m}$. The magnetic field can be assumed to be locally constant if the typical scale of variation w of the inhomogeneity is much larger than the virtual particles' Compton wavelength. For strong laser fields in the optical region, $w = O(1\,\mathrm{eV})$ and therefore this approximation is well justified.

Let us now implement the steps (2.16) outlined above. A partial Fourier transformation to position space of (1.49) results in

$$\Pi^{\mu\nu}(\mathrm{x} - \mathrm{x}') = \sum_{n=0}^{\infty} (eB)^{2n} \int \frac{dk_x}{2\pi} \Pi^{\mu\nu}_{(2n)}(-k_x) e^{ik_x(\mathrm{x}-\mathrm{x}')}. \quad (2.17)$$

Substitution $B \to B(\mathrm{x})$ and subsequent transformation back to momentum space yields

$$\Pi^{\mu\nu}(k_x, k_x') = \sum_{n=0}^{\infty} \Pi^{\mu\nu}_{(2n)}(k_x') \int dx \; e^{-i(k_x + k_x')\mathrm{x}} (eB(x))^{2n}. \quad (2.18)$$

Finally, we need to symmetrize in order to arrive at

$$\tilde{\Pi}^{\mu\nu}(k_x, k_x') = \frac{1}{2} \sum_{n=0}^{\infty} \left[\Pi^{\mu\nu}_{(2n)}(k_x') + \Pi^{\mu\nu}_{(2n)}(k_x) \right] \int dx \; e^{-i(k_x + k_x')\mathrm{x}} (eB(\mathrm{x}))^{2n}. \quad (2.19)$$

Up to this point, no approximation (other than the one-loop-approximation) has been employed. It is worth mentioning that the entire complication of the calculation of the reflection coefficient is shifted to the evaluation of the photon polarization tensor in momentum space. There are certain field inhomogeneities for which the procedure sketched in (2.16) can be performed explicitly. The one-loop polarization tensor (1.40) carries its entire field strength dependence in the phase and the Fourier transformation can, for instance, be expressed in terms of Gaussian integrals for an inhomogeneity of the special form $B(x) = 1/(1 + \mathrm{x}^2)$. However, a perturbative treatment as will be performed in this work offers the possibility to study the effect of quantum reflection for a wide range of different field profiles due to the simplicity of the resulting formulae, as will be seen later.

We now have to evaluate the symmetrized polarization tensor (2.19) on the light-cone, i.e.

$$\tilde{\Pi}^{\mu\nu}(-\tilde{\omega}, -\tilde{\omega}) = \frac{1}{2} \sum_{n=0}^{\infty} \left[\Pi^{\mu\nu}_{(2n)}(k_x' = -\tilde{\omega}) + \Pi^{\mu\nu}_{(2n)}(k_x = -\tilde{\omega}) \right] \int dx \; e^{i2\tilde{\omega}\mathrm{x}} (eB(\mathrm{x}))^{2n}, \quad (2.20)$$

for the lowest orders. As can be seen from Eq. (1.50), the polarization tensor vanishes on the light-cone for the lowest order $n = 0$. To evaluate the second order, $n = 1$, we rewrite (1.52). Setting $k^2 = 0$, the second order simplifies to

$$\Pi_{p,(2)}(k) = -\frac{\alpha}{12\pi} \int_0^1 d\nu \frac{(1-\nu^2)^2}{m^4} \left[\left\{ \begin{matrix} -\frac{2}{1-\nu^2} \\ 1 \end{matrix} \right\} k_\parallel^2 + \left\{ \begin{matrix} 1 \\ \frac{5-\nu^2}{2(1-\nu^2)} \end{matrix} \right\} k_\perp^2 \right], \qquad (2.21)$$

where we only concentrate on the relevant polarization modes $p = \parallel, \perp$. Note that no reflection takes place for the zero-mode, since the polarization tensor is proportional to k^2 at all orders (cf. Eq. (1.40)). Now the angle $\theta = \sphericalangle(\mathbf{e}_B, \mathbf{k})$ is introduced, which puts the magnetic field direction and the direction of photon propagation in relation. Then, $k_\parallel^2 = \mathbf{k}^2 \cos^2\theta - \omega^2$, $k_\perp^2 = \mathbf{k}^2 \sin^2\theta$ and evaluation of the ν-integral leads to

$$\Pi_{p,2}(k^2 = 0) = -\frac{\alpha}{45m^4\pi} \mathbf{k}^2 \sin^2\theta \left\{ \begin{matrix} 7 \\ 4 \end{matrix} \right\} = -\frac{\alpha}{45m^4\pi} \omega^2 \sin^2\theta \left\{ \begin{matrix} 7 \\ 4 \end{matrix} \right\}. \qquad (2.22)$$

Inserting this result into Eq. (2.20) and (2.15), the final result for the reflection coefficient to lowest order is given by

$$R_p = \left| \frac{c_p}{\pi} \tilde{\omega} \int d\mathbf{x}\, e^{i2\tilde{\omega}\mathbf{x}} \left(\frac{e\mathbf{B}(\mathbf{x})}{m^2} \right)^2 \right|^2 + \mathcal{O}\left((\frac{eB}{m^2})^6 \right), \qquad (2.23)$$

with

$$\left\{ \begin{matrix} c_\parallel \\ c_\perp \end{matrix} \right\} = \frac{\alpha}{180} \left[\sin^2\theta + \sin^2\theta' \right] \left(\frac{\omega}{\tilde{\omega}} \right)^2 \left\{ \begin{matrix} 7 \\ 4 \end{matrix} \right\}. \qquad (2.24)$$

The angles θ' and θ refer to the angles between the magnetic field and the incoming and reflected beam respectively. They can be related to each other in both the $\parallel$ and $\perp$ setting by means of momentum conservation. In the former case, it turns out that both angles coincide, i.e. $\theta = \theta'$, since the magnetic field may only have y and z components and hence

$$\mathbf{k} \cdot \mathbf{B} = k_y B_y = |\mathbf{k}||\mathbf{B}|\cos\theta = k_y' B_y = |\mathbf{k}'||\mathbf{B}|\cos\theta' = |\mathbf{k}||\mathbf{B}|\cos\theta'. \qquad (2.25)$$

In contrast, the perpendicular case $\mathbf{k}_\perp \cdot \mathbf{e}_x = 0$ differs and the angles can be expressed by the formulae (recall $k_x' = -k_x$)

$$\cos\theta' = \frac{-B_x k_x + B_y k_y}{|\mathbf{B}||\mathbf{k}|} \quad \text{and} \quad \cos\theta = \frac{B_x k_x + B_y k_y}{|\mathbf{B}||\mathbf{k}|}. \qquad (2.26)$$

Remarkably, the magnetic field directions are not fixed in both the parallel setting as well as the perpendicular setting. For the former setting there exists a configuration where the angles θ and θ' are independent of the incidence angle β. This is given if the magnetic field points into the z direction.

The perpendicular case permits no such setups and the angles θ and θ' are always dependent upon the direction of incidence of the probe photons. For the special setting of $\mathbf{e}_B = \mathbf{e}_x$, θ and θ' in the perpendicular case can be easily related to the angle β, in fact $\theta = \beta$ and $\theta' = \pi - \theta = \pi - \beta$. Therefore the terms $\sin\theta = \sin\theta'$ coincide and we can write

$$c_\perp = \frac{2\alpha}{45} \sin^2\beta \left(\frac{\omega}{\tilde{\omega}} \right)^2. \qquad (2.27)$$

From the constraint (2.2) we observe that for $\beta \to 0$ the only non-trivial case (i.e. $\mathbf{B} \neq 0$) fulfilling the requirement of the perpendicular case is exactly given for $\mathbf{e}_B = \mathbf{e}_x$.

Equation (2.23) can now be evaluated for different magnetic field inhomogeneities $\mathbf{B}(\mathbf{x})$. It is particularly simple to calculate the reflection coefficient in our case as it only requires a Fourier transformation of the squared magnetic field. However, the first contributing term to R_p is already of the order of $(B/B_{\mathrm{cr}})^4$ and thus expected to be rather small. A major task will consist of finding suitable and experimentally feasible beam profiles, which maximize the effect of reflection.

The derivation of R as performed in this chapter is not valid for arbitrary incidence angles β, but must be restricted to angles $\beta < \pi/2$. First of all, the case $\beta = \pi/2$ obviously does not make sense in our treatment. However, one even has to be careful for angles $\beta \to \pi/2$. The physical intuitive reason can be given by the fact that, for such angles, the incident photon beam is exposed to the inhomogeneity over a large distance. The artificial splitting, as it was performed in our derivation, of the photon vector field $a(k)$ into an independent incoming field $a_{\mathrm{in}}(k')$ and an induced field $a_{\mathrm{ind}}(k)$ cannot be performed anymore (cf. the step from Eq. (1.22) to (1.26)). Such a splitting corresponds to neglecting the field's own back reaction. As a result, the reflection coefficient as derived in Eq. (2.15) is not valid anymore for $\tilde{\omega} \to 0$ and will eventually diverge for $\tilde{\omega} = 0$. The quantum mechanical derivation in the next section will offer a more quantitative treatment of this limitation.

2.2. Quantum mechanical analogy

There exists an alternative way to derive the formula for the reflection coefficient (2.23) which employs the similarity to one dimensional scattering problems in ordinary quantum mechanics. A first hint that such a derivation might be possible is given by the similarity of Eq. (2.23) with scattering formulae derived within the Born approximation. As a first step, we derive a Schrödinger-like equation of motion for photons in the presence of a weak magnetic field, specializing to "on the light-cone" dynamics. We perform a Fourier transformation of this equation into position space and solve the resulting one dimensional scattering problem in the transfer matrix formalism. The specialization to the light-cone is permissible since we have seen in the last section that basically the entire dynamics of the problem are described by the evaluation of the polarization tensor for $k^2 = 0$. Note, however, that if we did not have any knowledge about the true solution, there would be no striking reason to make such an assumption beforehand. Still, it seems quite enlightening to show this alternative derivation nonetheless.

2.2.1. Equation of motion

In order to derive a Schrödinger-type equation of a propagating photon, we start with Eq. (2.3), where we do not distinguish between incoming and induced photon. We now impose momentum conservation $(2\pi)^4 \delta(k + k')$ on the photon polarization tensor and evaluate it on the light cone by employing the representation (2.22). Only keeping terms to the lowest non-trivial order $(eB/m^2)^2$, we arrive at the equation of motion in momentum space,

$$\left[k^2 - 2\tilde{\omega}^2 \frac{c_p}{\pi} \left(\frac{e\mathbf{B}}{m^2} \right)^2 \right] a_p(k) = 0, \tag{2.28}$$

and, following the above mentioned reasoning, a Fourier transformation to position space results in

$$\left[-\frac{d^2}{dx^2} - \tilde{\omega}^2 \left(1 + 2\frac{c_p}{\pi} \left(\frac{e\mathbf{B}}{m^2} \right)^2 \right) \right] a_p(x, k_y, \omega) = 0. \tag{2.29}$$

We now perform the replacement to an inhomogeneous magnetic field $\mathbf{B} \to \mathbf{B}(x)$. Then Equation (2.29) can be interpreted as a Schrödinger equation for the photon wave function $a_p(x, k_y, \omega)$ in the spatially localized potential

$$V(x) = -2\frac{c_p}{\pi}\tilde{\omega}^2 \left(\frac{e\mathbf{B}(x)}{m^2} \right)^2 \tag{2.30}$$

with the corresponding energy eigenvalue $\mathcal{E} = \tilde{\omega}^2$. Note that the ambiguity of $\tilde{\omega}^2 = k_x^2$, which arises when writing down the polarization tensor (2.22) and transforming Eq. (2.28) into position space, does not affect the result Eq. (2.29) due to our weak field approximation.

2.2.2. The quantum mechanical reflection coefficient for a smooth potential
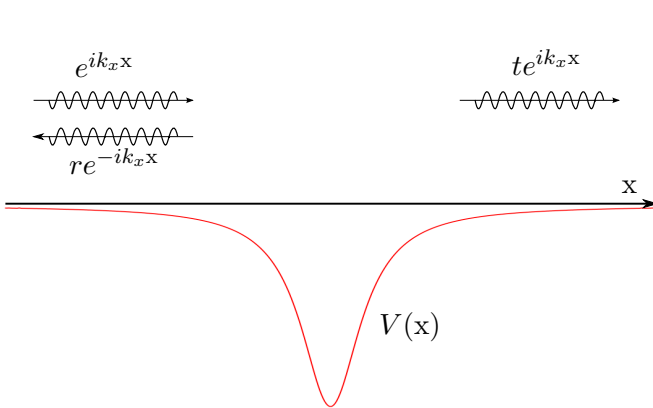
Figure 2.3.: One-dimensional above-barrier scattering in ordinary quantum mechanics for a smooth, spatially localized potential $V(x)$. The incident, normalized plane wave is given by $\exp(ik_x x)$ for asymptotic distances $x \to -\infty$. The reflected part of the wave is asymptotically given by $r \exp(-ik_x x)$, where $r = r(x \to -\infty)$ denotes the reflection amplitude. The transmission amplitude is given by $t = t(x \to \infty)$.
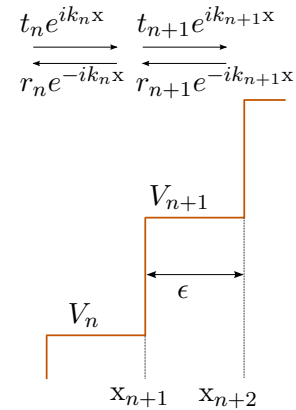
Figure 2.4.: Discretization of the smooth potential $V(x)$ into segments of even length ϵ with a constant value of the potential $V_n = V(x_n)$. The problem reduces to the case of determining the reflection and transition amplitudes r_n and t_n for a step potential.

We derive a formula for the calculation of the quantum mechanical reflection coefficient for above-barrier scattering in one dimension. The strategy is to first substitute the smooth, but otherwise arbitrary potential $V(x)$ by a piecewise continuous potential V_n for $x \in (n\epsilon, (n+1)\epsilon)$ and compute the reflection for the potential step $V_n \to V_{n+1}$ up to the first order in ϵ (cf. Figs. 2.3 and 2.4). At the end we retrieve our original problem by considering the limit $\epsilon \to 0$. This method is completely analogous to the transfer matrix approach known from optics. Using the plane wave solutions of the Schrödinger equation in a constant potential and furthermore employing the

matching conditions concerning the field and its first derivative, the following equations have to hold,

$$
t_n e^{ik_n \mathrm{x}_{n+1}} + r_n e^{-ik_n \mathrm{x}_{n+1}} = t_{n+1} e^{ik_{n+1} \mathrm{x}_{n+1}} + r_{n+1} e^{-ik_{n+1} \mathrm{x}_{n+1}},
$$
$$
k_n(t_n e^{ik_n \mathrm{x}_{n+1}} + r_n e^{-ik_n \mathrm{x}_{n+1}}) = k_{n+1}(t_{n+1} e^{ik_{n+1} \mathrm{x}_{n+1}} + r_{n+1} e^{-ik_{n+1} \mathrm{x}_{n+1}}).
$$
(2.31)

The coefficients t_n and r_n represent the amplitude for transmission and reflection respectively at the corresponding n-th potential step and $k_n = \sqrt{\mathcal{E} - V_n}$ is the constant wave vector for the propagation from $\mathrm{x}_n = n\epsilon$ to $\mathrm{x}_{n+1} = (n+1)\epsilon$. Equation (2.31) can be cast into the following form,

$$
\begin{pmatrix} t_n \\ r_n \end{pmatrix} = \begin{pmatrix} \frac{1}{2}(1 + \frac{k_{n+1}}{k_n})e^{i(k_{n+1} - k_n)\mathrm{x}_{n+1}} & \frac{1}{2}(1 - \frac{k_{n+1}}{k_n})e^{-i(k_{n+1} + k_n)\mathrm{x}_{n+1}} \\ \frac{1}{2}(1 - \frac{k_{n+1}}{k_n})e^{i(k_{n+1} + k_n)\mathrm{x}_{n+1}} & \frac{1}{2}(1 + \frac{k_{n+1}}{k_n})e^{-i(k_{n+1} - k_n)\mathrm{x}_{n+1}} \end{pmatrix} \begin{pmatrix} t_{n+1} \\ r_{n+1} \end{pmatrix},
$$
(2.32)

and taking the limit $\epsilon \to 0$ we get

$$
\begin{pmatrix} t(\mathrm{x}) \\ r(\mathrm{x}) \end{pmatrix} \approx \begin{pmatrix} 1 + (i\mathrm{x}k' + \frac{1}{2k}k')\epsilon & -e^{-i2k\mathrm{x}}\frac{1}{2k}k'\epsilon \\ -e^{i2k\mathrm{x}}\frac{1}{2k}k'\epsilon & 1 + (-i\mathrm{x}k' + \frac{1}{2k}k')\epsilon \end{pmatrix} \begin{pmatrix} t(\mathrm{x}+\epsilon) \\ r(\mathrm{x}+\epsilon) \end{pmatrix},
$$
(2.33)

where $k = k(\mathrm{x}) = \sqrt{\mathcal{E} - V(\mathrm{x})}$ and $k' = (d/dx)k(\mathrm{x})$. Here, the limitation to smooth potentials ensures that k' is finite. Due to the special structure of the matrix in Eq. (2.33), the relation

$$
\begin{pmatrix} 1 + a\epsilon & b\epsilon \\ c\epsilon & 1 + d\epsilon \end{pmatrix} \begin{pmatrix} 1 + a'\epsilon & b'\epsilon \\ c'\epsilon & 1 + d'\epsilon \end{pmatrix} = \begin{pmatrix} 1 + (a + a')\epsilon & (b + b')\epsilon \\ (c + c')\epsilon & 1 + (d + d')\epsilon \end{pmatrix}
$$
(2.34)

holds and thus we arrive at

$$
\begin{pmatrix} t(\mathrm{x}) \\ r(\mathrm{x}) \end{pmatrix} = \begin{pmatrix} 1 + \int_{\mathrm{x}}^{\mathrm{y}} d\tilde{\mathrm{x}}(\frac{k'}{2k} + i\tilde{\mathrm{x}}k') & -\int_{\mathrm{x}}^{\mathrm{y}} d\tilde{\mathrm{x}}\, e^{-i2k\tilde{\mathrm{x}}}\frac{k'}{2k} \\ -\int_{\mathrm{x}}^{\mathrm{y}} d\tilde{\mathrm{x}}\, e^{i2k\tilde{\mathrm{x}}}\frac{k'}{2k} & 1 + \int_{\mathrm{x}}^{\mathrm{y}} d\tilde{\mathrm{x}}(\frac{k'}{2k} - i\tilde{\mathrm{x}}k') \end{pmatrix} \begin{pmatrix} t(\mathrm{y}) \\ r(\mathrm{y}) \end{pmatrix}.
$$
(2.35)

Now we make use of the requirement that the potential has to vanish quickly enough at $|\mathrm{x}| \to \infty$. Then we can assume that there will not be any reflected part to the right of the inhomogeneity, i.e. $r(\mathrm{y} \to \infty) = 0$. The amplitude for the reflection then reduces to

$$
r(\mathrm{x}) = -\left[\int_{\mathrm{x}}^{\infty} d\tilde{\mathrm{x}}\, e^{i2k\tilde{\mathrm{x}}}\frac{k'}{2k}\right] t(\mathrm{y} \to \infty).
$$
(2.36)

The first line of Eq. (2.35) reduces to

$$
t(\mathrm{x} \to -\infty) = \left[1 + \int_{-\infty}^{\infty} d\tilde{\mathrm{x}}(\frac{k'}{2k} + i\tilde{\mathrm{x}}k')\right] t(\mathrm{y} \to \infty).
$$
(2.37)

For a normalized incident wave, i.e. $t(\mathrm{x} \to -\infty) = 1$, we can eliminate $t(\mathrm{y} \to \infty)$ from Eq. (2.36) to arrive at

$$
r(\mathrm{x} \to -\infty) = -\left[\int_{-\infty}^{\infty} d\tilde{\mathrm{x}}\, e^{i2k\tilde{\mathrm{x}}}\frac{k'}{2k}\right]\left[1 + \int_{-\infty}^{\infty} d\tilde{\mathrm{x}}(\frac{k'}{2k} + i\tilde{\mathrm{x}}k')\right]^{-1}.
$$
(2.38)

The reflection coefficient $R = |r(\mathrm{x} \to -\infty)|^2$ relates the intensities and is therefore given by

$$
R = \left|\frac{\int_{-\infty}^{\infty} d\mathrm{x}\, e^{2ik\mathrm{x}}\frac{k'}{2k}}{1 + \int_{-\infty}^{\infty} d\mathrm{x}\left(\frac{k'}{2k} + i\mathrm{x}k'\right)}\right|^2.
$$
(2.39)

The transmission coefficient T reads

$$
T = \left|\frac{1}{1 + \int_{-\infty}^{\infty} d\mathrm{x}\left(\frac{k'}{2k} + i\mathrm{x}k'\right)}\right|^2.
$$
(2.40)

Weak field approximation

The quantum mechanical reflection coefficient can now be brought in direct agreement with Eq. (2.23). First, we note that in the case of small magnetic fields

$$k(\mathrm{x}) = \tilde{\omega}\sqrt{1 + 2\frac{c_p}{\pi}\left(\frac{e\mathbf{B}(\mathrm{x})}{m^2}\right)^2} = \tilde{\omega}\left(1 + \frac{c_p}{\pi}\left(\frac{e\mathbf{B}(\mathrm{x})}{m^2}\right)^2 + \mathcal{O}\left((\frac{eB}{m^2})^4\right)\right) \qquad (2.41)$$

and

$$k' = 2\tilde{\omega}\frac{c_p}{\pi}\frac{e^2}{m^4}\mathbf{B}(\mathrm{x})\cdot\mathbf{B}'(\mathrm{x}) + \mathcal{O}\left((\frac{eB}{m^2})^4\right) \qquad , \qquad \frac{k'}{2k} = \tilde{\omega}\frac{c_p}{\pi}\frac{e^2}{m^4}\mathbf{B}(\mathrm{x})\cdot\mathbf{B}'(\mathrm{x}) + \mathcal{O}\left((\frac{eB}{m^2})^4\right). \quad (2.42)$$

Plugging these formulae into the reflection coefficient R and performing the same weak field expansion, i.e. keeping only terms up to $(eB/m^2)^2$, the denominator simplifies to 1 and we arrive at

$$\begin{aligned} R &= \left|\int_{-\infty}^{\infty} d\mathrm{x}\, e^{i2\tilde{\omega}\mathrm{x}}\tilde{\omega}\frac{c_p}{\pi}\frac{e^2}{m^4}\mathbf{B}(\mathrm{x})\cdot\mathbf{B}'(\mathrm{x})\right|^2 + \mathcal{O}\left((\frac{eB}{m^2})^6\right) \\ &= \left|\frac{c_p}{\pi}\tilde{\omega}\int d\mathrm{x}\, e^{i2\tilde{\omega}\mathrm{x}}\left(\frac{e\mathbf{B}(\mathrm{x})}{m^2}\right)^2\right|^2 + \mathcal{O}\left((\frac{eB}{m^2})^6\right), \end{aligned} \qquad (2.43)$$

where a partial integration has been performed and the boundary term vanishes due to the requirement $\mathbf{B}(|\mathrm{x}| \to \infty) = 0$. The derivation is only valid for smooth, localized beam profiles which, however, is completely compatible with our requirement that the inhomogeneity may only vary on length scales much larger than the Compton wavelength. Furthermore, the weak field expansions (2.41), (2.42) and the subsequent simplification of the Eq. (2.39) can only be performed for

$$2\frac{c_p}{\pi}\left(\frac{e\mathbf{B}}{m^2}\right)^2 \ll 1 \qquad \Longleftrightarrow \qquad R_p \ll 1. \qquad (2.44)$$

This condition, however, is violated for incidence angles $\beta \to \pi/2$, since $\tilde{\omega} \to 0$ and consequently $c_p \to \infty$. Equation (2.44) may thus be regarded as a subsequent quantification of the validity range of R as a function of the angle β and therefore also serves as a measure of when the splitting, as it was performed in Eq. (1.26), of the photon vector field into incoming and induced beam fails. It becomes apparent that such a splitting corresponds to a loop expansion as well and since we are only interested in lowest order effects, we have to neglect back reactions of the photon field onto itself.

2.3. Evaluation of R for different beam profiles

In this section, we take a closer look at some special beam profiles in order to obtain first magnitude estimates for the effect of quantum reflection and secondly to enhance the effect by a suitable choice of magnetic beam profiles.

2.3.1. Experimental setup

The experimental setup is given by an all optics pump-probe setup, whose basics were already described by Fig. 2.1. The lowest order of the reflection coefficient scales with $(B/B_{\mathrm{cr}})^4$, which

leads us to turn our attention to high intensity laser systems. These are at present the only systems capable of achieving field strengths which are sufficiently large for our purposes. Thus, we consider the background magnetic field $\mathbf{B}(x) = B(x)\mathbf{e}_B$ to be generated in the focal spot of a pump-laser with wavelength λ_{pump}. A purely magnetic field in the focal spot could be generated at least to a good approximation by superimposing two counter-propagating laser beams [29]. The probe laser with wavelength λ_{probe} hits the focal spot at an angle β and the amount of reflected photons is measured by a suitably placed detector.

Laser beams are usually characterized by the beam parameters λ, $\mathcal{E}$ and τ. The laser wavelength λ corresponds to the photon energy ω via $\omega = 2\pi/\lambda$. $\mathcal{E}$ denotes the pulse energy of the laser pulse and τ its duration. The maximum field strength in the focus-cross section area $\sigma = \pi(d/2)^2$ is related to the intensity $I = \mathcal{E}/(\tau\sigma)$ via $B = \sqrt{2I}$. Laser beams are usually well described by Gaussian beams and therefore the effective focus cross section area σ is assumed to contain 86% of the beam energy. The waist spot size $w_0 = d/2$ characterizes the distance from the focal spot where the intensity dropped to $1/e^2$ of its maximum value. Since we are only interested in obtaining first estimates, we will also apply this rule for shapes of the inhomogeneity which differ from the Gaussian transverse profile and will be examined later. Laser beams cannot be focused down to an arbitrary small focal spot, but are restricted by the diffraction limit. The minimal beam diameter is given by $d = 2f^{\#}\lambda$, where $f^{\#}$ denotes the so called f-number which can be as low as $f^{\#} = 1$, see [30] and [25]. Hence, for given laser parameters, the maximum field strength B can be approximated according to

$$B \approx \sqrt{0.86\frac{2}{\pi}\frac{\mathcal{E}}{\tau\, w_0^2}} \approx \sqrt{0.86\frac{2}{\pi}\frac{\mathcal{E}}{\tau\, f^{\#}\lambda^2}}. \tag{2.45}$$

In all future discussions we will assume $f^{\#} = 1$. The number of photons N_{in} contained in the laser pulse can be approximated by

$$N_{\text{in}} \approx \frac{\mathcal{E}}{\omega}. \tag{2.46}$$

The number of reflected photons per shot can be calculated according to

$$N_{p,\text{ref}} = R_p f_{\text{int}} N_{\text{in}}. \tag{2.47}$$

We introduced a factor $f_{\text{int}} = \text{Min}\left\{1, \frac{\tau_{\text{pump}}}{\tau_{\text{probe}}}\right\}$ being a first estimate of the fraction of incident probe photons interacting with the magnetic background field for the case of $\tau_{\text{pump}} < \tau_{\text{probe}}$.

To calculate explicit numerical values, we adopt the design parameters of the two high-intensity laser systems POLARIS and JETI200 currently under development and soon-to-be available in Jena [31]. The list below gives an overview of the important parameters:

Design Parameters POLARIS @ Jena

$$\lambda = w_0 = 1035\,\text{nm} \qquad\qquad\qquad = 5.25\,\text{eV}^{-1} \tag{2.48}$$

$$B = 1.46 \cdot 10^6\,\text{T} \qquad\qquad\qquad = 2.86 \cdot 10^8\,\text{eV}^2 \tag{2.49}$$

$$\omega = 1.821\,\text{PHz} \qquad\qquad\qquad = 1.20\,\text{eV} \tag{2.50}$$

$$\mathcal{E} = 150\,\text{J} \qquad\qquad\qquad = 9.36 \cdot 10^{20}\,\text{eV} \tag{2.51}$$

$$N_{\text{in}} = 7.8 \cdot 10^{20}\,\text{Photons per shot} \tag{2.52}$$

$$\tau = 150\,\text{fs} \qquad\qquad\qquad = 228\,\text{eV}^{-1} \tag{2.53}$$

Design Parameters JETI200 @ Jena

$$\lambda = w_0 = 800\,\text{nm} \qquad\qquad\qquad = 4.06\,\text{eV}^{-1} \qquad (2.54)$$

$$B = 0.84 \cdot 10^6\,\text{T} \qquad\qquad\qquad = 1.65 \cdot 10^8\,\text{eV}^2 \qquad (2.55)$$

$$\omega = 2.36\,\text{PHz} \qquad\qquad\qquad = 1.55\,\text{eV} \qquad (2.56)$$

$$\mathcal{E} = 4\,\text{J} \qquad\qquad\qquad = 2.50 \cdot 10^{19}\,\text{eV} \qquad (2.57)$$

$$N_{\text{in}} = 1.61 \cdot 10^{19}\;\text{Photons per shot} \qquad\qquad (2.58)$$

$$\tau = 20\,\text{fs} \qquad\qquad\qquad = 30.4\,\text{eV}^{-1} \qquad (2.59)$$

Let us mention that although neither of these two laser systems has currently reached its respective stage of completion, similar systems have been realized experimentally. As an example, let us take the BERKELEY LAB LASER ACCELERATOR (BELLA), a petawatt laser system which, as of August 2012, achieved to generate 40 fs-pulses with a compressed energy of $\mathcal{E} = 42\,\text{J}$ at a repetition rate of 1 Hz (see [32] and [33]). A long term prospect for future examinations of quantum vacuum effects is given by the "Extreme light infrastructure" (ELI) currently in its planning stage, which aspires to achieve laser powers of $P = 200\,\text{PW}$ (cf. [34]).

The experimental setting, as described in this section, of course clearly violates both the requirement of time independency as well as homogeneity of the magnetic field in the longitudinal direction, i.e. the y-direction. The time scale of the temporal variation of the magnetic field is of approximately the same order as the time needed for the probe beam to cross the region of the inhomogeneity. More precisely, the probe beam needs about $t \approx 2w_0/c \approx 2\lambda/c$ to traverse the inhomogeneity, which already corresponds to two temporal cycles of the pump laser field. The only scenario where the assumption of stationarity could be considered a valid approximation is the case of focusing far below the diffraction limit, i.e. $f^\# < 1$. A special setup, where such strong focussing is at least theoretically conceivable, will be examined in more detail below. In any case, the longitudinal profile for generic laser beams can generally not be considered to be constant either, which plays a role for probe beams with $k_y \neq 0$. These remarks should make it clear that any results obtained in this chapter have to be regarded as first estimates and that for properly investigating realistic laser scenarios, the temporal dependency has to be taken into account as well. One might wonder whether a setup similar to the PVLAS experiment ([12] and [35]), aimed at detecting magnetic vacuum birefringence, could be feasible. Here, a static magnetic field of about $B = 5\,\text{T}$, shining through a 1m Fabry-Perot cavity of high finesse, is generated by rotating dipole magnets. The photon probe laser beam runs through the cavity about 10^5 times and thus the nonlinear effects are increased by this factor. Such a setup is arguably closer to our theoretical treatment. However, due to the extremely small factor of $(B/B_{\text{cr}})^4$, the effect of reflection will be magnitudes smaller than with a laser-laser setting. Furthermore, the inherent signal-background separation is lost and the induced quantum vacuum signature, in this case reflected photons which are of same frequency as the ingoing probe photons, would have to be isolated from the comparatively enormous background signal. A last point which argues against such a setting is given by the rather large length scale of the field strength variation, which can be realized in static configurations. Reflection inherently requires inhomogeneous profiles and shorter scales of spatial variation likely increase the effect, as is known from ordinary quantum mechanics.

We can now combine the two lasers POLARIS and JETI200 in several ways according to our experimental layout: The POLARIS laser is employed as the pump laser and the JETI200 laser

serves as the probe beam (Setup (a)) or vice versa (Setup (b)). To relate the laser parameters for the different setups to the quantities contained in the formula for the reflection coefficient R, Eq. (2.23), they are listed below:

Setup (a) POLARIS: Background beam, JETI200: Probe beam

$$B = 2.86 \cdot 10^8 \text{eV}^2,$$
$$w_0 = 5.25 \text{eV}^{-1},$$
$$\omega = 1.55 \text{eV}, \tag{2.60}$$
$$N_{\text{in}} = 1,61 \cdot 10^{19} \text{ Photons per shot},$$
$$f_{\text{int}} = 1,$$

Setup (b) POLARIS: Probe beam, JETI200: Background beam

$$B = 1.65 \cdot 10^8 \text{eV}^2,$$
$$w_0 = 4.06 \text{eV}^{-1},$$
$$\omega = 1.20 \text{eV}, \tag{2.61}$$
$$N_{\text{in}} = 7.8 \cdot 10^{20} \text{ Photons per shot},$$
$$f_{\text{int}} = 0.13 .$$

It is already safe to assume that in most cases Setup (a) will yield higher reflection rates due to the greater maximum field amplitude B. For the sake of completeness, let us state the numerical value for the remaining constant $C_p := e^2/(\pi m^4)c_p$ occurring in Eq. (2.23) as well. With the fine structure constant $\alpha = 1/137$, the electron charge $e = \sqrt{4\pi\alpha} = 0.303$, the electron mass $m = 5.11 \cdot 10^5$ eV and the reduced frequency

$$\tilde{\omega}^2 = \omega^2 - k_y^2 = \omega^2 - \omega^2 \sin^2 \beta = \omega^2 \cos^2 \beta, \tag{2.62}$$

C_p evaluates to

$$C_p = \left\{ \begin{matrix} C_{\parallel} \\ C_{\perp} \end{matrix} \right\} = \frac{\alpha}{180} \frac{e^2}{\pi m^4} \frac{\left[\sin^2 \theta + \sin^2 \theta' \right]}{\cos^2 \beta} \left\{ \begin{matrix} 7 \\ 4 \end{matrix} \right\} = \frac{\left[\sin^2 \theta + \sin^2 \theta' \right]}{\cos^2 \beta} 1.74 \cdot 10^{-29} \left\{ \begin{matrix} 7 \\ 4 \end{matrix} \right\} \text{eV}^{-4}, \tag{2.63}$$

which stills depends on the angles θ, θ' and β. The reflection coefficient can then be written to the lowest order as

$$R_p = \left| C_p \tilde{\omega} \int_{-\infty}^{\infty} dx\, e^{i2\tilde{\omega}x} B^2(x) \right|^2. \tag{2.64}$$

Finally, the restriction on the incidence angle β, Eq. (2.44), evaluates for the different setups to

$$\text{Setup (a):} \quad \left\{ \begin{matrix} 7 \\ 4 \end{matrix} \right\} \cdot 2.85 \cdot 10^{-12} \ll \frac{\cos^2 \beta}{\left[\sin^2 \theta + \sin^2 \theta' \right]} \quad \longrightarrow \quad 6.3 \cdot 10^{-6} \ll \cos \beta,$$
$$\text{Setup (a):} \quad \left\{ \begin{matrix} 7 \\ 4 \end{matrix} \right\} \cdot 9.47 \cdot 10^{-13} \ll \frac{\cos^2 \beta}{\left[\sin^2 \theta + \sin^2 \theta' \right]} \quad \longrightarrow \quad 3.6 \cdot 10^{-6} \ll \cos \beta. \tag{2.65}$$

Thus, practically all angles of physical relevance can be dealt with within our approximation. In the investigations to follow, we always implicitly assume the "one" background beam to consist of two superimposed counter-propagating laser beams which approximately cancel the electric field.

2.3.2. Case 1: Lorentz profile

To begin with, we investigate a symmetric Lorentz-shaped inhomogeneity of the form

$$B(x) = \frac{B}{1 + \left(\frac{x}{w_0}\right)^2}, \tag{2.66}$$

whose profile is solely characterized by the full width at half maximum (FWHM) given by w_0 (cf. the remark in the previous section) and the maximum field strength B. The Lorentz profile is a representative of power-like decreasing fields for large values of $|x|$, in this case

$$B(x) \sim B \left(\frac{x}{w_0}\right)^{-2} \qquad \text{as} \qquad |x| \to \infty. \tag{2.67}$$

The reflection coefficient R according to Eq. (2.64) is then given by

$$R_p = \left| \frac{\pi}{2} C_p B^2 \, \tilde{\omega} w_0 (1 + 2\tilde{\omega} w_0) e^{-2\tilde{\omega} w_0} \right|^2. \tag{2.68}$$

We see that in addition to the smallness of the parameter $C_p B^2$, the coefficient is exponentially suppressed with $2\tilde{\omega} w_0$. Clearly, increasing the incidence angle $\beta \to \pi/2$ leads to a diverging reflection coefficient, since the exponential suppression can be overcome and the overall factor of $1/\cos^2 \beta$ dominates. This agrees well with the discussion of the validity of R in the last sections. The reflection coefficient increases monotonically for increasing angle β. For a given angle of β, the maximum of R is given for $(\tilde{\omega} w_0)_{\max} = \frac{1+\sqrt{5}}{4}$. However, the values of w_0 and ω are generally fixed by the laser parameters. A plot of the profile and the $w_0 \tilde{\omega}$ dependence is given in Fig. 2.5 and 2.6 respectively.

2.3.3. Case 2: Exponential profiles

Exponential profiles of the form

$$B(x) = \frac{B}{\cosh\left(\frac{x}{w_0}\right)}, \qquad B(x) = \frac{B}{\cosh^2\left(\frac{x}{w_0}\right)}, \qquad \dots \qquad , \tag{2.69}$$

are as well characterized by the single parameter w_0 being a measure for its width. It is related to the FWHM via $w_0 \operatorname{arcosh} \sqrt[n]{2}$ for a given order n. The asymptotic behavior is exponential, i.e.

$$B(x) \sim B \, 2^n e^{-n \frac{|x|}{w_0}} \qquad \text{as} \qquad |x| \to \infty. \tag{2.70}$$

The reflection coefficients for those field inhomogeneities are given by

$$R_p = \left| 2\pi C_p B^2 \frac{\tilde{\omega}^2 w_0^2}{\sinh(\pi \tilde{\omega} w_0)} \right|^2, \qquad R_p = \left| \frac{4\pi}{3} C_p B^2 \frac{\tilde{\omega}^2 w_0^2 (1 + \tilde{\omega}^2 w_0^2)}{\sinh(\pi \tilde{\omega} w_0)} \right|^2, \qquad \dots \qquad , \tag{2.71}$$

which again only depend on the quantity $\tilde{\omega} w_0$ and are exponentially suppressed. Each order of n results in one more quadratic polynomial factor to the polynomial in the numerator. The dependence on the angle β and on $\tilde{\omega} w_0$ for each order is similar the behavior observed for the Lorentz profile, as can be seen in Fig. 2.6.

2.3.4. Case 3: Gaussian profile

Another example of an exponential profile characterized by a single parameter is given by the Gaussian profile

$$B(\mathrm{x}) = B\, e^{-\left(\frac{\mathrm{x}}{w_0}\right)^2}. \tag{2.72}$$

The parameter w_0 describes the width at which the pulse has dropped to $1/e^2$ of its peak intensity, which is related to the FWHM via $w_0\sqrt{\ln 2}$. The reflection coefficient evaluates to

$$R_p = \left| \sqrt{\frac{\pi}{2}} C_p B^2 \tilde{\omega} w_0 e^{-\frac{1}{2}(\tilde{\omega} w_0)^2} \right|^2. \tag{2.73}$$

In contrast to the two previously treated examples, reflection is exponentially suppressed with $(1/2)(\tilde{\omega} w_0)^2$. This time, the maximum of R for a given angle β is given by $(\tilde{\omega} w_0)_{\max} = 1$.

2.3.5. Plots of the cases and numerical values

We now numerically evaluate the three cases treated above in order to get first estimates of the magnitude of the effect of quantum reflection. We make use of the two setups described in Section 2.3.1. As was mentioned at the end of Sect. (2.1), the angles θ and θ' in the parallel case can be independent of the incidence angle β for the special setting $\mathbf{e}_B = \mathbf{e}_z$. However, for the perpendicular case we make the observation that (cf. Eq.(2.27))

$$R_\perp \sim \beta^2 \qquad \text{as} \quad \beta \to 0, \tag{2.74}$$

i.e. the reflection coefficient always approaches zero.
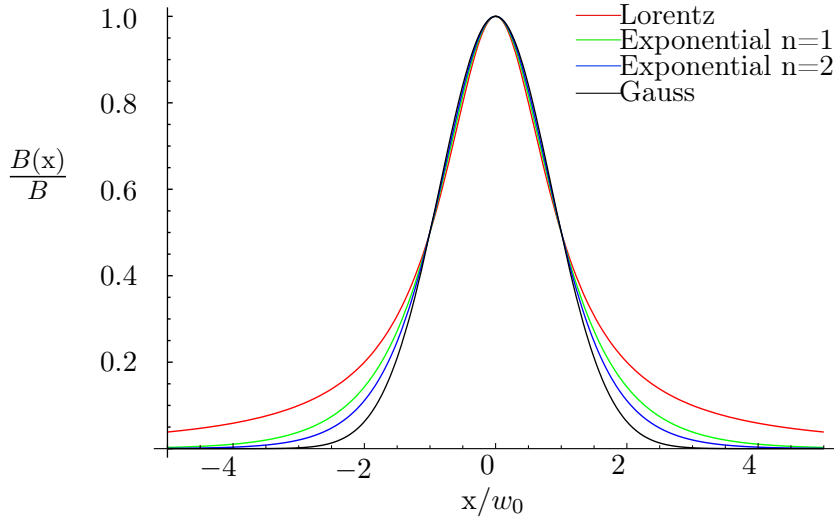
Figure 2.5.: Plot of the normalized magnetic field strength $B(\mathrm{x})/B$ for the cases 1 to 3 described above.

Figure 2.5 shows a plot of the four inhomogeneities for equal FWHM and Fig. 2.6 a plot of the resulting reduced reflection coefficient $R_p/(C_p^2\pi^2 B^4)$ for a fixed angle of β. The field profiles considered so far are very similar in shape and therefore it is not surprising that the value of R_p is of the same order and shows the same basic dependencies in all cases. Among this class of profiles, the Gaussian type yields the highest reflection rate if the laser parameters
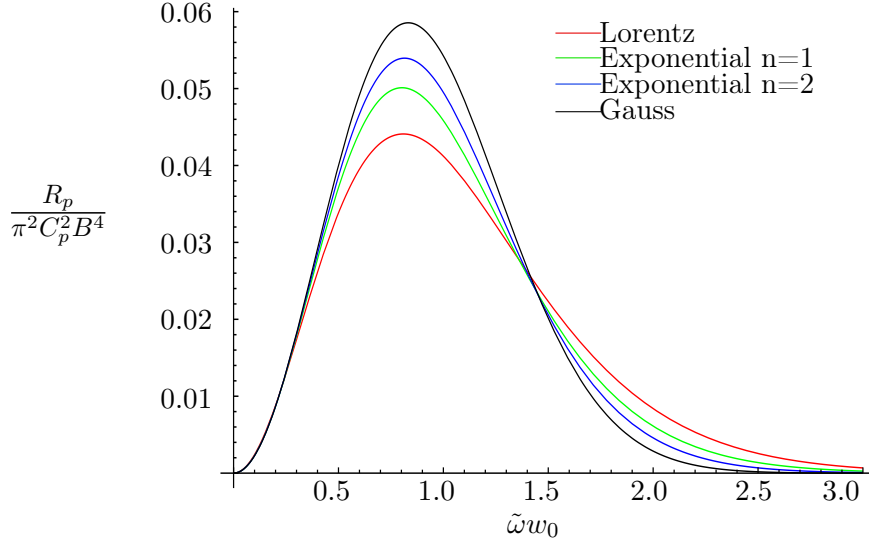
Figure 2.6.: Plot of the reduced (dimensionless) reflection coefficients $R_p/(\pi^2 C_p^2 B^4)$ for the different inhomogeneity profiles of the cases 1 to 3. The angle β is considered fixed and the coefficient then depends solely on the combination ωw_0.

match the maximum condition. The plot may be a little misleading due to the impression it gives that by adjusting the incidence angle β to achieve $\tilde{\omega}w_0 = (\tilde{\omega}w_0)_{\text{max}}$, we have reached the highest possible reflection rate. However, it is important to remember that the reduced reflection coefficient $R_p/(C_p^2 \pi^2 B^4)$ depends on β via C_p. Instead, R_p is a monotonically increasing function of $\beta = 0 \ldots \pi/2$ and eventually diverges, as was argued above. Figure 2.7 illustrates the point by plotting $R_p/(C_p^2 \pi^2 B^4 \cos^4 \beta)$ as a function of β for the different cases, choosing the value $\omega w_0 = 8.14$, corresponding to the Setup (a). Keep in mind that in general the angles θ and θ' still depend on β and in particular the reflection approaches zero for the perpendicular case, as was argued above.

The above plots already show that the effect of reflection is rather small. Let us exemplarily calculate some values for R_p and the number of reflected photons N_p choosing rather high angles of $\beta = 82.9°$ (Setup a) and $\beta = 78.2°$ (Setup b). Since the profiles are nearly identical, we limit ourselves to the case of the Gaussian shape and then the chosen angles fulfill exactly the matching condition. Employing Eq. (2.73) and (2.47), the result is given by

$$\text{Setup (a):} \quad R_p = \left[\sin^2 \theta + \sin^2 \theta'\right]^2 \cdot 5.1 \cdot 10^{-21} \begin{Bmatrix} 49 \\ 16 \end{Bmatrix}, \tag{2.75}$$

$$N_p = \left[\sin^2 \theta + \sin^2 \theta'\right]^2 \begin{Bmatrix} 4.1 \\ 1.3 \end{Bmatrix}, \tag{2.76}$$

$$\text{Setup (b):} \quad R_p = \left[\sin^2 \theta + \sin^2 \theta'\right]^2 \cdot 7.3 \cdot 10^{-23} \begin{Bmatrix} 49 \\ 16 \end{Bmatrix}, \tag{2.77}$$

$$N_p = \left[\sin^2 \theta + \sin^2 \theta'\right]^2 \begin{Bmatrix} 0.36 \\ 0.12 \end{Bmatrix}. \tag{2.78}$$

As expected, the reflection is lower for Setup (b) due to the lower magnetic field strength, although in this case it is partly outweighed by the higher number of incoming photons N_{in}. Those reflection rates should be considered upper bounds, since an experimental realization is unlikely
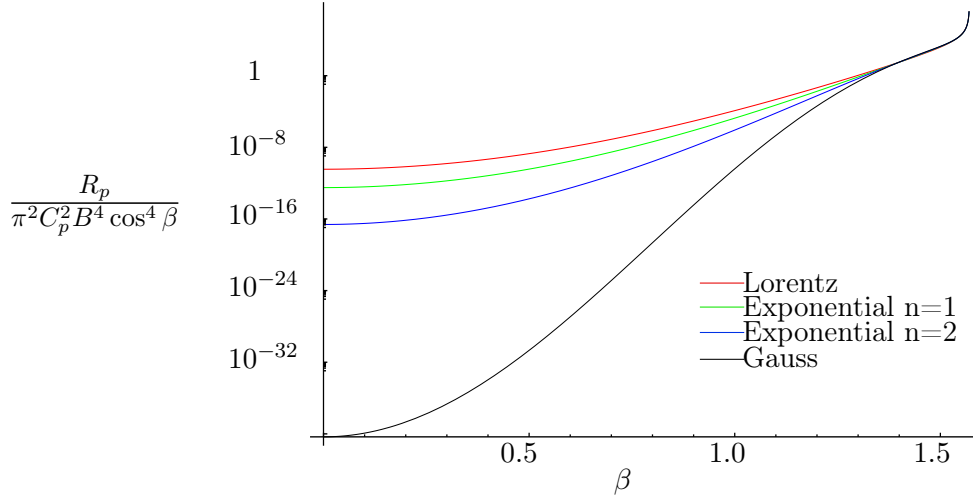
Figure 2.7.: Logarithmic plot of the reduced (dimensionless) reflection coefficients $R_p/(\pi^2 C_p^2 B^4 \cos^4 \beta)$ as a function of β for the different inhomogeneity profiles of the cases 1 to 3. All functions are monotonous in β and at $\beta = \pi/2$ the reflection coefficients diverge. The value of $\omega w_0 = 8.14$ was chosen according to setup (a).

to achieve the assumed precision in superimposing the laser beams. Nevertheless, the number of reflected photons is already quite sizable, especially if compared to other signatures of the electrodynamic quantum vacuum.

2.3.6. Modulated Gaussian inhomogeneity

The first four magnetic fields under consideration were only dependent on ωw_0, and the angle β provided the only handle to increase the effect. Sizable effects, however, could only be achieved for rather large angles, as was shown in Fig. 2.7. Such a setting, while theoretically devisable, leads to complications on the experimental side. Generating a clear superposition of the laser beams over a long longitudinal distance in order to cancel out the electric field is hardly possible and furthermore, for very large angles the clear signal-background separation gets lost. Furthermore, if the background beam is treated as a Gaussian beam, the assumption of a constant beam radius in the longitudinal direction gradually looses validity for increasing angles. A more quantitative discussion of this aspect is given in the appendix B.

In this section, we strive to achieve reflection effects of the same order, while requiring smaller angles at the same time. The way to accomplish this goal is by introducing modulated inhomogeneities characterized by a modulation length λ_m. In principle, we could use each of the previous profiles to modify by the modulation. However, results can be expected to be quite similar. Therefore, we only treat the Gaussian profile as a generic case in the upcoming examples. Laser beams are generally well described by Gaussian beams, whose transverse profile in the focus is indeed given by a Gaussian envelope and therefore justifies our choice. A short overview of Gaussian beams is given in appendix B.

The profile under investigation is given by

$$B(\mathrm{x}) = Be^{-\left(\frac{\mathrm{x}}{w_0}\right)^2}\cos(\omega_m \mathrm{x} + \varphi), \tag{2.79}$$

31

with the modulation frequency $\omega_m = 2\pi/\lambda_m$ and an additional phase φ. The reflection coefficient R_p can be computed straightforwardly in terms of Gaussian integrals and is given by

$$R_p = \left| \frac{1}{4}\sqrt{\frac{\pi}{2}} C_p B^2 \tilde{\omega} w_0 \left(2e^{-\frac{1}{2}w_0^2\tilde{\omega}^2} + e^{-\frac{1}{2}w_0^2(\tilde{\omega}+\omega_m)^2+2i\varphi} + e^{-\frac{1}{2}w_0^2(\tilde{\omega}-\omega_m)^2-2i\varphi} \right) \right|^2. \qquad (2.80)$$

For $\omega_m = \varphi = 0$ the equations (2.79) and (2.80) reduce to their respective forms of case 3. Again, we encounter the exponential suppression already observed in the last cases. However, this time the modulation frequency adds the possibility to overcome said suppression by matching $\tilde{\omega} = \omega_m$, which can be achieved by combined means of adjusting the angle and the modulation. Realistic laser parameters as given by our setups (a) and (b) yield rather large values for $\tilde{\omega} w_0$ and $\omega_m w_0$ and for these instances R_p is well approximated by

$$R_p = \left| \frac{1}{4}\sqrt{\frac{\pi}{2}} C_p B^2 \tilde{\omega} w_0 e^{-\frac{1}{2}w_0^2(\tilde{\omega}-\omega_m)^2} \right|^2, \qquad (2.81)$$

which does not depend on the phase φ anymore. There are now several ways to experimentally achieve such a transverse modulation within our stationary approximation.

Parallelly propagating laser beams

A first idea to realize such a modulation includes two identical Gaussian laser beams, which are propagating parallelly in the y direction (see [28]). If their respective beam axes are, within their focal parameters, a distance of λ_{pump} apart and they furthermore possess a relative phase shift of $\lambda_{\text{pump}}/2$ leading to magnetic fields pointing in opposite directions in the focus, then the resulting transverse profile will approximately exhibit a structure close to Eq. (2.79) with $\lambda_m = 2\lambda_{\text{pump}}$, $\phi = \pi/2$ and a width of $w_0 = 2\lambda_{\text{pump}}$. A plot of the magnetic field for the two setups (a) and (b) is shown in Fig. 2.10 in Subsection 2.3.8. Given such a setup and fixed parameters, the function $R_p(\beta)$ now shows a different behavior as can be observed in Fig. 2.8.
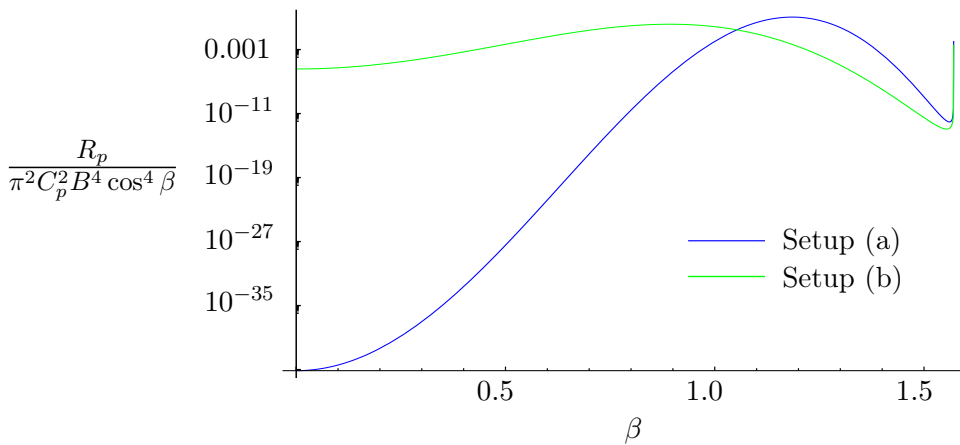
Figure 2.8.: Logarithmic plot of the normalized reflection coefficients $R_p/(\pi^2 C_p^2 B^4 \cos^4\beta)$ as a function of β for the case of an exponential inhomogeneity with a modulation frequency ω_m. The plot shows the two different setups under investigation. One can see the respective maxima at $\beta_{\max} \approx \arccos(0.49\,\lambda/\lambda_{\text{pump}})$ and the minima at $\beta_{\min} \approx \arccos(0.013\,\lambda/\lambda_{\text{pump}})$. For $\beta \to \pi/2$, the reflection coefficient diverges.

The extreme points of the function $R_p(\beta)$ as in Eq. (2.81) for $\beta \in [0, \pi/2)$ are given by

$$(\cos\beta)_{1/2} = \frac{\omega_m}{2\omega}\left(1 \pm \sqrt{1 - \frac{4}{(\omega_m w_0)^2}}\right) = \frac{\lambda}{\lambda_{\text{pump}}}\frac{1}{4}\left(1 \pm \sqrt{1 - \frac{4}{(2\pi)^2}}\right), \qquad (2.82)$$

where λ denotes the wave length of the probe beam. The positive sign corresponds to a local maximum, while the negative sign denotes a local minimum. For $\beta \to \pi/2$, the coefficient is again divergent. The modulation now permits us to achieve reflection rates of almost the same order as in the previous cases, albeit at lower angles, by adjusting $\beta = \beta_{\text{max}}$. The resulting, maximizing angles for the setups are then given by

$$\text{Setup (a):} \quad \beta_{\text{max}} \approx 67.9° \qquad \text{and} \qquad \text{Setup (b):} \quad \beta_{\text{max}} \approx 50.9°. \qquad (2.83)$$

Keep in mind that these angles are only estimates since the θ and θ' dependency on β has not been taken into account. The reflection rates and the reflected number of photons are an order lower than for the previously treated cases, i.e.

$$\text{Setup (a):} \quad R_p = \left[\sin^2\theta + \sin^2\theta'\right]^2 \cdot 3.6 \cdot 10^{-22}\left\{\begin{matrix} 49 \\ 16 \end{matrix}\right\}, \qquad (2.84)$$

$$N_p = \left[\sin^2\theta + \sin^2\theta'\right]^2 \left\{\begin{matrix} 0.29 \\ 0.093 \end{matrix}\right\}, \qquad (2.85)$$

$$\text{Setup (b):} \quad R_p = \left[\sin^2\theta + \sin^2\theta'\right]^2 \cdot 5.2 \cdot 10^{-24}\left\{\begin{matrix} 49 \\ 16 \end{matrix}\right\}, \qquad (2.86)$$

$$N_p = \left[\sin^2\theta + \sin^2\theta'\right]^2 \left\{\begin{matrix} 0.026 \\ 0.0084 \end{matrix}\right\}. \qquad (2.87)$$

Crossed field configuration

Another way to achieve a modulating frequency ω_m is illustrated in Fig. 2.9: The probe beam travels strictly along the x axis. The background beam is split into two identical laser beams with respective magnetic fields $B_1(\text{x}, \text{y})$ and $B_2(\text{x}, \text{y})$, which are restricted to the x-y plane and whose focal points meet at the origin. Beam 1 is directed at an angle δ with respect to the x axis, while beam 2 is directed at an angle $-\delta$. Both laser beams are assumed to be standing plane waves with wavelength λ_m along their respective directions $\mathbf{e}_i$, while their transversal shape (directions $\mathbf{e}_{i,\perp}$) is again characterized by a Gaussian profile of width $2w_0$. Each beam thus has the form

$$B_i(\text{x}, \text{y}) = \frac{B}{2}\exp\left[-\left(\frac{\mathbf{r}\cdot\mathbf{e}_{i,\perp}}{w_0}\right)^2\right]\cos(\omega_m\mathbf{r}\cdot\mathbf{e}_i + \varphi_i) \qquad (2.88)$$

with

$$\mathbf{e}_1 = \cos\delta\,\mathbf{e}_x + \sin\delta\,\mathbf{e}_y, \qquad\qquad \mathbf{e}_{1,\perp} = -\sin\delta\,\mathbf{e}_x + \cos\delta\,\mathbf{e}_y, \qquad (2.89)$$
$$\mathbf{e}_2 = \cos\delta\,\mathbf{e}_x - \sin\delta\,\mathbf{e}_y, \qquad\qquad \mathbf{e}_{2,\perp} = \sin\delta\,\mathbf{e}_x + \cos\delta\,\mathbf{e}_y, \qquad (2.90)$$

where ϕ_i denotes an arbitrary phase and $\mathbf{r} = \text{x}\,\mathbf{e}_x + \text{y}\,\mathbf{e}_y$. The problem reduces to a one-dimensional one and can be handled like before if we confine ourselves to the x axis. The magnetic field then reduces to

$$B(\text{x}, \text{y} = 0) = \frac{B}{2}e^{-\frac{\text{x}^2}{w_0^2}\sin^2\delta}\left[\cos(\omega_m\text{x}\cos\delta + \varphi_1) + \cos(\omega_m\text{x}\cos\delta + \varphi_2)\right] \qquad (2.91)$$
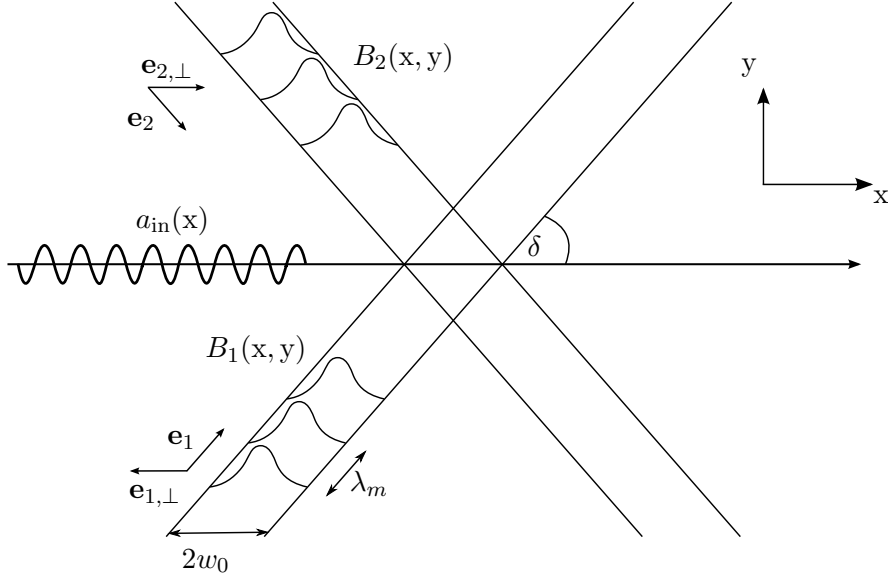
Figure 2.9.: The setup of the crossed fields configuration. The background beam is split into two identical beams in the x-y plane with angles $\pm\delta$ with respect to the x axis. The problem is reduced to a one dimensional task by considering only the x axis.

and the corresponding reflection coefficient is given by

$$R_p = \left| \frac{1}{4}\sqrt{\frac{\pi}{2}} C_p B^2 \frac{\omega w_0}{\sin\delta} \cos^2\left[\frac{1}{2}(\varphi_1 + \varphi_2)\right] \right.$$

$$\left. \left[2e^{-\frac{1}{2}\left(\frac{\omega w_0}{\sin\delta}\right)^2} + e^{-\frac{1}{2}\left(\frac{w_0}{\sin\delta}\right)^2(\omega - \omega_m \cos\delta)^2 - i(\varphi_1 + \varphi_2)} + e^{-\frac{1}{2}\left(\frac{w_0}{\sin\delta}\right)^2(\omega + \omega_m \cos\delta)^2 + i(\varphi_1 + \varphi_2)}\right] \right|^2 . \quad (2.92)$$

The result resembles the one from Eq. (2.80), but this time the dependency on the angle δ is different than the one on β from the previous cases. First of all, let us note that for $\delta = 90°$ and $\varphi_1 = \varphi_2 = 0$, R_p reduces to that of case 3, Eq. (2.71). Secondly, the reflection coefficient depends of course on the relative phases of the background beams: A maximum is given for $\varphi_1 + \varphi_2 = 2\pi k$ with $k \in \mathbb{Z}$ and it is zero for $\varphi_1 + \varphi_2 = (2k + 1)\pi$, since destructive interference causes the magnetic field to vanish. For our future discussion, we will assume the maximum possible value, i.e. $\varphi_1 + \varphi_2 = 0$. For

$$\omega - \omega_m \cos\delta << \omega, \quad (2.93)$$

which is fulfilled for our laser parameters if the angle δ is sufficiently small, we can again simplify Eq. (2.92) to yield

$$R_p = \left| \frac{1}{4}\sqrt{\frac{\pi}{2}} C_p B^2 \frac{\omega w_0}{\sin\delta} e^{-\frac{1}{2}\left(\frac{w_0}{\sin\delta}\right)^2(\omega - \omega_m \cos\delta)^2} \right|^2 . \quad (2.94)$$

The matching condition to achieve maximum reflection is given by the cubic equation in $\cos\delta$,

$$-\cos\delta(1 - \cos^2\delta) = w_0^2(1 - \omega_m \cos\delta)(1 - \omega\cos\delta). \quad (2.95)$$

Since the LHS of (2.95) is smaller than zero, the maximum we are interested in must be located in $\cos\delta \in \left(\text{Min}\left(\frac{\omega}{\omega_m}, \frac{\omega_m}{\omega}\right), 1\right)$. The real root of such cubic equations can be conveniently found numerically. The result for the two setups under consideration reads

$$\text{Setup (a):} \quad \delta_{\text{max}} \approx 38.2° \qquad \text{and} \qquad \text{Setup (b):} \quad \delta_{\text{max}} \approx 37.5°. \tag{2.96}$$

The result for the reflection coefficient and the number of reflected photons is

$$\text{Setup (a):} \quad R_p = \left[\sin^2\theta + \sin^2\theta'\right]^2 \cdot 1.0 \cdot 10^{-34} \begin{Bmatrix} 49 \\ 16 \end{Bmatrix}, \tag{2.97}$$

$$N_p = \left[\sin^2\theta + \sin^2\theta'\right]^2 \cdot 10^{-14} \begin{Bmatrix} 7.9 \\ 2.6 \end{Bmatrix}, \tag{2.98}$$

$$\text{Setup (b):} \quad R_p = \left[\sin^2\theta + \sin^2\theta'\right]^2 \cdot 1.4 \cdot 10^{-24} \begin{Bmatrix} 49 \\ 16 \end{Bmatrix}, \tag{2.99}$$

$$N_p = \left[\sin^2\theta + \sin^2\theta'\right]^2 \begin{Bmatrix} 0.0070 \\ 0.0023 \end{Bmatrix}. \tag{2.100}$$

In this case, Setup (b) yields a higher reflection rate, since no angle δ can nullify the exponential suppression for Setup (a). If Setup (a) could be modified in such a way that the frequency of the background beam be doubled, then the exponent could be more or less matched to zero, yielding a much higher reflection coefficient. This could be done in principle by creating SHG at the cost of an intensity loss (the conversion efficiency Q ranges from 30% to 70%). Considering a frequency doubled background beam and including the conversion efficiency Q, the optimal angle for Setup (a) changes to

$$\delta_{\text{max}} \approx 48.5°, \tag{2.101}$$

Here it is assumed that the background beam can again be focused with an f-number of 1, which leads to $w_0 = 517.5nm = 2.63\,\text{eV}^{-1}$ and a doubled magnetic field of $B = 5.72 \cdot 10^8\,\text{eV}^2$. The reflection increases to

$$R_p = Q^2 \left[\sin^2\theta + \sin^2\theta'\right]^2 \cdot 0.92 \cdot 10^{-22} \begin{Bmatrix} 49 \\ 16 \end{Bmatrix}, \tag{2.102}$$

$$N_p = Q^2 \left[\sin^2\theta + \sin^2\theta'\right]^2 \begin{Bmatrix} 0.073 \\ 0.024 \end{Bmatrix}. \tag{2.103}$$

Depending on the conversion efficiency Q, the reflection for Setup (a) was increased by about 10 orders of magnitude and, as a result of the exact matching and higher focussing of the background field, is now of the same order of magnitude as Setup (b).

2.3.7. Two Gaussian potentials a distance l apart

The potential (2.79) is only an approximation to the field configuration generated by two parallelly propagating beams as described in the last section. Of course, we can also calculate the exact expression for the reflection coefficient for such a configuration

$$B(\text{x}) = B\left(e^{-\left(\frac{\text{x}+l}{w_0}\right)^2} - e^{-\left(\frac{\text{x}-l}{w_0}\right)^2}\right), \tag{2.104}$$

where l denotes the distance of either beam axis from the origin. To compare it directly with the experimental setup in the last section, we would have to choose $l = \lambda_{\text{pump}} = w_0$. However,

we should rather make use of the additional free parameter l and leave it unspecified for now. The reflection coefficient evaluates to

$$R_p = \left| \sqrt{2\pi} C_p B^2 \tilde{\omega} w_0 e^{-\frac{1}{2}\tilde{\omega}^2 w_0^2} \left(\cos(2\tilde{\omega}l) - e^{-2\frac{l^2}{w_0^2}} \right) \right|^2. \tag{2.105}$$

We can already see that the exponential suppression cannot be overcome by the modification of the exponent with a modulating frequency of some kind. Instead, the behavior of R_p is closer to that of the very first examples where the exponential suppression can be overcome by simply increasing the angle of incidence β. However, the dependency on the angle β is not strictly monotonous anymore owing to the possible cancelation of the terms in the brackets (...). For a given angle β, we can adjust the separation length l according to

$$2\omega\, l \cos\beta = (2k+1)\pi \qquad\qquad \text{with } k \in \mathbb{N} \tag{2.106}$$

We now choose angles of the same order as for the treatment of the pure modulation in the last section, i.e.

$$\text{Setup (a):} \quad \beta_{\max} \approx 67.9° \qquad \text{and} \qquad \text{Setup (b):} \quad \beta_{\max} \approx 50.9°, \tag{2.107}$$

and make use of the additional freedom by picking the smallest separation length l fulfilling the condition (2.106). The values are given by

$$\text{Setup (a):} \quad l_{\max} \approx 2.69\,\text{eV}^{-1} \qquad \text{and} \qquad \text{Setup (b):} \quad l_{\max} \approx 2.08\,\text{eV}^{-1}. \tag{2.108}$$

Plugging those values into the formula for the reflection coefficient Eq. (2.105), we find

$$\text{Setup (a):} \quad R_p = \left[\sin^2\theta + \sin^2\theta' \right]^2 \cdot 1.3 \cdot 10^{-24} \begin{Bmatrix} 49 \\ 16 \end{Bmatrix}, \tag{2.109}$$

$$N_p = \left[\sin^2\theta + \sin^2\theta' \right]^2 \cdot 10^{-3} \begin{Bmatrix} 1.0 \\ 0.33 \end{Bmatrix}, \tag{2.110}$$

$$\text{Setup (b):} \quad R_p = \left[\sin^2\theta + \sin^2\theta' \right]^2 \cdot 1.7 \cdot 10^{-26} \begin{Bmatrix} 49 \\ 16 \end{Bmatrix}, \tag{2.111}$$

$$N_p = \left[\sin^2\theta + \sin^2\theta' \right]^2 \cdot 10^{-5} \begin{Bmatrix} 8.4 \\ 2.8 \end{Bmatrix}. \tag{2.112}$$

Employing the same angles as in the case with ideal modulation, the reflection for both setups is about two orders of magnitude lower in the former case. Of course, higher reflection rates are accessible by choosing higher angles β and adjusting the separation length l accordingly. However, the mechanism of circumventing the exponential suppression is then basically the same as for the very first discussed beam profiles (Lorentz, pure Gaussian etc.) and leads again to rather large angles to achieve a sizable rate of reflection. This discussion shows that the parallelly propagating beam setup does not actually help to reduce the angle $\beta_{\max}$ unless an ideal modulation resembling Eq. (2.79) can be created.

2.3.8. 4π focussed pulses

We have seen in the last examples that, in order to maximize the effect of quantum reflection, one first has to overcome the exponential suppression and secondly provide a focus w_0 as small as possible, as this will lead via Eq. (2.45) to an increased amplitude of the magnetic background

field. According to [36], 4π focused laser pulses provide the most efficient focus of all possible configurations, even allowing to go lower than the diffraction limit. In their paper the authors proposed an experimental setup which generates such dipole pulses by employing a parabolic mirror. This section deals with calculating the reflection coefficient for such a setup, where "quasi-Gaussian" pulses are used as input beams. First, let us review the most important points.

The starting point is a virtual electric dipole moment at the focus point $\mathbf{r} = 0$, where the singularities at the origin are eliminated by the addition of retarded and advanced potentials. The corresponding exact, singularity free solution for the magnetic and electric fields is given by (quoting the paper using Gaussian units)

$$\mathbf{H}(\mathbf{r}, t) = -(\mathbf{n} \times \mathbf{d}_0) \left[\frac{1}{c^2} \frac{\ddot{g}_+(t, R)}{R} + \frac{1}{c} \frac{\dot{g}_-(t, R)}{R^2} \right], \tag{2.113}$$

$$\mathbf{E}(\mathbf{r}, t) = -\frac{\mathbf{n} \times (\mathbf{n} \times \mathbf{d}_0)}{Rc^2} \ddot{g}_-(t, R) + \frac{3\mathbf{n}(\mathbf{n}\mathbf{d}_0) - \mathbf{d}_0}{R^3} \left[\frac{R}{c} \dot{g}_+(t, R) + g_-(t, R) \right]. \tag{2.114}$$

Here $R = |\mathbf{r}|$ and $\mathbf{n} = \mathbf{r}/R$. The quantity $\mathbf{d}_0 = $ const. denotes the virtual dipole moment and $g_\pm(t, R) = g(t - R/c) \pm g(t + R/c)$, where $g(\tilde{t})$ is the dimensionless driving function of the dipole moment, i.e. $\mathbf{d}(t \pm R/c) = g(t \pm R/c)\mathbf{d}_0$. The virtual dipole moment can be approximately related to the input energy of the laser pulse by means of the relation

$$\mathcal{E} = \frac{2d_0^2}{3c^3} \int_{-\infty}^{\infty} \ddot{g}^2(\tilde{t}) d\tilde{t}, \tag{2.115}$$

where the approximation of an infinitely large focusing system and dipole pulses of finite duration was made. This setup maximizes the electric field at the time $t = 0$, while the magnetic field at that moment vanishes. To switch to our case of a desirably strong magnetic field the electric dipole has to be substituted by a magnetic dipole leading to a continued validity of the given formulas provided one substitutes

$$\mathbf{H}^{MD} \longleftarrow \mathbf{E}^{ED}, \qquad \mathbf{E}^{MD} \longleftarrow -\mathbf{H}^{ED}. \tag{2.116}$$

Furthermore, we consider a dipole moment $\mathbf{d}_0 = d_0 \mathbf{e}_z$ and our probe beam will be traveling along the x-axis meeting the focus point at time $t = 0$. Therefore, the following field configurations are the starting points of our considerations

$$\mathbf{E} = (\mathbf{n} \times \mathbf{d}_0) \left[\frac{1}{c^2} \frac{\ddot{g}_+(t, R)}{R} + \frac{1}{c} \frac{\dot{g}_-(t, R)}{R^2} \right], \tag{2.117}$$

$$\mathbf{H} = -\frac{\mathbf{d}_0}{Rc^2} \ddot{g}_-(t, R) - \frac{\mathbf{d}_0}{R^3} \left[\frac{R}{c} \dot{g}_+(t, R) + g_-(t, R) \right]. \tag{2.118}$$

More specifically,

$$E_y(t, R) = -d_0 \left[\frac{1}{c^2} \frac{\ddot{g}_+(t, R)}{R} + \frac{1}{c} \frac{\dot{g}_-(t, R)}{R^2} \right], \tag{2.119}$$

$$H_z(t, R) = -\frac{d_0}{Rc^2} \ddot{g}_-(t, R) - \frac{d_0}{R^3} \left[\frac{R}{c} \dot{g}_+(t, R) + g_-(t, R) \right] \tag{2.120}$$

are the only non-vanishing components of the fields. The restriction to this setting implies vanishing parallel components, i.e. $\mathbf{k}_\parallel = 0$, and consequently the parallel case is the one under consideration here. The perpendicular component, on the other hand, is not unaffected by the

inhomogeneity and therefore this case must not be considered. Since $\mathbf{k}$ and $\mathbf{B}$ are perpendicular, the angles evaluate to $\sin\theta = \sin\theta' = 1$. To treat quasi-Gaussian pulses, we take the driving function

$$g(\tilde{t}) = e^{-a^2\tilde{t}^2}\sin(\omega_m\tilde{t}). \tag{2.121}$$

The quantities appearing in Eq. (2.121) can be related directly to the incoming laser pulse (the background beam) because in the far field the field amplitudes are proportional to the second derivative of $g(\tilde{t})$,

$$\ddot{g}(\tau) = e^{-a^2\tilde{t}^2}\left[-4a^2\omega_m\tilde{t}\cos(\omega_m\tilde{t}) + (4a^4\tilde{t}^2 - \omega_m^2 - 2a^2)\sin(\omega_m\tilde{t})\right], \tag{2.122}$$

since in (2.118) the terms $\propto \frac{1}{R}$ dominate. This still has a "quasi-Gaussian" shape and hence ω_m can be related to the mean frequency of the background beam, while $\frac{1}{a} = \frac{\tau}{2}$ corresponds to the duration of the background beam pulse. Here, $\frac{\tau}{2}$ is the time when the magnetic field envelope decreases to $\frac{1}{e}$ of its maximum value, τ thus denotes the pulse length.

Calculation of the reflection coefficient

For the calculation of $R_\parallel$ we assume the probe beam to hit the "static" background field evaluated at time $t = 0$. Explicitly calculating (2.118) for the Gaussian driving function (2.121) at the time $t = 0$ and switching to SI-units leads to

$$B(\mathrm{x}) = B_z(t=0, R) = \frac{d_0}{\sqrt{\pi}}e^{-a^2\mathrm{x}^2}\left[\cos(\omega_m\mathrm{x})\left(4a^2\omega_m + \frac{\omega_m}{\mathrm{x}^2}\right) + \sin(\omega_m\mathrm{x})\left(\frac{\omega_m^2}{\mathrm{x}} - 4a^4\mathrm{x} - \frac{1}{\mathrm{x}^3}\right)\right], \tag{2.123}$$

where

$$d_0 = \frac{\sqrt{3\mathcal{E}a}}{\omega_m^2\left(\frac{\pi}{2}\right)^{\frac{1}{4}}\left[\left(1 + 6\frac{a^2}{\omega_m^2} + 3\frac{a^4}{\omega_m^4}\right) - 3\frac{a^4}{\omega_m^4}e^{-\frac{\omega_m^2}{2a^2}}\right]^{\frac{1}{2}}}. \tag{2.124}$$

Figure 2.10 shows a plot of the resulting magnetic field (2.123) for the setups (a) and (b) and compares them to the case modulated field of the parallelly propagating beams from Sec. (2.3.6). Employing Eq. (2.64) for the reflection coefficient $R_\parallel$,

$$R_\parallel = \left|C_\parallel\omega\int_{-\infty}^{\infty}e^{2i\omega\mathrm{x}}B^2(x)d\mathrm{x}\right|^2 = \left|C_\parallel\omega\frac{d_0^2}{\pi}I(\omega,\omega_m,a)\right|^2, \tag{2.125}$$

we have to calculate the integral

$$I(\omega,\omega_m,a) = \int_{-\infty}^{\infty}dx\, e^{2i\omega\mathrm{x}}e^{-2a^2\mathrm{x}^2}\left[S_1(\mathrm{x}) + a^2S_2(\mathrm{x}) + a^4S_3(\mathrm{x}) + S_4(\mathrm{x})\right], \tag{2.126}$$

where

$$S_1(\mathrm{x}) = \frac{\omega_m^2}{\mathrm{x}^4} + \sin^2(\omega_m\mathrm{x})\left(\frac{\omega_m^4}{\mathrm{x}^2} + \frac{1}{\mathrm{x}^6} - 3\frac{\omega_m^2}{\mathrm{x}^4}\right) + 2\cos(\omega_m\mathrm{x})\sin(\omega_m\mathrm{x})\left(\frac{\omega_m^3}{\mathrm{x}^3} - \frac{\omega_m}{\mathrm{x}^5}\right), \tag{2.127}$$

$$S_2(\mathrm{x}) = 8\cos^2(\omega_m\mathrm{x})\frac{\omega^2}{\mathrm{x}^2} + 8\cos(\omega_m\mathrm{x})\sin(\omega_m\mathrm{x})\left(\frac{\omega_m^3}{\mathrm{x}} - \frac{\omega_m}{\mathrm{x}^3}\right), \tag{2.128}$$

$$S_3(\mathrm{x}) = 8\sin^2(\omega_m\mathrm{x})\frac{1}{\mathrm{x}^2} - 8\cos(\omega_m\mathrm{x})\sin(\omega_m\mathrm{x})\frac{\omega_m}{\mathrm{x}}, \tag{2.129}$$

$$S_4(\mathrm{x}) = 16\cos^2(\omega_m\mathrm{x})a^4\omega_m^2 - 8\sin^2(\omega_m\mathrm{x})a^4\omega_m^2$$
$$- 32\cos(\omega_m\mathrm{x})\sin(\omega_m\mathrm{x})a^6\omega_m\mathrm{x} + 16\sin^2(\omega_m\mathrm{x})a^8\mathrm{x}^2. \tag{2.130}$$
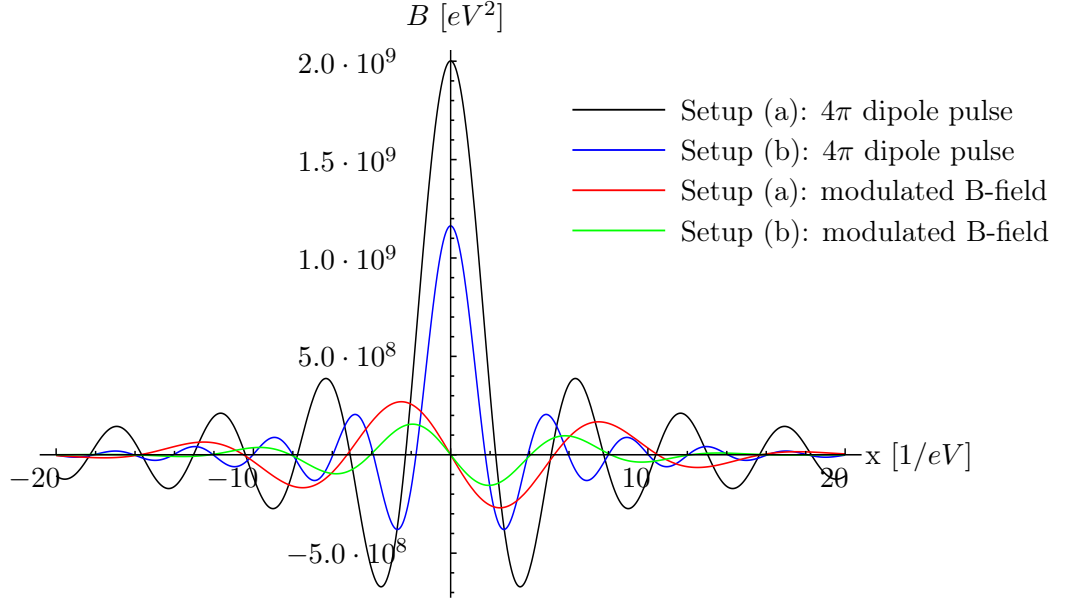
Figure 2.10.: Plot of the magnetic field $B(x)$ for the 4π dipole pulses and the approximated modulated field from the last section for parallelly propagating beams employing values from setups (a) and (b). The smaller focus area leads to an increased peak amplitude of the magnetic field for the 4π dipole pulses.

The terms $S_i(x)$ are regular, although the individual sum terms contained in them diverge for $x \to 0$. Therefore, the integral has to be handled with care. Dealing with each of the terms S_i individually, the general strategy is to write the integrand as a divergent part $\frac{1}{x^n}$ times a regular part and reduce the negative order by partial integration until only $\frac{1}{x}$ factors remain. The only difficulty left is to compute integrals of the kind

$$\int_{-\infty}^{\infty} dy\, \frac{\sin \gamma y}{y} e^{-\alpha^2 y^2 + i\beta y} = \frac{1}{2i} \int_{-\infty}^{\infty} dy\, \frac{1}{y} e^{-\alpha^2 y^2 + i(\beta+\gamma)y} - \frac{1}{2i} \int_{-\infty}^{\infty} dy\, \frac{1}{y} e^{-\alpha^2 y^2 + i(\beta-\gamma)y}$$
$$=: f_+ - f_- \,, \tag{2.131}$$

where dimensionless units y have been introduced and $\alpha, \gamma \in \mathbb{R}$, $\beta \in \mathbb{C}$ denote real and complex constants respectively. These can be solved by introducing a parameter s via a proper-time integral and solve the integrals by switching the order of integration. The calculation is performed as follows,

$$f_{\pm} = \frac{1}{2i} \int_{-\infty}^{\infty} dy\, \frac{1}{y} e^{-\alpha^2 y^2 + i(\beta \pm \gamma)y} = \frac{1}{2i} \lim_{\Lambda \to \infty} \int_0^{\Lambda} ds \int_{-\infty}^{\infty} dy\, e^{-\alpha^2 y^2 + i(\beta \pm \gamma + is)y} \tag{2.132}$$

$$= \frac{1}{2i} \frac{\sqrt{\pi}}{\alpha} \lim_{\Lambda \to \infty} \int_0^{\Lambda} ds\, e^{\frac{1}{4\alpha^2}(s - i(\beta \pm \gamma))^2} \tag{2.133}$$

$$= \frac{\pi}{2} \lim_{\Lambda \to \infty} \left[\operatorname{erf}\left(\frac{1}{2i\alpha}(\Lambda - i(\beta \pm \gamma)) \right) + \operatorname{erf}\left(\frac{1}{2\alpha}(\beta \pm \gamma) \right) \right], \tag{2.134}$$

and in the limit $\Lambda \to \infty$ the result reads

$$\int_{-\infty}^{\infty} dy\, \frac{\sin \gamma y}{y} e^{-\alpha^2 y^2 + i\beta y} = \frac{\pi}{2} \left[\operatorname{erf}\left(\frac{1}{2\alpha}(\beta + \gamma) \right) - \operatorname{erf}\left(\frac{1}{2\alpha}(\beta - \gamma) \right) \right], \tag{2.135}$$

which is regular. The Gaussian error function $\text{erf}(z)$ for arbitrary, complex arguments z is defined as

$$\text{erf}(z) := \frac{2}{\sqrt{\pi}} \int_0^z dt \, e^{-t^2}. \tag{2.136}$$

Performing the outlined procedure, the final result for the Integral I is given by

$$
I(\omega, \omega_m, a) = \frac{a\sqrt{2\pi}}{30} \left[P_+ e^{-\frac{(\omega+\omega_m)^2}{2a^2}} + P_- e^{-\frac{(\omega-\omega_m)^2}{2a^2}} - 2Q e^{-\frac{\omega^2}{2a^2}} \right]
$$
$$
+ \frac{\pi}{30} \left[R_+ \text{erf}\left(\frac{\omega + \omega_m}{\sqrt{2}a} \right) + R_- \text{erf}\left(\frac{\omega - \omega_m}{\sqrt{2}a} \right) - (R_+ + R_-)\text{erf}\left(\frac{\omega}{\sqrt{2}a} \right) \right], \tag{2.137}
$$

where $P_\pm$, $R_\pm$ and Q are polynomials in ω, ω_m and a given by

$$
\begin{aligned}
P_\pm = P(\omega, \pm\omega_m, a) =\,& 121a^4 + 33a^2\omega^2 + 2\omega^4 + 73a^2\omega_m^2 + 12\omega^2\omega_m^2 + 7\omega_m^4 \\
& \pm (76a^2\omega\omega_m + 8\omega\omega_m^3 - 2\omega^3\omega_m), \\
R_\pm = R(\omega, \pm\omega_m, a) =\,& 150a^4\omega + 20a^2\omega^3 + 2\omega^5 + 150a^2\omega\omega_m^2 + 10\omega^3\omega_m^2 + 15\omega\omega_m^4 \\
& \pm (180a^4\omega_m + 120a^2\omega^2\omega_m + 80a^2\omega_m^3 + 20\omega^2\omega_m^3 + 7\omega_m^5), \\
Q = Q(\omega, \omega_m, a) =\,& 121a^4 + 33a^2\omega^2 + 2\omega^4 + 110a^2\omega_m^2 + 10\omega^2\omega_m^2 + 15\omega_m^4.
\end{aligned} \tag{2.138}
$$

Numerical results

We again evaluate the result for the two setups (a) and (b). The magnitude of the reflection coefficient depends on the parameter $a = 2/\tau$, with shorter incoming pulses yielding a higher reflection. The 4π dipole pulses are of very little spatial extension, however, their time dependence in the focal point $R = 0$ is given by (in Gaussian units)

$$\mathbf{H} = \frac{4}{3c^3} \dddot{\mathbf{d}}(t) \tag{2.139}$$

and in our case possesses the same Gaussian envelope $e^{-a^2\tilde{t}^2}$ as the far field. Therefore, the same factor f_{int} as in the previous examples can be employed. Note however, that since the temporal dependence in the focus is basically given by the time derivative of the far field, very short dipole pulses can be created by using input beams featuring sharp pulse fronts and therefore the maximum field amplitude can be further increased. The reflection coefficients for our two setups are given by

$$\text{Setup (a):} \quad R_\parallel = 3.0 \cdot 10^{-48}, \tag{2.140}$$
$$N_\parallel = 4.8 \cdot 10^{-29}, \tag{2.141}$$
$$\text{Setup (b):} \quad R_\parallel = 6.9 \cdot 10^{-20}, \tag{2.142}$$
$$N_\parallel = 6.8 \qquad . \tag{2.143}$$

The reflection for Setup (a) is negligible, which is a consequence of the special dependence of the result (2.137) on ω and ω_m. Interestingly, the higher input power of the POLARIS laser does little to outweigh the longer pulse duration. Setup (b) yields reflection rates of about 7 photons per shot and is thus comparable to the very first cases considered, albeit there it always was Setup (a) providing better results.

2.4. Conclusions

In the previous section, we discussed a variety of beam profiles and calculated their respective reflection coefficients and number of reflected photons per shot employing the laser parameters of the Jena based laser facilities POLARIS and JETI200. By means of inducing a modulation of the background field or by shining the probe beam under an angle β, the effect could be maximized to yield reflection rates of the order of 1 photon per shot. In principle, employing single photon detection techniques ([37]) over a large number of repetitions should produce measurable results and thus quantum reflection might turn out to be an interesting candidate for probing the quantum vacuum nonlinearity. However, as was mentioned earlier, the temporal structure of the background beams was completely neglected, which means that reliable quantitative predictions are not yet possible. Rather, the present chapter provides first estimates and, more importantly, insights into some of the effects and techniques related to the quantification of this phenomenon.

It is interesting to note that the formal analogy to atomic quantum reflection also persists on the level of the resulting equations. As was shown in [15], the rate of reflection is exponentially suppressed, i.e. $R \sim \exp(-Cv_x)$, where v_x denotes the normal component of the velocity of the incoming particles with respect to the surface. This fact necessitates the shining of the atomic probe beams under a grazing angle of incidence in order to achieve a normal velocity component as small as possible. It becomes clear that in our optical case $\tilde{\omega}$ plays exactly the same role as v_x and we were also forced to use grazing incidence to overcome the exponential suppression.

3. Reflection at time dependent magnetic fields

In the following chapter we now aim to extend the treatment to include time dependent magnetic fields. The first section describes the setup and shows a derivation of the corresponding Green's function solving the equation of motion in analogy to the last chapter. In the second section we suggest a definition of the reflection coefficient for the time dependent case. The third section gives an expression of the Fourier transform of the photon polarization to the lowest orders. A discussion of the calculation of the current $j_\perp$ concludes this chapter.

3.1. The Green's function for the time dependent case

The general setting is again the same as for the static case, see Fig. 2.1. We especially consider the probe photon beam to be restricted to the x-y plane as well as the background field to be homogeneous in the y and z directions, but vary in the x direction with a maximum at x = 0 and approaching zero asymptotically for $|x| \to \infty$. Additionally, the magnetic field now varies over time. We demand this temporal variation to be well localized, i.e. to fall off sufficiently rapidly for large times $|t| \to \infty$. The background field is defined to reach its peak intensity around the time $t = 0$. If a plane wave now travels through the origin and interacts with the background field, the result will be an induced wave packet with finite spatial and temporal extension, since the interaction can only take place for a finite amount of time. Furthermore, if the incoming beam is already a wave packet of finite extent, it has to pass through the origin at times when the magnetic field has its peak amplitude in order for notable interaction to occur.

Since we aim to utilize the same strategy as in the last chapter, i.e. employ the expression for the photon polarization tensor in a constant magnetic field and substitute $B \to B(x, t)$ to account for the inhomogeneity, we have to require the magnetic field to vary sufficiently slowly. The time scale τ for the existence of the virtual electron-positron pairs with energy E is given by $\tau E \sim 1$. Hence, the polarization tensor probes time scales of the order of the Compton time, i.e. $\tau \approx 1/m \approx 1.98 \cdot 10^{-6}\,\text{eV}^{-1} \approx 1.3 \cdot 10^{-21}\,\text{s}$. The approximation of a locally time independent field should hold true as long as the temporal variation of the laser pulse is much larger than τ, which is the case for practically all viable setups.

For the calculation of the reflected field, we again make use of the equation of motion (1.26) which also served as a starting point in the static case. Using the same strategy as in Sec. (2.1), we strive to rid ourselves of the complicated tensor structure, but at the same time still try to consider cases as general as possible. In analogy to the last chapter, we can again identify settings $\parallel$ and $\perp$ with the potential to simplify the equations of motion. However, keeping in mind that this time we will have to apply Fourier transformations (A.13) acting on space as well as time coordinates, it becomes clear that the parallel setting has to be dropped from our discussion. The projector $P_\parallel(k)$ does not remain unaffected anymore by the inhomogeneity, as $k_\parallel = (\omega, \mathbf{k}_\parallel)$ possesses a k^0-component which will be affected by the temporal variation. Hence, $P_\parallel(k) \neq P_\parallel(k')$. We furthermore see that the temporal inhomogeneity will likely induce frequency

conversions between incoming and induced photon beam in the general case.

The above consideration leaves us only with the perpendicular component to apply on a similar procedure as in the last chapter. For the remainder of this work we shall only consider this component. The equation of motion for this particular case again simplifies to the scalar equation

$$k^2 a_{\perp,\text{ind}}(k) = -\int \frac{d^4k'}{(2\pi)^4} \tilde{\Pi}_\perp(k, -k'|\mathbf{B}) a_{\perp,\text{in}}(k'), \tag{3.1}$$

and, limiting ourselves to the two-dimensional case, we arrive at

$$\left(k_x^2 - \omega^2 + k_y^2\right) a_{\perp,\text{ind}}(k_x, k_y, \omega) = -\int \frac{dk_x'}{2\pi} \int \frac{d\omega'}{2\pi} \tilde{\Pi}_\perp(k_x, -k_x', \omega, -\omega', k_y|\mathbf{B}) a_{\perp,\text{in}}(k_x', k_y, \omega'). \tag{3.2}$$

A transformation to position space employing (A.13) results in

$$\left[-\frac{\partial^2}{\partial \mathrm{x}^2} + \frac{\partial^2}{\partial t^2} + k_y^2\right] a_{\perp,\text{ind}}(\mathrm{x}, k_y, t) = -\int d\mathrm{x}' \tilde{\Pi}_\perp(\mathrm{x}, \mathrm{x}', t, t', k_y) a_{\perp,\text{in}}(\mathrm{x}', k_y, t') = j_\perp(\mathrm{x}, k_y, t), \tag{3.3}$$

with the symmetrized polarization tensor in position space

$$\tilde{\Pi}(\mathrm{x}, \mathrm{x}', t, t') = \frac{1}{2}\left[\Pi(\mathrm{x}, \mathrm{x}', t, t', k_y) + \Pi(\mathrm{x}', \mathrm{x}, t', t, k_y)\right]. \tag{3.4}$$

We now calculate the corresponding Green's function solving

$$\left[-\frac{\partial^2}{\partial \mathrm{x}^2} + \frac{\partial^2}{\partial t^2} + k_y^2\right] G(\mathrm{x}, \mathrm{x}', t, t', k_y) = \delta(\mathrm{x} - \mathrm{x}')\delta(t - t'), \tag{3.5}$$

or in position space

$$\left(k_x^2 - \omega^2 + k_y^2\right) G(k_x, k_x', \omega, \omega') = 2\pi\delta(k_x + k_x')2\pi\delta(\omega + \omega'). \tag{3.6}$$

In order to maintain causality, we have to use the integration prescription which produces the retarded Green's function, reading

$$G(\mathrm{x}, \mathrm{x}', t, t') = \int_{-\infty}^{\infty} \int_{-\infty}^{\infty} \frac{dk_x}{2\pi} \frac{d\omega}{2\pi} \frac{e^{ik_x(\mathrm{x}-\mathrm{x}')}e^{-i\omega(t-t')}}{\left(\omega - \sqrt{k_x^2 + k_y^2} + i\epsilon\right)\left(\omega + \sqrt{k_x^2 + k_y^2} + i\epsilon\right)}. \tag{3.7}$$

The contour of the ω integration is such that it circumvents the poles in clockwise half circles. Closing the integration path below for $t - t' > 0$ picks up both poles, while for $t - t' < 0$ and a path in the upper half plane picks up none. Therefore we arrive at

$$G(\mathrm{x}, \mathrm{x}', t, t') = -\theta(t - t')\int_{-\infty}^{\infty} \frac{dk_x}{2\pi} e^{ik_x(\mathrm{x}-\mathrm{x}')} \frac{\sin\left(\sqrt{k_x^2 + k_y^2}(t - t')\right)}{\sqrt{k_x^2 + k_y^2}}$$

$$= -\theta(t - t')\int_{-\infty}^{\infty} \frac{dk_x}{2\pi} \cos\left(k_x|\mathrm{x} - \mathrm{x}'|\right) \frac{\sin\left(\sqrt{k_x^2 + k_y^2}(t - t')\right)}{\sqrt{k_x^2 + k_y^2}}. \tag{3.8}$$

The solution to this Fourier cosine transformation is given in [38], page 26 and reads

$$G(\mathrm{x}, \mathrm{x}', t, t') = -\frac{1}{2}\Theta(t - t' - |\mathrm{x} - \mathrm{x}'|) J_0\left(|k_y|\sqrt{(t - t')^2 - (\mathrm{x} - \mathrm{x}')^2}\right), \tag{3.9}$$

where

$$J_0(\mathrm{z}) := \frac{1}{\pi} \int_0^\pi \cos(\mathrm{z}\sin\phi)\, d\phi \tag{3.10}$$

defines the Bessel function of the first kind. The condition for the non-vanishing of the Green's function can be rewritten to read

$$\mathrm{x} + t - t' > \mathrm{x}' > \mathrm{x} - (t - t') \tag{3.11}$$

and is exactly the condition of causality: points outside the past light-cone cannot influence the value of the field at the point (x, t). From Eq. (3.10) we see right away that $J_0(0) = 1$. The result for the special case of $k_y = 0$ consequently takes on a quite simple form, i.e.

$$G(\mathrm{x}, \mathrm{x}', t, t') = -\frac{1}{2}\Theta(t - t') \begin{cases} 1 & \text{for} \quad -(t-t') < \mathrm{x} - \mathrm{x}' < t - t', \\ \frac{1}{2} & \text{for} \quad |\mathrm{x} - \mathrm{x}'| = |t - t'|, \\ 0 & \text{otherwise.} \end{cases} \tag{3.12}$$

The general result for the induced field $a_{\perp,\mathrm{ind}}$ is given by

$$\begin{aligned}
a_{\perp,\mathrm{ind}}(\mathrm{x}, t, k_y) &= -\frac{1}{2}\int_{-\infty}^t dt' \int_{\mathrm{x}-(t-t')}^{\mathrm{x}+t-t'} d\mathrm{x}'\, J_0\left(|k_y|\sqrt{(t-t')^2 - (\mathrm{x}-\mathrm{x}')^2}\right) j_\perp(\mathrm{x}', k_y, t') \\
&= \frac{1}{2}\int_{-\infty}^t dt' \int_{\mathrm{x}-(t-t')}^{\mathrm{x}+t-t'} d\mathrm{x}' \int d\mathrm{x}'' \int dt'' \\
&\quad \times J_0\left(|k_y|\sqrt{(t-t')^2 - (\mathrm{x}-\mathrm{x}')^2}\right) \tilde{\Pi}_\perp(\mathrm{x}', \mathrm{x}'', t', t'', k_y)\, a_{\perp,\mathrm{in}}(\mathrm{x}'', k_y, t'').
\end{aligned} \tag{3.13}$$

We can now implement the spatially and temporally inhomogeneous magnetic field $\mathbf{B}(\mathrm{x}, t)$ in the polarization tensor in analogy to the last chapter. The general procedure is outlined as follows,

$$\tilde{\Pi}^{\mu\nu}(k_x', \omega')\, (2\pi)\, \delta(k_x + k_x')\, (2\pi)\, \delta(\omega + \omega') \xrightarrow{\mathrm{F.T.}} \tilde{\Pi}^{\mu\nu}(\mathrm{x} - \mathrm{x}', t - t') \xrightarrow{B \to B(\mathrm{x},t)} \tilde{\Pi}^{\mu\nu}(\mathrm{x}, \mathrm{x}', t, t'). \tag{3.14}$$

A Fourier transformation on the x component of the momentum vector and on the energy component according to A.13 results in a polarization tensor solely depending on the differences $\mathrm{x} - \mathrm{x}'$ and $t - t'$, since translational and temporal invariance must hold. Inserting the space and time dependence of the magnetic field, i.e. $\mathbf{B} \to \mathbf{B}(\mathrm{x}, t)$, breaks both invariances and we arrive at the required expression $\tilde{\Pi}^{\mu\nu}(\mathrm{x}, \mathrm{x}', t, t')$. An inverse Fourier transformation would result in a polarization tensor $\tilde{\Pi}^{\mu\nu}(k_x, k_x', \omega, \omega')$ mediating between two distinct momenta k_x and k_x' as well as two distinct photon energies ω and ω'.

3.2. Definition of the reflection coefficient

In the last chapter, the reflection coefficient for the one-dimensional static case was defined as the ratio of the squared amplitude $|A_{\mathrm{ref}}|^2$ of the reflected beam to the squared amplitude $|A_{\mathrm{in}}|^2$ of the incoming beam. In the static case this is equal to the ratio of intensities, which is also the physical quantity a measuring device registers at a given moment of time (i.e. a photo-diode measures the number of photons hitting its area). Therefore, a reasonable definition of the reflection coefficient for the time dependent case is given by the ratio of the time integrated

intensities of the incoming and reflected beams, which suitably placed detectors with a certain area measure. This quantity characterizes the total energy $\mathcal{E}_{\text{ref}}$, which gets reflected and passes the area of the detector, set in relation to the incoming beam energy $\mathcal{E}_{\text{in}}$. We set the maximum of interaction at time $t = 0$ and place x $= 0$. The incoming beam starts at a time $t = -\infty$ and at position x $= -\infty$ and travels in positive x direction. The detector is appropriately set up at a large negative position x $= -L$ and is assumed to span an area A_{dec} in the y-z plane. Hence, the majority of the reflected beam photons will have passed the detector at some large, positive time. We define the intensity of the photon beam at a certain spatial point $\mathbf{x}$ and time t as

$$
\begin{aligned}
I(\mathbf{x}, t) &= \text{energy density} \cdot \text{group velocity} \\
&= w(\mathbf{x}, t) \cdot c_{\text{gr}}(\mathbf{x}, t),
\end{aligned}
\tag{3.15}
$$

where the energy in a given volume V can be obtained from

$$
\mathcal{E}(t) = \int_V d^3\text{x}\, w(\mathbf{x}, t) = \frac{1}{2} \int_V d^3\text{x}\, \left(\mathfrak{e}^2(\mathbf{x}, t) + \mathfrak{b}^2(\mathbf{x}, t) \right).
\tag{3.16}
$$

In our case, the position of measurement is already far outside the interaction region and therefore the beam travels with group velocity $c_{\text{gr}} = 1$. The electric field $\mathfrak{e}(\mathbf{x}, t)$ and the magnetic field $\mathfrak{b}(\mathbf{x}, t)$ of the photon beam are related to the vector potential $a(\mathbf{x}, t)$ by means of the field strength tensor $F_{\mu\nu} = \partial_\mu a_\nu - \partial_\nu a_\mu$, see the appendix A. More specifically, the electric and magnetic field components are given by

$$
\mathfrak{e}_i = F^{0i} = \partial^0 a^i - \partial^i a^0 \qquad \longrightarrow \qquad \mathfrak{e} = -\partial_t \mathbf{a}(\mathbf{x}, t) - \text{grad}\, a^0(\mathbf{x}, t),
\tag{3.17}
$$

$$
\mathfrak{b}_i = \frac{1}{2} \epsilon_{ijk} F^{jk} \qquad \longrightarrow \qquad \mathfrak{b} = \text{rot}\, \mathbf{a}(\mathbf{x}, t).
\tag{3.18}
$$

We can now derive an expression for the reflection coefficient $R_\perp$. This will be done only for the perpendicular component and the justification was given in the last section. Consulting Eq. (1.47), the corresponding photon polarization mode for the perpendicular case is given by

$$
a_\perp^\mu(\mathbf{x}, t) = a_\perp(\mathbf{x}, t) \left[0, \frac{\mathbf{e}_k \times \mathbf{e}_B}{|\mathbf{e}_k \times \mathbf{e}_B|} \right] = a_\perp(\mathbf{x}, t) \left[0, \frac{\mathbf{e}_k \times \mathbf{e}_B}{\sin\theta} \right] =: a_\perp(\mathbf{x}, t)\, [0, \mathbf{e}_a].
\tag{3.19}
$$

The electric field then simplifies to

$$
\mathfrak{e}(\mathbf{x}, t) = -\partial_t a_\perp(\mathbf{x}, t)\, \mathbf{e}_a,
\tag{3.20}
$$

and the magnetic field can be simplified by using an identity from vector analysis, in which case we obtain

$$
\mathfrak{b}(\mathbf{x}, t) = \text{rot}\, \left(a_\perp(\mathbf{x}, t)\, \mathbf{e}_a \right) = -\mathbf{e}_a \times \text{grad}\, a_\perp(\mathbf{x}, t).
\tag{3.21}
$$

In the last section we saw that the y and z components of the probe photon momentum $\mathbf{k}$ are not affected by the inhomogeneity and we obtained an expression for the potential $a_\perp(\text{x}, k_y, t)$ as a function of x, t and k_y. This quantity can be related to $a_\perp(\text{x}, \text{y}, t)$ by means of the partial Fourier transformations (A.12), i.e.

$$
a_\perp(\text{x}, \text{y}, t) = \int \frac{dk_y}{2\pi} a_\perp(x, k_y, t) e^{ik_y \text{y}}.
\tag{3.22}
$$

We now put the time and area integrated intensity of the reflected beam $a_{\perp, \text{ref}}(\text{x}, \text{y}, t)$ in relation to the incoming beam $a_{\perp, \text{in}}(\text{x}, \text{y}, t)$ and define this quantity as the reflection coefficient, i.e.

$$
R_\perp := \left. \frac{\int_{-\infty}^{\infty} dt \iint_{A_{\text{dec}}} dy\, dz \left[(\mathfrak{Re}\, \mathfrak{e}_{\perp,\text{ref}})^2(\text{x}, \text{y}, t) + (\mathfrak{Re}\, \mathfrak{b}_{\perp,\text{ref}})^2(\text{x}, \text{y}, t) \right]}{\int_{-\infty}^{\infty} dt \iint_{A_{\text{dec}}} dy\, dz \left[(\mathfrak{Re}\, \mathfrak{e}_{\perp,\text{in}})^2(\text{x}, \text{y}, t) + (\mathfrak{Re}\, \mathfrak{b}_{\perp,\text{in}})^2(\text{x}, \text{y}, t) \right]} \right|_{\text{x}=-L}.
\tag{3.23}
$$

The reflection coefficient thus measures the energy which hits a detector with area A_dec positioned at a large negative distance $-L$ and puts it in relation to the incoming beam energy. The latter we formally assume to be measured by another detector with the same area A_dec, but put into such a position that it registers the incoming beam. Since our problem is z independent, the z integrals in the numerator and denominator cancel out. One requirement for the use of this formula is that both the incoming and the reflected beam are wave packets localized in time and x direction. If the wave packet is furthermore localized in the y direction and we assume the detector's area large enough to pick up the bulk of the energy of the reflected beam, we can formally extend the integration limits in the y direction to $\pm\infty$. Keep in mind that Eq. (3.23) requires the evaluation of the real parts of the electric and magnetic field components if we are dealing with complex quantities. For beams with such properties, the reflection coefficient takes the form

$$R_\perp := \left.\frac{\int_{-\infty}^{\infty} dt \int_{-\infty}^{\infty} dy \, \left[(\mathfrak{Re}\, \mathfrak{e}_{\perp,\text{ref}})^2(\text{x},\text{y},t) + (\mathfrak{Re}\, \mathfrak{b}_{\perp,\text{ref}})^2(\text{x},\text{y},t)\right]}{\int_{-\infty}^{\infty} dt \int_{-\infty}^{\infty} dy \, \left[(\mathfrak{Re}\, \mathfrak{e}_{\perp,\text{in}})^2(\text{x},\text{y},t) + (\mathfrak{Re}\, \mathfrak{b}_{\perp,\text{in}})^2(\text{x},\text{y},t)\right]}\right|_{\text{x}=-L}, \tag{3.24}$$

where the electric and magnetic fields have to be evaluated according to Eqs. (3.20) and (3.21). As shown in the last chapter, the perpendicular setting restricts the possible directions of the magnetic field. If the magnetic field points into the direction of the inhomogeneity, i.e. $\mathbf{e}_B = \mathbf{e}_x$, the equations for the field components simplify substantially, since $\mathbf{e}_a = -\mathbf{e}_z$. The reflection coefficient can then be written as

$$R_\perp = \left.\frac{\int_{-\infty}^{\infty} dt \int_{-\infty}^{\infty} dy \, \left[(\mathfrak{Re}\, \partial_t a_{\perp,\text{ref}})^2 + (\mathfrak{Re}\, \partial_\text{x} a_{\perp,\text{ref}})^2 + (\mathfrak{Re}\, \partial_\text{y} a_{\perp,\text{ref}})^2\right]}{\int_{-\infty}^{\infty} dt \int_{-\infty}^{\infty} dy \, \left[(\mathfrak{Re}\, \partial_t a_{\perp,\text{in}})^2 + (\mathfrak{Re}\, \partial_\text{x} a_{\perp,\text{in}})^2 + (\mathfrak{Re}\, \partial_\text{y} a_{\perp,\text{in}})^2\right]}\right|_{\text{x}=-L}. \tag{3.25}$$

In most cases, it will be easier to evaluate incoming plane waves in the x and y direction and use these to approximately describe the incoming probe laser pulse, as was already done in the last chapter. Under these circumstances, Eq. (3.23) cannot be used to calculate the fraction of reflected photons since the numerator and denominator diverge. However, then one can substitute the denominator by the total pulse energy $\mathcal{E}_\text{in}$ of the incoming probe laser pulse. We therefore define the reflection coefficient in the case of an incoming plane wave with specific k_x and k_y as

$$R_\perp(k_x, k_y) := \left.\frac{\int_{-\infty}^{\infty} dt \iint_{A_\text{dec}} dy \, dz \, \left[(\mathfrak{Re}\, \mathfrak{e}_{\perp,\text{ref}})^2(\text{x},\text{y},t) + (\mathfrak{Re}\, \mathfrak{b}_{\perp,\text{ref}})^2(\text{x},\text{y},t)\right]}{2\mathcal{E}_\text{in}}\right|_{\text{x}=-L}. \tag{3.26}$$

The amplitude $A_{\perp,\text{in}}$ of the incoming beam $a_{\perp,\text{in}}(\mathbf{x},t)$ has to be matched to correspond to a given energy $\mathcal{E}_\text{in}$ of the incoming probe beam, when the area of the detector A_dec is taken into account. This can be done easily for the special case of $\mathbf{e}_B = \mathbf{e}_x$, as is demonstrated now. The incoming plane wave $a_{\perp,\text{in}}(\mathbf{x},t) = -\mathbf{e}_z A_{\perp,\text{in}} \exp[i(k_x\text{x} + k_y\text{y} - \omega t)]$ with a constant and real amplitude $A_{\perp,\text{in}}$ has an energy density of

$$w(\mathbf{x},t) = \omega^2 A_{\perp,\text{in}}^2 \sin^2[k_x\text{x} + k_y\text{y} - \omega t], \tag{3.27}$$

where $\omega^2 = k_x^2 + k_y^2$. We can now choose the area of the detector to be of following extent in y and z directions: $A_\text{dec} = (\text{y} = 0...2\pi/k_y, \text{z} = 0...2\pi/k_y)$. Furthermore, choosing the temporal integration to be of the order of the incoming pulse length τ and demanding that this corresponds to 86% of the energy contained within the pulse, we obtain the formula

$$A_{\perp,\text{in}} \approx \sqrt{0.86 \frac{k_y^2 \mathcal{E}_\text{in}}{2\pi^2 \tau \omega^2}}. \tag{3.28}$$

Equation (3.28) approximately relates the amplitude A_{in} to the incoming beam energy for the case of plane waves, if $k_y \neq 0$. For the case of $k_y = 0$ the only length scale left is given by k_x, so we choose a detector area $A_{\mathrm{dec}} = (\mathrm{y} = 0...2\pi/k_x, \mathrm{z} = 0...2\pi/k_x)$. The integrations will be independent of y and the energy relates to the amplitude by

$$A_{\perp,\mathrm{in}} \approx \sqrt{0.86 \frac{k_x^2 \mathcal{E}_{\mathrm{in}}}{2\pi^2 \tau \omega^2}}. \tag{3.29}$$

Such a plane wave approximation as done here should comply well with the Setup (b) described in the last chapter, since the pulse duration of the POLARIS probe laser is about eight times longer than that of the JETI200 pump laser.

3.3. Fourier transform of the polarization tensor

In this section, we perform a partial Fourier transformation (A.13) on the perpendicular component of the weak field photon polarization tensor (1.49). Again, we only consider the lowest orders (1.50) and (1.52). The perpendicular component of the photon momentum $\mathbf{k}_\perp = k_y \mathbf{e}_y$ can be identified with the y component in our case of two dimensions.

Order n=0

Starting with $2\pi\delta(k_x + k_x')2\pi\delta(\omega + \omega')\Pi_{\perp,(0)}(k)$ according to our procedure (3.14), we must evaluate the expression

$$\Pi_{\perp,(0)}(\mathrm{x} - \mathrm{x}', t - t', \mathbf{k}_\perp) = \frac{\alpha}{4\pi} \int_0^1 d\nu \left(\frac{\nu^2}{3} - 1\right) \nu^2$$
$$\int \frac{dk_x}{2\pi} \int \frac{d\omega}{2\pi} \frac{\left(k_x^2 - \omega^2 + \mathbf{k}_\perp^2\right)^2 e^{ik_x(\mathrm{x}-\mathrm{x}') - i\omega(t-t')}}{m^2 - i\epsilon + \left(k_x^2 - \omega^2 + \mathbf{k}_\perp^2\right)\frac{1-\nu^2}{4}}. \tag{3.30}$$

Substituting

$$u = k_x - \omega, \quad v = k_x + \omega, \quad \mathrm{x}_\pm := \mathrm{x} - \mathrm{x}' \pm (t - t') \quad \text{and} \quad \eta := 4\frac{m^2 - i\epsilon}{1 - \nu^2}, \tag{3.31}$$

the expression can be cast into

$$\Pi_{\perp,(0)}(\mathrm{x} - \mathrm{x}', t - t', \mathbf{k}_\perp) = \frac{\alpha}{2\pi} \int_0^1 d\nu \frac{\left(\frac{\nu^2}{3} - 1\right)\nu^2}{1 - \nu^2} \int \frac{du}{2\pi} e^{\frac{i}{2}\mathrm{x}_+ u} \int \frac{dv}{2\pi} \frac{\left(uv + \mathbf{k}_\perp^2\right)^2}{uv + \eta + \mathbf{k}_\perp^2} e^{\frac{i}{2}\mathrm{x}_- v}. \tag{3.32}$$

Let us first compute the innermost integral, i.e.

$$I_v := \int_{-\infty}^{\infty} \frac{dv}{2\pi} \frac{\left(uv + \mathbf{k}_\perp^2\right)^2}{\frac{\eta + \mathbf{k}_\perp^2}{u} + v} e^{\frac{i}{2}\mathrm{x}_- v}. \tag{3.33}$$

Depending on the sign of u, the poles of v lie in the upper ($u > 0$) or lower ($u < 0$) complex plane. The contour has to be closed in the upper plane for $\mathrm{x}_- > 0$ and in the lower plane for $\mathrm{x}_- < 0$. Hence, I_v evaluates to

$$I_v = i\left[\Theta(u)\Theta(\mathrm{x}_-) - \Theta(-u)\Theta(-\mathrm{x}_-)\right]\eta^2 e^{-\frac{i}{2}\frac{\mathrm{x}_-}{u}(\eta + k_\perp^2)}, \tag{3.34}$$

and therefore

$$
\Pi_{\perp,(0)}(\mathrm{x}-\mathrm{x}',t-t',\mathbf{k}_\perp) = \frac{\alpha}{2\pi}\int_0^1 d\nu \frac{\left(\frac{\nu^2}{3}-1\right)\nu^2}{1-\nu^2}\eta^2
$$
$$
\left[\Theta(\mathrm{x}_-)\int_0^\infty \frac{dy}{2\pi}\frac{1}{\mathrm{y}}e^{-\frac{i}{2}\left(-(\eta+\mathbf{k}_\perp^2)\mathrm{x}_- - y - \frac{-\mathrm{x}_+}{y}\right)} + \Theta(-\mathrm{x}_-)\int_0^\infty \frac{dy}{2\pi}\frac{1}{y}e^{\frac{i}{2}\left((\eta+\mathbf{k}_\perp^2)\mathrm{x}_- - y - \frac{\mathrm{x}_+}{y}\right)}\right],
\tag{3.35}
$$

where the substitution $u = 1/y$ has been performed. The y-integral can be solved in terms of modified Bessel functions by employing formula 3.3241 from [39],

$$
\int_0^\infty dx\, e^{-\frac{\beta}{4x}-\gamma x} = \sqrt{\frac{\beta}{\gamma}}K_1\left(\sqrt{\beta\gamma}\right) \qquad \text{for} \qquad \mathfrak{Re}\,\beta \geq 0,\ \mathfrak{Re}\,\gamma > 0.
\tag{3.36}
$$

Differentiating with respect to the parameter β to generate the inverse powers of x and employing the recurrence relation 9.6.26 from [40],

$$
K_\nu'(z) = K_{\nu-1}(z) - \frac{\nu}{z}K_\nu(z),
\tag{3.37}
$$

we arrive at the formula

$$
\int_0^\infty dx\,\frac{1}{x}e^{-\frac{\beta}{4x}-\gamma x} = -2K_0\left(\sqrt{\beta\gamma}\right) \qquad \text{for} \qquad \mathfrak{Re}\,\beta \geq 0,\ \mathfrak{Re}\,\gamma > 0.
\tag{3.38}
$$

Hence, the solution for the lowest order is given by

$$
\Pi_{\perp,(0)}(\mathrm{x}-\mathrm{x}',t-t',\mathbf{k}_\perp) = -\frac{i\alpha}{2\pi^2}\int_0^1 d\nu \frac{\left(\frac{\nu^2}{3}-1\right)\nu^2}{1-\nu^2}\eta^2 K_0\left(\sqrt{\mathrm{x}_+\mathrm{x}_-(\eta+\mathbf{k}_\perp^2)}\right).
\tag{3.39}
$$

Order n=1

The first nontrivial order is given by $n = 1$. Again, we compute the Fourier transform of $2\pi\delta(k_x + k_x')2\pi\delta(\omega + \omega')\Pi_{\perp,(2)}(k)$ along the same lines as in the last section, i.e.

$$
\Pi_{\perp,(2)}(\mathrm{x}-\mathrm{x}',t-t',\mathbf{k}_\perp^2) = -\frac{\alpha}{12\pi}\int_0^1 d\nu(1-\nu^2)\cdot\int\frac{dk_x}{2\pi}\int\frac{d\omega}{2\pi}e^{ik_x(\mathrm{x}-\mathrm{x}')-i\omega(t-t')}
$$
$$
\frac{1}{\phi_0^2}\left\{(k_x^2-\omega^2)(1-\nu^2) + \left(1+\frac{1+\nu^2}{2}+(1-\nu^2)\frac{m^2}{\phi_0^2}\right)\mathbf{k}_\perp^2\right\}.
\tag{3.40}
$$

Performing the same substitutions as in the last section, we arrive at

$$
\Pi_{\perp,(2)}(\mathrm{x}-\mathrm{x}',t-t',\mathbf{k}_\perp^2) = -\frac{2\alpha}{3\pi}\int_0^1 d\nu \frac{1}{1-\nu^2}\int\frac{du}{2\pi}e^{\frac{i}{2}\mathrm{x}_+ u}\int\frac{dv}{2\pi}e^{\frac{i}{2}\mathrm{x}_- v}
$$
$$
\frac{1}{\left[uv+\eta+\mathbf{k}_\perp^2\right]^2}\left\{uv(1-\nu^2)+\left(1+\frac{1+\nu^2}{2}+\frac{4m^2}{\left[uv+\eta+\mathbf{k}_\perp^2\right]^2}\right)\mathbf{k}_\perp^2\right\},
\tag{3.41}
$$

and the innermost integral is given by

$$
I_v := \int\frac{dv}{2\pi}e^{\frac{i}{2}\mathrm{x}_- v}\left\{\frac{1}{u}\frac{v(1-\nu^2)}{\left[\frac{\eta+\mathbf{k}_\perp^2}{u}+v\right]^2}+\left(\frac{1}{u^2}\frac{\left(1+\frac{1+\nu^2}{2}\right)}{\left[\frac{\eta+\mathbf{k}_\perp^2}{u}+v\right]^2}+\frac{1}{u^3}\frac{4m^2}{\left[\frac{\eta+\mathbf{k}_\perp^2}{u}+v\right]^3}\right)\mathbf{k}_\perp^2\right\}.
\tag{3.42}
$$

Now the poles are of higher order, but they still have the same location in the complex plane as for the zero-th order. The integral evaluates to

$$
I_v = i\left[\Theta(u)\Theta(\mathrm{x}_-) - \Theta(-u)\Theta(-\mathrm{x}_-)\right] e^{-\frac{i}{2}\frac{\mathrm{x}_-}{u}(\eta+\mathbf{k}_\perp^2)}
$$
$$
\times \left\{ (1-\nu^2)\left(\frac{1}{u} - \frac{1}{u^2}\frac{i}{2}\mathrm{x}_-(\eta+\mathbf{k}_\perp^2)\right) - \left(\left(1+\frac{1+\nu^2}{2}\right)\frac{1}{u^2}\frac{i}{2}\mathrm{x}_- + \frac{m^2}{2u^3}\mathrm{x}_-^2\right)\mathbf{k}_\perp^2 \right\} \quad (3.43)
$$

and Eq. (3.41) therefore becomes

$$
\Pi_{\perp,(2)}(\mathrm{x}-\mathrm{x}', t-t', \mathbf{k}_\perp^2) = -\frac{2i\alpha}{3\pi}\int_0^1 d\nu \frac{1}{1-\nu^2}
$$
$$
\times \left[\Theta(\mathrm{x}_-)\int \frac{dy}{2\pi} e^{\frac{i}{2}\left(-\mathrm{x}_-(\eta+\mathbf{k}_\perp^2)y - \frac{\mathrm{x}_-}{y}\right)} \right.
$$
$$
\times \left\{ (1-\nu^2)\left(\frac{1}{y} - \frac{i}{2}\mathrm{x}_-(\eta+\mathbf{k}_\perp^2)\right) - \left(\left(1+\frac{1+\nu^2}{2}\right)\frac{i}{2}\mathrm{x}_- + \frac{m^2}{2}\mathrm{x}_-^2 y\right)\mathbf{k}_\perp^2 \right\}
$$
$$
- \Theta(-\mathrm{x}_-)\int \frac{dy}{2\pi} e^{\frac{i}{2}\left(\mathrm{x}_-(\eta+\mathbf{k}_\perp^2)y - \frac{\mathrm{x}_-}{y}\right)}
$$
$$
\left. \times \left\{ (1-\nu^2)\left(-\frac{1}{y} - \frac{i}{2}\mathrm{x}_-(\eta+\mathbf{k}_\perp^2)\right) - \left(\left(1+\frac{1+\nu^2}{2}\right)\frac{i}{2}\mathrm{x}_- - \frac{m^2}{2}\mathrm{x}_-^2 y\right)\mathbf{k}_\perp^2 \right\} \right].
$$
$$
(3.44)
$$

The y integrals can again be evaluated according to the procedure of the last section. The one missing integral is generated from the integral (3.36) by differentiation with respect to γ and its solution therefore given by

$$
\int_0^\infty dx\; x\; e^{-\frac{\beta}{4x}-\gamma x} = -\left[\sqrt{\frac{\beta}{\gamma^3}}K_1\left(\sqrt{\beta\gamma}\right) + \frac{1}{2}\frac{\beta}{\gamma}K_0\left(\sqrt{\beta\gamma}\right)\right] \qquad \text{for} \qquad \mathfrak{Re}\,\beta \geq 0,\; \mathfrak{Re}\,\gamma > 0.
$$
$$
(3.45)
$$

Keeping in mind that the square root in Eq. (3.36) has to be taken using the positive solution, the result for the second order Fourier transformed polarization tensor can be conveniently stated as follows,

$$
\Pi_{\perp,(2)}(\mathrm{x}-\mathrm{x}', t-t', \mathbf{k}_\perp^2) = -\frac{i\alpha}{6\pi^2}\int_0^1 d\nu \left\{ \left[-4 - \frac{2m^2\mathbf{k}_\perp^2}{\eta+\mathbf{k}_\perp^2}\frac{\mathrm{x}_+\mathrm{x}_-}{1-\nu^2}\right] K_0\left(\sqrt{\mathrm{x}_+\mathrm{x}_-(\eta+\mathbf{k}_\perp^2)}\right) \right.
$$
$$
+ \left[\Theta(\mathrm{x}_+\mathrm{x}_-) + i\Theta(-\mathrm{x}_+\mathrm{x}_-)\right]\sqrt{|\mathrm{x}_+\mathrm{x}_-|}\sqrt{\eta+\mathbf{k}_\perp^2}
$$
$$
\left. \times \left[2 - \left(\frac{4m^2}{(\eta+\mathbf{k}_\perp^2)^2}\frac{1}{1-\nu^2} + \frac{3+\nu^2}{1-\nu^2}\frac{1}{\eta+\mathbf{k}_\perp^2}\right)\mathbf{k}_\perp^2\right] K_1\left(\sqrt{\mathrm{x}_+\mathrm{x}_-(\eta+\mathbf{k}_\perp^2)}\right) \right\}. \quad (3.46)
$$

Note that the result is invariant with respect to translations as it only depends on the quantities $\mathrm{x}-\mathrm{x}'$ and $t-t'$. More specifically, the photon polarization tensor in position space is a pure function of $\mathrm{x}_+\mathrm{x}_- = (\mathrm{x}-\mathrm{x}')^2 - (t-t')^2$, since the polarization tensor in momentum space, Eq. (1.50) and (1.52), depends solely on combinations $uv = k_x^2 - \omega^2$. The full solution up to the second order is therefore given by

$$
\Pi_\perp(\mathrm{x}-\mathrm{x}', t-t', \mathbf{k}_\perp^2) = \Pi_{\perp,(0)}(\mathrm{x}-\mathrm{x}', t-t', \mathbf{k}_\perp^2) + (eB)^2\,\Pi_{\perp,(2)}(\mathrm{x}-\mathrm{x}', t-t', \mathbf{k}_\perp^2) + \mathcal{O}\left((eB)^4\right), \quad (3.47)
$$

together with Eqs. (3.39) and (3.46).

3.4. Calculation of the current $j_\perp$

The current $j_\perp(x', t', k_y)$ as the source of the induced photon field can be expanded in powers of $(eB)^2$, i.e.

$$j_\perp(x', t', k_y) = j_{\perp,(0)}(x', t', k_y) + (eB)^2 \, j_{\perp,(2)}(x', t', k_y) + \mathcal{O}\left((eB)^4\right), \qquad (3.48)$$

where the expansion coefficients are given by

$$j_{\perp,(0)}(x', t', k_y) = \int dx'' \int dt'' \, \Pi_{\perp,(0)}(x' - x'', t' - t'', k_y) \, a_{\perp,\text{in}}(x'', k_y, t''), \qquad (3.49)$$

$$j_{\perp,(2)}(x', t', k_y) = \int dx'' \int dt'' \, \tilde{\Pi}_{\perp,(2)}(x', x'', t', t'', k_y) \, a_{\perp,\text{in}}(x'', k_y, t''). \qquad (3.50)$$

The polarization tensor at the lowest order $n = 0$ is still invariant with respect to translations, since it does not depend on the magnetic field. We thus expect this order to vanish, which is confirmed by an explicit calculation. It is advantageous to not employ the special representation of the polarization tensor Eq. (3.46), but instead leave the evaluation of the momentum integrals for a later stage. Furthermore, we only consider an ingoing plane wave

$$a_{\text{in}}(x'', k_y, t'') = e^{i(k_{\text{in}}x'' - \omega_{\text{in}}t'')} \qquad (3.51)$$

with photon energy $\omega_{\text{in}} = \sqrt{k_{\text{in}}^2 + k_y^2}$. The lowest order of the current is then given by

$$j_{\perp,(0)}(x', k_y, t') = -\frac{\alpha}{4\pi} \int dx'' \int dt'' \int_0^1 d\nu \left(\frac{\nu^2}{3} - 1\right) \nu^2 \int \frac{dk_x}{2\pi} \int \frac{d\omega}{2\pi}$$
$$\frac{\left(k_x^2 - \omega^2 + k_y^2\right)^2}{\phi_0} e^{ik_x(x' - x'') - i\omega(t' - t'')} \, e^{i(k_{\text{in}}x'' - \omega_{\text{in}}t'')}. \quad (3.52)$$

Switching the order of integration, i.e. first performing the x''- and t''-integrals, yields delta-functions

$$2\pi \, \delta(k_x - k_{\text{in}}) \, 2\pi \, \delta(\omega - \omega_{\text{in}}) \qquad (3.53)$$

and, upon evaluation,

$$j_{\perp,(0)}(x', k_y, t') = -\frac{\alpha}{4\pi} \int_0^1 d\nu \left(\frac{\nu^2}{3} - 1\right) \nu^2 \frac{\left(k_{\text{in}}^2 - \omega_{\text{in}}^2 + k_y^2\right)^2}{m^2 - i\epsilon + \left(k_{\text{in}}^2 - \omega_{\text{in}}^2 + k_y^2\right)\frac{1-\nu^2}{4}} e^{i(k_{\text{in}}x' - \omega_{\text{in}}t')}$$
$$\equiv \quad 0 \,, \qquad (3.54)$$

because $\omega_{\text{in}}^2 = k_{\text{in}}^2 + k_y^2$. Since we can generate wave packets of arbitrary shape by the superposition of plane waves, this result also holds for the general case of arbitrary incoming photon beams. As expected, the effect of quantum reflection manifests itself again as an effect which is suppressed by at least B^2/B_{cr}^2 on the level of the reflected field a_{ref}. The second order current $j_{\perp,(2)}(x', k_y, t')$ cannot be evaluated easily, since the inclusion of an inhomogeneous magnetic field breaks the translational invariance. Furthermore, it does not seem possible to reach a closed expression for the reflection coefficient for arbitrary magnetic fields as was done in the last chapter. Rather, one has to specify the spatial and temporal variation $B(x, t)$ early in order to solve the remaining

integrals. A promising generic shape, which is sufficiently close to experimental reality, might be given by a Gaussian spatial and temporal profile exhibiting a temporal modulation, i.e.

$$B^2(\mathrm{x}, t) = B^2 e^{-\left(\frac{\mathrm{x}}{\lambda_x}\right)^2} e^{-\left(\frac{t}{\lambda_t}\right)^2} e^{i\omega_m t}. \tag{3.55}$$

Especially the inclusion of the temporal modulation, which is an inherent property of laser beams, might give an extra handle to increase the effect of reflection in analogy to the static case. The computation of the current for such a profile is still under investigation.

Once the current is calculated, one still has to find an expression for the induced field by means of the equation (3.13). The integrals are not easy to evaluate due to the Bessel-function contained in them. However, physical results for the induced field should exhibit some basic properties, which are a direct consequence of the spatial and temporal locality of the inhomogeneity. For asymptotic times $t \to \infty$, the induced wave should reduce to basically two parts, which correspond to reflected and induced contributions. These should only depend on the relative coordinates $\mathrm{x} + \tilde{c}t$ and $\mathrm{x} - \tilde{c}t$ respectively, where $\tilde{c} = \tilde{c}(k_y) > 0$ denotes a constant. By means of singling out these contributions, one can therefore in principle compute the reflection coefficient via Eq. (3.23), which in the end should not depend on the position $\mathrm{x} = -L$ of the detector and, formally, the limit $L \to \infty$ can be taken as was done in the static case.

4. Conclusion and outlook

This work dealt with the investigation of quantum reflection as a new means to probe the QED quantum vacuum nonlinearity. The main body of this thesis examined this phenomenon for the case of static magnetic background fields and the obtained results can be considered as first estimates for the effects expected to be observed in feasible high intensity laser experiments. Naturally, the treatment has to be extended to involve the time dependency as well. Spatial and temporal variations of the field strength were required to be large compared with Compton wavelength of the involved virtual particles. In the context of QED, practically all available high intensity laser systems in the optical region comply easily with this restriction. Contrary to the traditional signatures of the QED vacuum, which were briefly outlined in the introduction, quantum reflection manifestly requires an inhomogeneous background field. This fact necessitated the treatment of the problem in position space and hence information about the entire momentum dependence of the photon polarization tensor had to be maintained. In particular, no a priori approximation to on the light-cone dynamics can be applied, which considerably complicates the calculation for the time dependent case.

In the second chapter, two different strategies of deriving the reflection coefficient were presented. Especially the second derivation via the quantum mechanical analogy highlights the close connection of optical quantum reflection with the case of atomic quantum reflection, as was already mentioned in the introduction. The resulting equation for the reflection coefficient in the static case turned out to be particularly simple and allowed the study of a plethora of different beam profiles in order to maximize the effect. The exploitation of this freedom, while interesting and enlightening, is also highly necessary, since in addition to the suppression stemming from the fourth order coupling $(B/B_{\mathrm{cr}})^4$, reflection is usually further suppressed exponentially in the reduced frequency $\tilde{\omega}$. However, sizable rates of reflection for current laser systems could already be achieved by considering varying angles of incidence β as well as utilizing modulated as well as 4π focused laser pulses. Near-future laser facilities such as ELI will provide additional improvement by drastically increasing the maximum field strength available.

The last chapter depicted a first attempt to generalize the treatment to space and time dependent background fields. While the calculation of the Green's function as well as the zeroth-order current for this case could be achieved in a straightforward manner, the inclusion of generic background beam shapes is still not completed. Additionally, a possible definition of the reflection coefficient for the time dependent case was given. It seems rather challenging to estimate the effect of temporal variation on quantum reflection. However, since we have observed that a modulated inhomogeneity can help to overcome the exponential suppression, and that such a modulation ω_m will likely be induced by the temporal oscillation of the background field, the prospect seems promising at first sight. Hence, it might not even be necessary to experimentally realize very complicated field profiles in order to yield measurable reflection rates.

Of course, solving the time dependent case is the most pressing issue at the moment, since it would allow for solid quantitative predictions with regard to a possible experimental realization. However, there are many alternative aspects which deserve attention. First of all, in contrast to this work which dealt within a weak field approximation one can also investigate the strong field

limit $B/B_{\text{cr}} \gg 1$. Although such a treatment does not possess any connection to currently feasible experiments, it opens up the possibility to study manifestly non-perturbative effects. A deeper investigation of the Lorentz potential $1/(1+x^2)$ also falls under this category. Secondly, a further generalization and a way to ease the not to be underestimated experimental confinement to purely magnetic background beams is given by the investigation of crossed field configurations with non-vanishing electric and magnetic field components. Exact solutions of the photon polarization tensor in such backgrounds to one loop order have been obtained, as was already mentioned at the end of chapter 1. However, it is not certain that such a setup would permit the simple treatment of the tensor structure of the equations of motion, as was possible in the present work for the case of a purely magnetic background field. Consequently, this necessitates a detailed inspection of how specific photon polarization modes are affected and mixed by inhomogeneous magnetic and electric background fields, which also constitutes an interesting effect in its own regard.

All of the aforementioned aspects eventually deserve attention on the path to a more accurate description of the phenomenon of optical quantum reflection and its subsequent utilization as a means to probe the QED vacuum. Hopefully, this work was able to give first insights into the effect of quantum vacuum reflection and help establish its feasibility as a possible complementary signature of the quantum vacuum nonlinearity.

Bibliography

[1] P. A. M. Dirac, "The Quantum theory of electron," Proc. Roy. Soc. Lond. A **117**, 610 (1928).

[2] P. A. M. Dirac, "Theory of the positron," Report to 7th Solvay Conference (1933).

[3] W. Heisenberg and H. Euler, "Consequences of Dirac's theory of positrons," Z. Phys. **98**, 714 (1936) [physics/0605038].

[4] J. S. Schwinger, "On gauge invariance and vacuum polarization," Phys. Rev. **82**, 664 (1951).

[5] G. V. Dunne, "The Heisenberg-Euler Effective Action: 75 years on," Int. J. Mod. Phys. A **27**, 1260004 (2012) [Int. J. Mod. Phys. Conf. Ser. **14**, 42 (2012)] [arXiv:1202.1557 [hep-th]].

[6] J. S. Toll, "The Dispersion relation for light and its application to problems involving electron pairs," Ph.D. thesis, Princeton Univ., 1952 (unpublished).

[7] Z. Bialynicka-Birula and I. Bialynicki-Birula, "Nonlinear effects in Quantum Electrodynamics. Photon propagation and photon splitting in an external field," Phys. Rev. D **2**, 2341 (1970).

[8] J. S. Heyl and L. Hernquist, "Birefringence and dichroism of the QED vacuum," J. Phys. A **30**, 6485 (1997) [hep-ph/9705367].

[9] R. Karplus and M. Neuman, "The scattering of light by light," Phys. Rev. **83**, 776 (1951).

[10] S. L. Adler, "Photon Splitting And Photon Dispersion In A Strong Magnetic Field," Annals Phys. **67**, 599 (1971).

[11] S. Z. Akhmadaliev, G. Y. Kezerashvili, S. G. Klimenko, R. N. Lee, V. M. Malyshev, A. L. Maslennikov, A. M. Milov and A. I. Milstein *et al.*, "Experimental investigation of high-energy photon splitting in atomic fields," Phys. Rev. Lett. **89**, 061802 (2002) [hep-ex/0111084].

[12] G. Cantatore [PVLAS Collaboration], "Recent results from the PVLAS experiment on the magnetized vacuum," Lect. Notes Phys. **741**, 157 (2008).

[13] P. Berceau, R. Battesti, M. Fouche and C. Rizzo, "The vacuum magnetic birefringence experiment: A test for quantum electrodynamics," Can. J. Phys. **89**, 153 (2011).

[14] H. B. G. Casimir, "On the Attraction Between Two Perfectly Conducting Plates," Kon. Ned. Akad. Wetensch. Proc. **51**, 793 (1948).

[15] C. Henkel, C. I. Westbrook, and A. Aspect, "Quantum reflection: atomic matter-wave optics in an attractive exponential potential," J. Opt. Soc. Am. B **13**, 233 (1996).

[16] H. Gies, "Physics of the Quantum Vacuum," Lecture Notes WS 2012, Friedrich-Schiller-Universität Jena.

[17] L. S. Brown, *Quantum Field Theory*, Cambridge University Press (1994).

[18] M. E. Peskin and D. V. Schroeder, *An Introduction to Quantum Field Theory (Frontiers in Physics)*, Westview Press (1995).

[19] W. Dittrich and M. Reuter, "Effective Lagrangians In Quantum Electrodynamics," Lect. Notes Phys. **220**, 1 (1985).

[20] F. Karbstein, L. Roessler, B. Dobrich and H. Gies, "Optical Probes of the Quantum Vacuum: The Photon Polarization Tensor in External Fields," Int. J. Mod. Phys. Conf. Ser. **14**, 403 (2012) [arXiv:1111.5984 [hep-ph]].

[21] I. A. Batalin and A. E. Shabad, "Photon green function in a stationary homogeneous field of the most general form," Zh. Eksp. Teor. Fiz. **60**, 894 (1971).

[22] W. Dittrich and H. Gies, "Probing the quantum vacuum. Perturbative effective action approach in quantum electrodynamics and its application," Springer Tracts Mod. Phys. **166**, 1 (2000).

[23] L. F. Urrutia, "Vacuum Polarization In Parallel Homogeneous Electric And Magnetic Fields," Phys. Rev. D **17**, 1977 (1978).

[24] B. Dobrich, H. Gies, N. Neitz and F. Karbstein, "Magnetically amplified light-shining-through-walls via virtual minicharged particles," Phys. Rev. D **87**, 025022 (2013) [arXiv:1203.4986 [hep-ph]].

[25] B. Dobrich and H. Gies, "Axion-like-particle search with high-intensity lasers," JHEP **1010**, 022 (2010) [arXiv:1006.5579 [hep-ph]].

[26] W. -y. Tsai and T. Erber, "The Propagation of Photons in Homogeneous Magnetic Fields: Index of Refraction," Phys. Rev. D **12**, 1132 (1975).

[27] F. Shimizu, "Specular Reflection of Very Slow Metastable Neon Atoms from a Solid Surface," Phys. Rev. Lett. **86**, 987 (2001).

[28] H. Gies, F. Karbstein and N. Seegert, "Quantum Reflection as a New Signature of Quantum Vacuum Nonlinearity," New J. Phys. **15**, 083002 (2013) [arXiv:1305.2320 [hep-ph]].

[29] Y. Monden and R. Kodama, "Interaction of two counterpropagating laser beams with vacuum," Phys. Rev. A **86**, 033810 (2012).

[30] A. E. Siegman, *Lasers*, First Edition, University Science Books, USA (1986).

[31] Homepage of the Helmholtz Institute Jena: http://www.hi-jena.de

[32] W. P. Leemans, R. Duarte, E. Esarey, S. Fournier, C. G. R. Geddes, D. Lockhart, C. B. Schroeder and C. Toth *et al.*, "The Berkeley Lab Laser Accelerator (BELLA): A 10-GeV laser plasma accelerator," AIP Conf. Proc. **1299**, 3 (2010).

[33] http://www.photonics.com/Article.aspx?AID=51563

[34] http://www.extreme-light-infrastructure.eu/

[35] M. Bregant *et al.* [PVLAS Collaboration], "Limits on Low Energy Photon-Photon Scattering from an Experiment on Magnetic Vacuum Birefringence," Phys. Rev. D **78**, 032006 (2008) [arXiv:0805.3036 [hep-ex]].

[36] I. Gonoskov, A. Aiello, S. Heugel and G. Leuchs, "Dipole pulse theory: Maximizing the field amplitude from 4π focussed laser pulses," Phys. Rev. A **86**, 053836 (2012).

[37] R. T. Thew, N. Curtz, P. Eraerds, N. Walenta, J. -D. Gautier, E. Koller, J. Zhang, N. Gisin and H. Zbinden, "Approaches to single photon detection," Nuclear Instruments and Methods in Physics Research A **610**, 16 (2009).

[38] F. Oberhettinger, *Tables of Fourier transforms and Fourier transforms of distributions*, Springer Verlag (1990).

[39] I. S. Gradshteyn and J. M. Ryzhik, *Table of Integrals, Series, and Products*, Ed. by A. Jeffrey and D. Zwillinger, 6th edition, Academic Press (2000).

[40] M. Abramowitz and I. Stegun, *Handbook of Mathematical Functions: With Formulas, Graphs, and Mathematical Tables*, Applied mathematics series, National Bureau of Standards (1964).

[41] D. Meschede, *Optik, Licht und Laser*, Teubner Studienbücher, Vieweg+Teubner Verlag (2008).

A. Notation and conventions

Throughout this work we work in the Heaviside-Lorentz system and use natural units, i.e.

$$\hbar \equiv c \equiv 1. \tag{A.1}$$

In this system, the unit of electric charge e is related to the fine structure α by

$$e = \sqrt{4\pi\alpha} \approx 0.303 \qquad . \tag{A.2}$$

As a convention for the flat Minkowski metric, we choose

$$g_{\mu\nu} = g^{\mu\nu} = \text{diag}\,(-1, 1, 1, 1). \tag{A.3}$$

Greek indices run from $\mu = 0, \dots, 3$, while Latin indices run from $i = 1, \dots, 3$. Indices, which occur twice in a single term, are being summed over in accordance with the Einstein summation convention. The components of the momentum four-vectors k in Minkowski space are given by $k^\mu = (\omega, k_x, k_y, k_z) = (\omega, \mathbf{k})$. The spatio-temporal four-vector x uses Roman letters to denote its spatial components, i.e. $x^\mu = (t, \mathrm{x}, \mathrm{y}, \mathrm{z}) = (t, \mathbf{x})$. Bold quantities represent ordinary Euclidean vectors in three-space, the corresponding unit vectors are given by $\mathbf{e}_x$, $\mathbf{e}_y$ and $\mathbf{e}_z$. The only exception was made in chapter 3. There, $\mathfrak{e}$ and $\mathfrak{b}$ denote the Euclidean electric and magnetic field strength vectors respectively and $\mathfrak{e}_i$, $\mathfrak{b}_i$ their components. The product of two four-vectors is given by

$$kx = -\omega t + \mathbf{k} \cdot \mathbf{x} = -\omega t + k_x \mathrm{x} + k_y \mathrm{y} + k_z \mathrm{z}. \tag{A.4}$$

The γ-matrices in their standard representation

$$\gamma^0 = \begin{pmatrix} 1 & 0 \\ 0 & -1 \end{pmatrix} \qquad \text{and} \qquad \gamma^i = \begin{pmatrix} 0 & \sigma^i \\ -\sigma^i & 0 \end{pmatrix} \tag{A.5}$$

satisfy by definition the anti-commutation relations

$$\{\gamma^\mu, \gamma^\nu\} = -2g^{\mu\nu}. \tag{A.6}$$

The Pauli matrices are given by

$$\sigma^1 = \begin{pmatrix} 0 & 1 \\ 1 & 0 \end{pmatrix}, \qquad \sigma^2 = \begin{pmatrix} 0 & -i \\ i & 0 \end{pmatrix}, \qquad \sigma^3 = \begin{pmatrix} 1 & 0 \\ 0 & -1 \end{pmatrix} \tag{A.7}$$

and the matrices $\sigma^{\mu\nu}$ are defined by

$$\sigma^{\mu\nu} := \frac{i}{2}\big[\gamma^\mu, \gamma^\nu\big]. \tag{A.8}$$

The Feynman slash denotes a contraction of a four-vector with γ-matrices, i.e.

$$\slashed{a} = \gamma_\mu a^\mu = -\gamma^0 a^0 + \gamma^i a^i. \tag{A.9}$$

In our metric, the electromagnetic field strength tensor $F^{\mu\nu} = \partial^\mu a^\nu - \partial^\nu a^\mu$ is given by

$$F^{\mu\nu} = \begin{pmatrix} 0 & E_1 & E_2 & E_3 \\ -E_1 & 0 & B_3 & -B_2 \\ -B_2 & -B_3 & 0 & B_1 \\ -B_3 & B_2 & -B_1 & 0 \end{pmatrix}. \tag{A.10}$$

Since many results involve the evaluation of numerical values, let us give the conversion factors between SI-units and natural units:

Quantity	SI-unit	Natural unit
Length	$1\,\mathrm{m}$	$5.07 \cdot 10^6$ eV^{-1}
Time	$1\,\mathrm{s}$	$1.52 \cdot 10^{15}$ eV^{-1}
Mass	$1\,\mathrm{kg}$	$5.61 \cdot 10^{35}$ eV
Energy	$1\,\mathrm{J}$	$6.24 \cdot 10^{18}$ eV
Intensity	$1\,\mathrm{W/cm^2}$	$1.59 \cdot 10^{-6}$ eV^4
Power	$1\,\mathrm{W}$	$4.11 \cdot 10^3$ eV^2
Magnetic field strength	$1\,\mathrm{T}$	195.5 eV^2
Electric field strength	$1\mathrm{V/m}$	$6.5 \cdot 10^{-7}$ eV^2

Fourier transformations

We switch between position and momentum space by means of the Fourier transformations

$$
a_\nu(x) = \int \frac{d^4k}{(2\pi)^4} a_\nu(k) e^{ikx} \qquad \text{and} \qquad \Pi^{\mu\nu}(x,x') = \int \frac{d^4k}{(2\pi)^4} \int \frac{d^4k'}{(2\pi)^4} e^{ikx} \Pi^{\mu\nu}(k,k') e^{ik'x'}.
$$
(A.11)

Furthermore, throughout the paper there are performed partial Fourier transformations on either only one spatial component, i.e.

$$
a_\nu(\mathrm{x}, k_y, k_z, \omega) = \int \frac{dk_x}{2\pi} a_\nu(k) e^{ik_x \mathrm{x}},
$$

$$
\Pi^{\mu\nu}(\mathrm{x}, \mathrm{x}', k_y, k_y', k_z, k_z', \omega, \omega') = \int \frac{dk_x}{2\pi} \int \frac{dk_x'}{2\pi} e^{ik_x \mathrm{x}} \Pi^{\mu\nu}(k,k') e^{ik_x' \mathrm{x}'},
$$
(A.12)

or on one spatial and the temporal component, i.e.

$$
a_\nu(\mathrm{x}, k_y, k_z, t) = \int \frac{dk_x}{2\pi} \int \frac{d\omega}{2\pi} a_\nu(k) e^{i(k_x \mathrm{x} - \omega t)},
$$

$$
\Pi^{\mu\nu}(\mathrm{x}, \mathrm{x}', k_y, k_y', k_z, k_z', t, t') = \int \frac{dk_x}{2\pi} \int \frac{dk_x'}{2\pi} \int \frac{d\omega}{2\pi} \frac{d\omega'}{2\pi} e^{i(k_x \mathrm{x} - \omega t)} \Pi^{\mu\nu}(k,k') e^{i(k_x' \mathrm{x}' - \omega' t')}.
$$
(A.13)

B. Gaussian beams

A short overview of the properties of Gaussian beams, propagating along the z-axis, is given (see for example [41]). The Gaussian beam is a special solution of the paraxial approximation to the Helmholtz equation. The amplitude $B(r, z)$, where r denotes the radial coordinate, is given by

$$B(r, z) = B_0 \frac{w_0}{w(z)} e^{-\left(\frac{r}{w(z)}\right)^2} e^{-ik\frac{r^2}{2R(z)}} e^{i(\zeta(z) - kz)}, \tag{B.1}$$

with

$$w(z) = w_0 \sqrt{1 + \left(\frac{z}{z_0}\right)^2}, \qquad\qquad \text{beam radius,} \tag{B.2}$$

$$R(z) = z\left(1 + \left(\frac{z_0}{z}\right)^2\right), \qquad\qquad \text{radius of curvature,} \tag{B.3}$$

$$\zeta(z) = \arctan\frac{z}{z_0}, \qquad\qquad \text{Gouy phase shift,} \tag{B.4}$$

$$z_0 = \frac{\pi w_0^2}{\lambda}, \qquad\qquad \text{Rayleigh length.} \tag{B.5}$$

The beam radius $w(z)$ indicates the radial position at which the field declined to $1/e$ of its maximum value at $r = 0$. It is characterized by the waist $2w_0$, which denotes the smallest extension of the laser beam. The Rayleigh zone extends from $-z_0$ to z_0 and marks the region of the biggest change of the laser beam, i.e. the transition from a plane wave for $z \approx 0$ to an approximate spherical wave for $z \gg z_0$. The beam radius in the focus $z \approx 0$ is almost constant, while it increases linearly for large z. The radius of curvature $R(z)$ near the focus resembles that of a plane wave, i.e. $R(z \to 0) \to 0$, while in the far field it increases linearly with z as well. The Gouy phase shift accounts for an extra phase shift near the focus compared with plane waves. In the center of the beam, i.e. $z = 0$, the transversal profile is given by a Gaussian profile

$$B(r, 0) = B_0 \, e^{-\left(\frac{r}{w_0}\right)^2}. \tag{B.6}$$

For the specific case of quantum reflection, we consider the background beam radius in the focal spot as constant and furthermore assume f-numbers of $f^\# = 1$. Therefore, the beam radius is given by $w_0 = \lambda$ and the Rayleigh length by $z_0 = \pi\lambda$. At the Rayleigh length, the waist of the Gaussian beam increases to $w(z_0) = \sqrt{2}w_0$. If the probe beam hits the background beam under an angle of β, it traverses the background beam in the longitudinal direction on a scale $(2\tan\beta 2\lambda)$. For our assumption of a nearly constant waist size in the interaction region to be valid, we require the longitudinal distance to be of not more than twice the Rayleigh length. This leads to an upper limit on the angle β, which is given by

$$\tan\beta \lesssim \frac{\pi}{2} \qquad \to \qquad \beta \lesssim 58°. \tag{B.7}$$

Hence, we should strive to achieve incidence angles β below this maximum value as such setups comply better with the approximation of a nearly constant background beam radius w_0.

Danksagung

Gerne möchte ich mich bei einigen Menschen bedanken, welche mich bei der Anfertigung dieser Arbeit direkt oder indirekt unterstützt haben . Auf akademischer Ebene gilt großer Dank meinem betreuenden Professor Holger Gies, welcher mich mit einem sehr interessanten Thema betraute und mir die Möglichkeit bietet, jenes auch in Zukunft zu verfolgen. Desweiteren möchte ich mich insbesondere bei Dr. Felix Karbstein bedanken. Er brachte stets gutgelaunt Zeit und Geduld für mich auf, wenn ich desöfteren mit meinen Fragen und Problemen plötzlich bei ihm im Büro erschien. Dank gebührt weiterhin Julia Borchardt und Courtney Hotchkiss für das Korrekturlesen der Arbeit. Allgemein geht mein Dank auch an die versammelte Physikergemeinde, insbesondere aber an W. Heisenberg, R. Feynman, J. Schwinger und Co. für die Entwicklung eines solch eleganten wie umfangreichen Theoriegebäudes "QED", welches auch nach mehr als 50 Jahren neue Aspekte zutage fördert und so jungen angehenden Physikern wie mir ausreichend Beschäftigung bietet. Glücklicherweise erweist sich die Beschaffenheit der Natur als kompliziert genug, so dass sie der damals schon Max Planck vorhergesagten Massenarbeitslosigkeit von Physikern bis heute stets Einhalt gebot.

Auf persönlicher Ebene gilt mein großer Dank natürlich meiner Familie, welche mich stets vorbehaltlos in all meinen Plänen unterstützte. Insbesondere meine Eltern Detlef und Kerstin Seegert boten einen sicheren Hafen, von welchem aus ich die entferntesten Exkursionen starten konnte mit der steten Gewissheit, sie bei meiner Rückkehr schon freudig winkend an der Pier zu finden. Meinen Großeltern Ruth und Werner Seegert widme ich diese Arbeit. Sie legten mit ihrer Liebe und Zuneigung das Fundament für viele glückliche Generationen, die Dank ihnen der Erkenntnis, worauf es im Leben ankommt, einen großen Schritt näher gerückt sind.

Eigenständigkeitserklärung

Ich erkläre, dass ich die vorliegende Arbeit selbständig und nur unter Verwendung der angegebenen Hilfsmittel und Quellen angefertigt habe. Die eingereichte Arbeit ist nicht anderweitig als Prüfungsleistung verwendet worden oder als Veröffentlichung erschienen.
Seitens des Verfassers bestehen keine Einwände, die vorliegende Arbeit für die öffentliche Benutzung zur Verfügung zu stellen.

Ort, Datum: Unterschrift: